Strål
säkerhets
myndigheten
Swedish Radiation Safety Authority

Authors: Peter Segle
Jessica Strömbro
Alexander Wulff
Johan Kölfors
Albin Larsson
Robert Persson

Research

2013:27

Numerical simulations of headed anchors break in reinforced and non-reinforced concrete structures

Report number: 2013:27 **ISSN:** 2000-0456
Available at www.stralsakerhetsmyndigheten.se

SSM perspective

Background

The design codes for anchorage of equipment in concrete structures have been developed since the time the Swedish power plants were designed. Furthermore, the design basis has been updated and in some cases new mechanical loads have been added. As a consequence, it can be difficult for some anchorages to meet the requirements of today.

In the design of anchorage equipment the beneficial effect of reinforcement was, in most cases, not considered. The American ASCI 349-06 code open up today for a more detailed analysis where the beneficial impact of reinforcement on anchor capacity can be taken into account. How this analysis can be done is, however, not explicitly described in the code. The European CEN/TS code provides a simplified way of calculate the capacity for the concrete edge failure mode if sufficient reinforcement is present.

Objectives

The objective of the project is to study the effect of reinforcement on the concrete breakout capacity of cast in headed bolts in concrete structures by numerical simulations. Both single anchors and anchor groups are studied for tension and shear loads.

Results

Numerical simulations show that reinforcement has a beneficial effect on anchor capacity both in tension and shear. For instance, it increases the global stiffness of the concrete structure which means that the risk for splitting of the concrete at the location of the anchor is reduced.

Some of the conclusions are as follows:

- Concrete cone failure and concrete edge failure of headed single anchors and anchor groups in non-reinforced concrete as well as in reinforced concrete can be simulated with confidence using finite element analysis.
- The simulations show good agreement with results from physical tests.
- For cases of single anchor in tension, simulated concrete cone failure loads in non-cracked reinforced concrete show better agreement with physical tests compared to anchors in pre-cracked reinforced concrete.
- Global stiffness of the concrete structures is normally not considered by design codes in the design of anchors. For anchor groups loaded in tension, this might result in reduced safety margin against concrete cone failure if the concrete structure is too flexible.
- The simulations show that reinforcement in the direction of the applied load leads to a substantial increase of the concrete edge failure capacity.
- In general, reinforcement makes the failure of anchors loaded in tension or shear more ductile.

Need for further research

More research is needed within this area in order to develop detailed recommendations for design of anchor plates by use of numerical simulations compatible with the European code CEN/TS.

Project information

Contact person SSM: Kostas Xanthopoulos
Reference: SSM2011-1003

Strål
säkerhets
myndigheten
Swedish Radiation Safety Authority

Authors: Peter Segle, Jessica Strömbro, Alexander Wulff, Johan Kölfors,
Albin Larsson and Robert Persson
Inspecta Nuclear AB, Scanscot Technology AB

2013:27

Numerical simulations of headed anchors break in reinforced and non-reinforced concrete structures

Date: Mars 2013
Report number: 2013:27 **ISSN:** 2000-0456
Available at www.stralsakerhetsmyndigheten.se

This report concerns a study which has been conducted for the Swedish Radiation Safety Authority, SSM. The conclusions and viewpoints presented in the report are those of the author/authors and do not necessarily coincide with those of the SSM.

SSM 2013:27

Summary

In this research project, the response of headed anchors in non-reinforced and reinforced concrete structures is investigated by means of finite element simulations. Single anchor and anchor groups loaded in tension or shear are studied. Focus is on anchors in reinforced concrete structures.

Simulations are conducted with the general purpose finite element program Abaqus. A number of parameters are investigated such as dilation angle, fracture energy of concrete, element size, width and thickness of concrete structure, number of anchors, eccentricity of anchor group, type of reinforcement, amount of reinforcement and boundary conditions.

Numerical simulations show good agreement with available results from testing of anchor bolts in tension and shear. The level of failure loads is better simulated than the shape of force-displacement curves. Results show that reinforcement has a beneficial effect on anchor capacity both in tension and shear. Firstly, it increases the global stiffness of the concrete structure which means that the risk for splitting of the concrete at the location of the anchor is reduced. Secondly, it increases the confinement in the vicinity of the anchor which increases the capacity. Thirdly, in the case of supplementary reinforcement close to the anchors, such as shear reinforcement for an anchor in shear, the reinforcement can directly transfer the load from the anchor into the concrete structure and thereby increase the capacity substantially. Fourthly, in general reinforcement makes the failure of anchors loaded in tension or shear more ductile.

Most important conclusions are:

1. Concrete cone failure and concrete edge failure of headed single anchors and anchor groups in non-reinforced as well as in reinforced concrete can be simulated with confidence using finite element analyses.

2. In general, reinforcement makes the failure of anchors loaded in tension or shear more ductile.

3. Global stiffness of the concrete structure is not considered by design codes such as CEN/TS in the design of anchors. For anchor groups loaded in tension, this lack might result in reduced safety margin against concrete cone failure if the concrete structure is too flexible. This is particularly true when non-cracked concrete is assumed.

4. The simulations show that reinforcement in the direction of the applied load leads to a substantial increase of the concrete edge failure capacity. However, the simulations show that the normal stress in the reinforcement bars close to the anchors is considerably higher than in the rest of the bars tying the breakout body to the concrete member.

Finally, a number of areas for further work on anchors in reinforced concrete structures are suggested.

Sammanfattning

I detta projekt har simuleringar av brott hos förankringar i oarmerad och armerad betong genomförts med hjälp av finita elementanalyser. Simuleringarna har omfattat utdragsbelastade förankringar samt tvärkraftsbelastade förankringar nära fri betongkant. Både enskilda förankringar och grupper av förankringar har studerats. Speciellt fokus har legat på att simulera den effekten som armering har på förankringarnas brottkapacitet.

Simuleringarna har genomförts med det generella finita elementprogrammet Abaqus. Studien omfattar undersökningar av ett stort antal viktiga parametrar såsom dilationsvinkel, brottenergi, elementstorlek, dimensioner hos betongkroppen, antalet förankringar, excentricitet, typ av armering, armeringsmängd och randvillkor.

De numeriska simuleringarna visar god överensstämmelse med resultat från provningar som har genomförts i andra projekt. Generellt kan sägas att den simulerade nivån på brottlasten stämmer bättre överens med resultat från provning än det simulerade sambandet mellan kraft och deformation. Resultaten visar att armering har en tydlig positiv effekt på betongförankringars brottkapacitet både vid utdragsbelastning och vid tvärkraftsbelastning. Man kan urskilja fyra huvudsakliga anledningar till denna positiva effekt. Den första är det bidrag till global styvhet som armeringen ger och som i sin tur minskar risken för stora böjsprickor i förankringarnas närområde. Den andra är den ökande grad av treaxligt spänningstillstånd i närbetongen som armeringen leder till. Den tredje effekten är den direkt lastöverförande effekten som fås av armering som är placerad i lastens riktning exempelvis tvärkraftsarmering. Simuleringarna visar dock vikten av att denna kraftöverförande armering är placerad i nära anslutning till förankringen för att erhålla denna effekt. Den fjärde effekten är att brottet för utdragsbelastade förankringar eller tvärkraftsbelastade förankringar oftast blir mer duktilt när betongstrukturen är armerad.

De viktigaste slutsatserna är:

1. Brottmoderna ”concrete cone failure” och ”concrete edge failure” kan simuleras med god tillförlitlighet med hjälp av finita elementanalyser.

2. Brottet för utdragsbelastade förankringar eller tvärkraftsbelastade förankringar blir oftast mer duktilt när betongstrukturen är armerad.

3. Den globala styvheten hos den strukturdel där förankringen är monterad beaktas ej i CEN/TS vid normativ bestämning av brottkapaciteten. För utdragsbelastade förankringar monterade i relativt veka betongkonstruktioner kan detta innebära en minskning av säkerhetsmarginalerna. Detta gäller framförallt när betongen antas osprucken.

4. Som väntat visar simuleringarna att armering placerad i lastens riktning kan ge en ansenlig höjning av brottkapaciteten. En förutsättning för att erhålla denna effekt är dock att armeringen är placerad i nära anslutning till förankringen.

Avslutningsvis ges förslag på områden för fortsatt arbete med förankringar i armerade betongstrukturer.

Content

Nomenclature

$^{0}_{,N}$	projected concrete failure area of single anchor [mm^2]
$_{,N}$	projected concrete failure area of anchor group [mm^2]
c_1	edge distance from anchor positioned close to a free concrete edge [mm]
d_t	concrete tension damage [-]
E	modulus of elasticity [MPa]
E_0	initial modulus of elasticity used in Abaqus [MPa]
G_F	fracture energy [Nm/m^2]
H	thickness of slab [m]
f_c	compressive cylinder strength of concrete [MPa]
f_{ck}	characteristic compressive cylinder strength of concrete [MPa]
f_{cm}	mean value of concrete cylinder compressive strength [MPa]
$f_{c,cube}$	compressive cube strength of concrete [MPa]
$f_{ck,cube}$	characteristic compressive cube strength of concrete [MPa]
$f_{cm,cube}$	mean value of concrete cube compressive strength [MPa]
f_{ct}	tensile strength of concrete [MPa]
f_{ctk}	characteristic tensile strength of concrete [MPa]
f_{ctm}	mean value of tensile strength of concrete [MPa]
h_{ef}	anchor embedment depth [mm]
L	width of slab [m]
$N^0_{Rk,c}$	characteristic resistance of a single anchor in tension [N]
N_u	failure load of a single anchor or anchor group in tension [N]
s, s_2	distance between anchors [mm]
u_t^{ck}	cracking displacement [m]
u_{t0}^{ck}	cracking displacement at which complete loss of strength takes place [m]
$V^0_{Rk,c}$	characteristic shear resistance of a single anchor loaded perpendicular to the edge [N]
$V^0_{Rm,c}$	mean concrete edge failure capacity for single anchor [N]
δ	displacement [mm]
ϵ	flow potential eccentricity used in Abaqus
ε	total strain [-]
ε_0^{el}	elastic strain corresponding to undamaged material [-]
ε^{in}	inelastic strain [-]
ε_{max}	maximum strain [-]
μ	viscosity parameter
ν	Poisson's ratio [-]
ψ	dilation angle [deg]
ρ	density [kg/m^3]
σ_{cu}	ultimate compressive stress used in Abaqus [MPa]
$\sigma_{\ 0}$	uniaxial initial compressive yield stress used in Abaqus [MPa]
σ_{b0}	initial equibiaxial compressive yield stress used in Abaqus [MPa]
σ_{t0}	failure stress in tension used in Abaqus [MPa]

1. Introduction

Currently, many of the Swedish nuclear power plant reactors are power uprated and modernised. Structural verification of mechanical equipment forms an essential part of this work. Structural embedments in concrete used to transmit mechanical loads between pressure equipment and concrete structures is an important area in this context.

Since the Swedish nuclear power plants were designed (the oldest reactor Oskarshamn 1 was started 1972 and the youngest reactors Oskarshamn 3 and Forsmark 3 were started 1985), the design codes for anchorage of equipment in concrete structures have been developed. Furthermore, mechanical loads in the design basis have been updated and in many cases new mechanical loads have been added. Only Oskarshamn 3 and Forsmark 3 were, for example, originally designed for a safe shut-down earthquake. A consequence of these changes is that some anchorage equipment that previously fulfilled the design code criteria, today seems to be overloaded at an initial calculation.

When the anchorage equipment first was designed, the beneficial effect of reinforcement was, in most cases, not considered. Taking reinforcement into account might thus give the extra capacity needed to fulfil the requirements of today.

In ACI 349-06, section D.4.4 and D.4.5, supplementary reinforcement is considered in a simplistic way when calculating the anchor capacity for the failure modes concrete breakout and side-face blowout [ACI 349-06 2006]. Two conditions are defined. Condition A applies where the potential concrete failure surfaces are crossed by supplementary reinforcement proportioned to tie the potential concrete failure prism into the concrete structure. Condition B applies where such supplementary reinforcement is not provided. Depending on condition, type of load and type of anchor, different strength-reduction factors ϕ are given. According to ACI 349-06, section D.4.4 and D.4.5, the concrete breakout and side-face blowout strength is between 7 and 15 % higher with supplementary reinforcement than without.

According to ACI 349-06, section D.4.2.1, the effect of supplementary reinforcement provided to confine or restrain the concrete breakout, or both, shall be permitted to be included in the design models used for determining the anchor capacity. The ACI code thus opens up for a more detailed analysis where the beneficial impact of reinforcement on anchor capacity can be taken into account. How this analysis can be done is, however, not explicitly described in the code.

In CEN/TS 1992-4-2, section 6.2 and 6.3, supplementary reinforcement is considered by means of replacing the concrete cone and/or concrete edge failure mode verification in tension and shear respectively with two reinforcement related failure modes [CEN/TS 1992-4-2 2009]. This approach means that the supplementary reinforcement should be designed to resist the total load. Requirements such as distance between anchor and reinforcing bar, diameter of reinforcement, type of reinforcement and anchorage lengths in the concrete failure prism and the concrete member has to be fulfilled. The rebars should also be organised as a wire mesh, enabling adequate transmission of the load (strut and tie).

In addition, CEN/TS 1992-4-2 section 6.3.5.2.7, provides a simplistic way of enumerate the capacity for the concrete edge failure mode if sufficient supplementary reinforcement is present. The uprating factor is either 1.2 or 1.4 depending on the position of the fastening.

In this project, the effect of reinforcement on the concrete breakout capacity of cast-in headed anchor bolts in concrete structures is investigated by numerical simulations. Both single anchors and anchor groups are studied for tension loads and shear loads. Analyses are performed with the finite element program solver Abaqus/Explicit version 6.10 which is a well-known and thoroughly tested general purpose finite element program [Dassault Systémes 2010]. Experimental results from mechanical testing of headed anchor bolts are rather few in the open literature. Available results from testing of single cast-in headed anchor bolts in non-reinforced and reinforced concrete blocks are utilized for validation of used numerical approach and modelling of the concrete material. A number of different parameters influencing the capacity of single anchors and anchor groups in concrete structures are investigated.

Parameters of interest are effective embedment depth of anchor, thickness and width of concrete structure, spacing of anchors in anchor group, amount and type of reinforcement, compressive strength of concrete, fracture energy of concrete, concrete constitutive model as well as mesh size and type of boundary conditions in finite element models. Other issues of interest are the interaction of local stress field in the vicinity of the anchor and global stress field in the concrete structure, the possibility to transmit mechanical loads from the embedded anchors to the concrete and its reinforcement and how to perform rational modelling and analysis of mechanically loaded anchors in concrete structures.

2. General about concrete

Concrete is the most used material in buildings and civil structures. The main advantages are low cost, high flexibility in the shaping of the structure and good capacity to resist fire.

Concrete is a complex material produced by mixing cement, water and aggregate. The aggregate consists of a mixture of sand, gravel and crushed stone. Immediately after the mixing, the material is plastic without compressive or tensile strength. The concrete is then poured into a formwork. Shortly after mixing, the stiffness and strength start to increase as a result of the chemical reaction between cement and water. This hardening of the concrete is called curing.

Concrete is a brittle material, strong in compression but very weak in tension. In compression the load is carried by the aggregate. However, in tension the cement between the aggregate will crack at rather low tensile stresses. Because of the low tensile strength, concrete is in most structures used in combination with steel reinforcement where the concrete carries the compressive loads and the reinforcement carries the tensile loads.

The stiffness and strength of concrete depends on the mix of the ingredients. A high ratio between water and cement leads to lower strength. On the other hand, a high ratio leads to a more liquid and workable concrete that is easier to cast and vibrate. The stiffness of concrete also depends on the duration of the load applied to it. For very short-term loads the stiffness is significantly higher than for long-term loads such as dead weight.

The reaction between water and cement is exothermic and leads to heating of the concrete. As a result of the heating, the concrete will expand. Later when the chemical reaction is slowing down, the concrete will start to cool and contract. In addition, the drying of the concrete during hardening will make the concrete shrink. In many cases the expansion and contraction is constrained by ground or adjacent structural members. This can result in significant internal stresses and cracking.

The most common way to describe the strength properties of concrete is to classify it in different strength classes. In the Eurocodes, concrete in classified based on the characteristic (5% fractile) compressive cylinder strength (f_{ck}) or cube strength ($f_{ck,cube}$) at the age of 28 days. The name of each class is based on these strengths e.g. C40/50 is the name of the strength class with f_{ck} = 40 MPa and $f_{ck,cube}$ = 50 MPa.

3. Size effect and fracture mechanics

Practical experiences from concrete structures indicate that the load-carrying capacity does not increase linearly with size but somewhat slower. This phenomenon is called the size effect. Traditionally, the size effect in failure of concrete structures has been explained by Weibull's statistical theory [Weibull 1939]. According to this theory, failure is determined by the minimum value of the strength of the material. The implication of the statistical size effect is that the larger the structure is, the smaller the minimum value of the strength is. This explanation of the size effect is valid for a one-dimensional structure (weakest link of a chain). However, for a structure with three dimensions, this description cannot fully explain experiences from the response of concrete structures.

In the mid-eighties, Bazant suggested a new approach for explaining the size effect in concrete structures [Bazant 1984]. The basis for his concept is the characteristics of concrete as a quasi-brittle material. In a quasi-brittle material with an initial crack, stress and strain redistributions take place in the fracture process zone as a result of material softening. This means that the stress peak moves across the failure zone, leaving a reduced stress in its wake, see figure 3-1. Type of structure, structure size and type of quasi-brittle material influence the stress and strain field in the fracture process zone. A structure made of a quasi-brittle material is characterised by its ability to develop large fractures in a stable manner prior to failure.

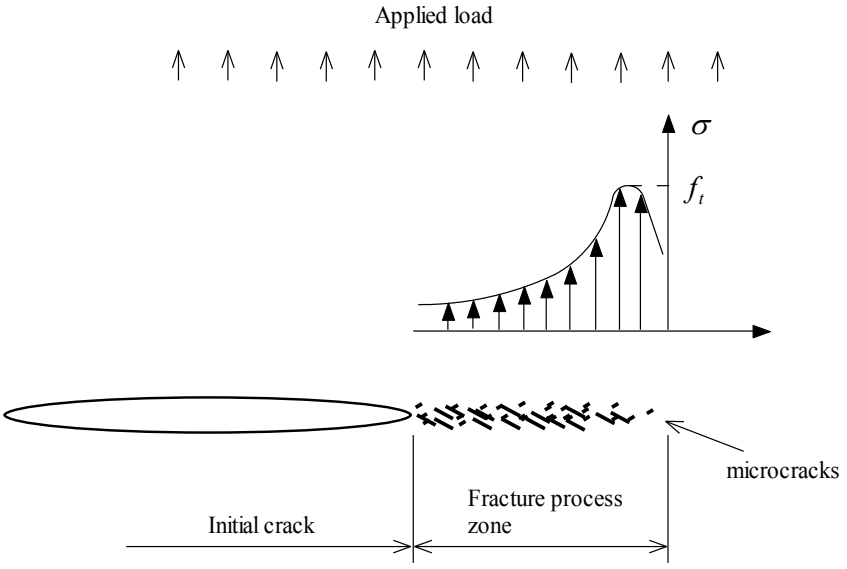

Figure 3-1: Stress field in the fracture process zone ahead of an initial crack in a quasi-brittle material such as concrete.

The relative size of the fracture process zone decreases with increasing size of the concrete structure. For a larger structure, this means that a larger volume fraction will respond elastically. In quasi-brittle failure that is preceded by large, stable growth of localised fracture or distributed cracking damage, the size effect mainly is caused by stress redistribution and localisation of cracking damage associated with

the release of energy stored in the structure. In a larger structure, more strain energy is available to drive the propagation of the failure zone, see figure 3-2.

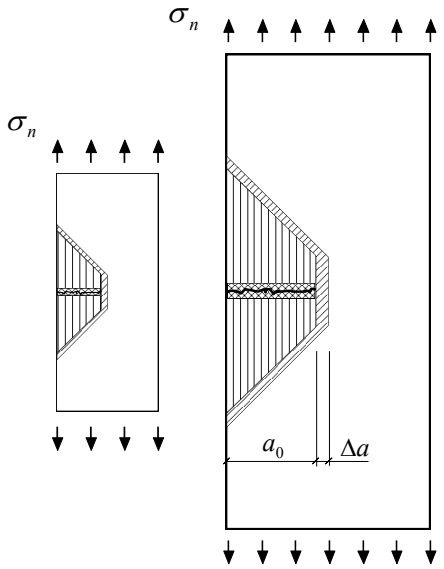

Figure 3-2: More strain energy is available to drive the propagation of the failure zone in a larger structure.

For very large structures, the fracture process zone can be regarded as infinitesimally small and the entire volume of the structure remains elastic. This means that linear elastic fracture mechanics can describe the fracture process. As the size of the structure is reduced, linear elastic fracture mechanics can no longer describe the fracture process and the size of the fracture process zone cannot be regarded as infinitesimally small. For specimens of practical size, the methodology of nonlinear fracture mechanics is needed to describe the fracture process.

In ACI 349 from 1978 [ACI 349-76 1978], the size effect according to Bazant was not considered and the ultimate load for an anchor in tension was expressed as

$$N_u = a \cdot \sqrt{f_c} \cdot h_{ef}^2 \qquad \text{(Eq. 3-1)}$$

where a is a constant, f_c is the concrete compressive strength and h_{ef} is the anchor embedment depth. It was assumed that the capacity of the anchor was directly related to the fracture surface of the concrete breakout cone. In ACI 349 of today [ACI 349-06 2006] and other codes for calculation of the capacity of anchors in tension, the size effect is considered and equation 3-1 is rewritten as

$$N_u = a \cdot \sqrt{f_c} \cdot h_{ef}^{1.5} \qquad \text{(Eq. 3-2)}$$

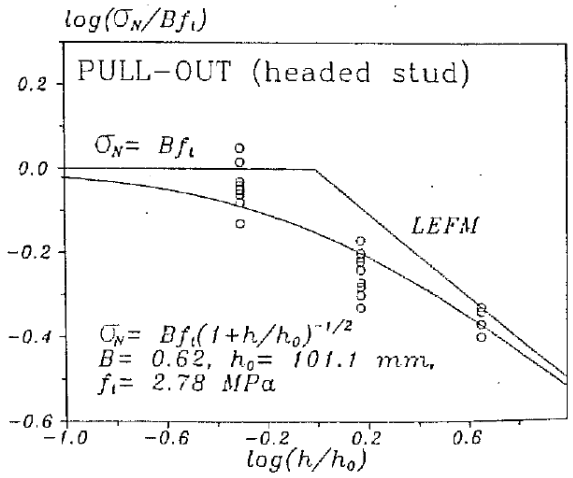

Figure 3-3 Size effect of the average tensile stress over the failure cone area [Eligehausen et al. 1992].

Figure 3-3 shows the average tensile stress over the failure cone area of a single anchor loaded in tension as a function of normalized embedment depth. The curved line represents equation 3-2. As the normalized embedment depth increases, i.e. the size of the structure increases, linear elastic fracture mechanics (LEFM) can be applied to describe the response.

4. Constitutive concrete material models in Abaqus

There are three constitutive models available in Abaqus for modelling mechanical response of concrete. The two most commonly used are described in this section.

4.1. Concrete damaged plasticity model

The concrete damaged plasticity model (CDP) is based on work carried out by [Lee et al. 1998] and [Lubliner et al. 1989] and is available in both the implicit and the explicit integration solver (Abaqus/Standard and Abaqus/Explicit). The CDP model uses the concept of isotropic damaged elasticity in combination with isotropic tensile and compressive plasticity to represent the inelastic behaviour of concrete. The model consists of the combination of non-associated multi-hardening plasticity and scalar (isotropic) damaged elasticity to describe the irreversible damage that occurs during the fracturing process. The model allows the definition of strain hardening in compression and can be defined to be sensitive to the straining rate, which resembles the behaviour of concrete more realistically.

The CDP model is applicable for applications in which concrete is subject to monotonic loading, cyclic loading with alternating tension compression loading, and/or dynamic loading. The model allows stiffness recovery during cyclic loading reversals. Under uniaxial tension the stress-strain response follows a linear elastic relationship until the value of the failure stress is reached. Beyond the failure stress the formation of micro-cracks is represented macroscopically with a softening stress-strain response, which induces strain localization in the concrete structure. Under uniaxial compression the response is linear until the value of initial yield. In the plastic regime the response is typically characterized by stress hardening followed by strain softening beyond the ultimate stress. Figure 4-1 illustrates the proceeding of a loading cycle starting in tension passing to compression.

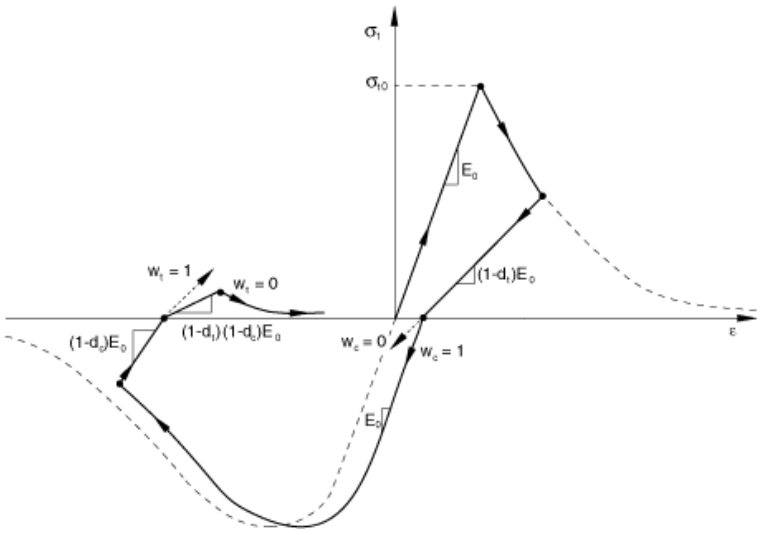

Figure 4-1: Uniaxial load cycle of the concrete damaged plasticity model [Dassault Systémes 2010].

When the concrete specimen is unloaded from any point on the strain softening branch of the stress-strain curve, the unloading response is weakened, i.e. the elastic stiffness of the material appears to be damaged (or degraded).

The material parameters needed to define the CDP model are described in chapter 5. The CDP model provides a general capability for modelling concrete materials in all types of structure elements, e.g. beams, trusses, shells, and solids.

4.2. Brittle cracking model

The brittle cracking material model is based on the work by [Hillerborg et al. 1976] and is only available in the explicit integration solver (Abaqus/Explicit). The concrete model has a linear elastic behaviour in compression as well as up to the concrete tensile strength in tension. For stresses exceeding the concrete tensile strength, cracked concrete behaviour is assumed. The brittle cracking model is hence designed for cases where the overall material behaviour is dominated by tensile cracking.

The brittle cracking model does not track individual cracks. Instead the effect of cracks enters into analysis by the way in which the cracks affect the structural stiffness. The fracture energy required to form a unit area of crack surface is used to decide if the crack will propagate in the structure. Cracking is irrecoverable in the sense that once a crack has developed it remains throughout the rest of the calculation. However, crack closing and reopening may take place along the directions of the crack surface normal. A benefit of the brittle cracking model in Abaqus is that the crack orientation is considered.

The material parameters needed to define the brittle cracking material model is the modulus of elasticity E, tensile strength f_{ct} and fracture energy G_f. Even if the model does not describe compressive failure the compressive strength f_c is also needed to verify that compressive stresses are acceptable. The reduced shear stiffness in cracked concrete is in the brittle cracking material model described by a “shear retention factor”, which is implemented as reduction of the shear modulus in elements exceeding the crack strain. The brittle cracking model may be used for modelling concrete material in all types of structure elements, e.g. beams, trusses, shells and solids provided that the dominating response is tensile cracking.

5. Determination of constants in constitutive models

5.1. General

The numerical simulations presented within this report are performed with the Abaqus material model named concrete damaged plasticity (CDP). This chapter reflects general implementation of values necessary for defining the CDP material model.

5.2. Determination of constants in CDP-model

The different parameters that need to be specified when using the CDP model are stated in table 5-1.

Table 5-1: Concrete damaged plasticity parameters.

Parameter	Description	Default value
ψ	Dilation angle	User defined
ϵ	Flow potential eccentricity	0.1
σ_{b0}/σ_{c0}	Ratio of initial equibiaxial compressive yield stress to initial uniaxial compressive yield stress	1.16
K_c	Ratio of the second stress invariant on the tensile meridian to that on the compressive meridian at initial yield for any given value of the pressure invariant such that the maximum principal stress is negative	0.6667
μ	Viscosity parameter	0.0 in Abaqus/Standard N/A in Abaqus/Explicit

The CDP model assumes non-associated potential plastic flow in which the Drucker-Prager hyperbolic function describes the flow potential G [Dassault Systémes 2010].

$$G = \sqrt{(\epsilon \cdot \sigma_{t0} \cdot tan\psi)^2 + \bar{q}^2} - \bar{p} \cdot tan\psi \qquad \text{(Eq. 5-1)}$$

In equation 5-1, $\bar{q}$ denotes effective Mises stress and $\bar{p}$ the effective stress caused by hydrostatic pressure. The dilation angle ψ is measured in the p-q plane at high confining pressure and indicates the ratio between the volume change and the shear strain. The dilation angle value for concrete is commonly specified in the range of 30° to 40°. The flow potential eccentricity ϵ defines the rate at which the function approaches the asymptote. With the default value of $\epsilon = 0.1$ the dilation angle is almost the same over a wide range of confining pressure stress values. The uniaxial failure tensile stress σ_{t0} is via the tension stiffening definition specified by the user [Dassault Systémes 2010].

The third and fourth parameter stated in table 5-1 is included in the yield function used in the CDP model, which in terms of effective stresses has the form:

$$F = \frac{1}{1-\alpha}(\bar{q} - 3\alpha\bar{p} + \beta(\tilde{\varepsilon}^{pl})\langle\hat{\bar{\sigma}}_{max}\rangle - \gamma\langle-\hat{\bar{\sigma}}_{max}\rangle) - \bar{\sigma}_c(\tilde{\varepsilon}_c^{pl}) = 0$$

With

$$\alpha = \frac{(\sigma_{b0}/\sigma_{c0})-1}{2(\sigma_{b0}/\sigma_{c0})-1}$$

$$\beta = \frac{\bar{\sigma}_c(\tilde{\varepsilon}_c^{pl})}{\bar{\sigma}_t(\tilde{\varepsilon}_t^{pl})}(1-\alpha) - (1+\alpha)$$

$$\gamma = \frac{3(1-K_c)}{2K_c-1}$$

In the numerical simulations presented in current report the default values presented in table 5-1 of both these parameters (σ_{b0}/σ_{c0} and K_c) have been used. Also since the analyses have been performed with the Abaqus/Explicit solver the viscosity parameter μ is not used.

Besides the parameters stated in table 5-1, the fundamental material parameters need to be defined. That is, modulus of elasticity E, density ρ and Poisson's ratio υ. If temperature analyses are to be performed, the thermal conductivity also needs to be specified.

5.2.1. Behaviour in compression

The concrete material behaviour in compression outside of the elastic regime is defined by the relation of yield stress σ_{c0} and inelastic strain $\tilde{\varepsilon}_c^{in}$. The inelastic strain is defined as the total strain minus the elastic strain corresponding to the undamaged material, see equation 5-2 and figure 5-1 [Dassault Systémes 2010].

$$\tilde{\varepsilon}_c^{in} = \varepsilon_c - \varepsilon_{0c}^{el} \qquad \text{(Eq. 5-2)}$$

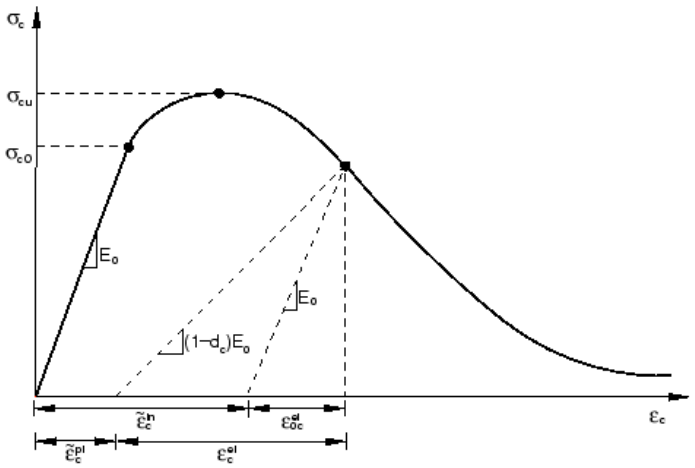

Figure 5-1: Definition of the compressive inelastic strain.

The uniaxial initial yield stress value σ_{c0} is according to [Boverket 2004] defined as 60 % of the ultimate compressive stress σ_{cu}. Corresponding strain is then calculated according to Hookes law, i.e. $\varepsilon_{0c}^{el} = \frac{\sigma_{c0}}{E_0}$ and the maximum strain is taken as $\varepsilon_{max} = \varepsilon_{0c}^{el} \cdot 20$. The inelastic stress curve is thenceforth defined according to [Lubliner et al. 1989] in the following manner:

$$\sigma_c = \sigma_{c0}\left[(1+a)\cdot e^{-b\cdot\tilde{\varepsilon}_c^{pl}} - a\cdot e^{-2\cdot b\cdot\tilde{\varepsilon}_c^{pl}}\right] \qquad \text{(Eq. 5-3)}$$

With:

$$a = 2\cdot\frac{f_{cm}}{\sigma_{c0}} - 1 + 2\sqrt{\left(\frac{f_{cm}}{\sigma_{c0}}\right)^2 - \frac{f_{cm}}{\sigma_{c0}}} \qquad \text{(Eq. 5-4)}$$

$$b = \frac{\left(\frac{d\sigma}{d\tilde{\varepsilon}_c^{pl}}\right)}{\sigma_{c0}(a-1)} \qquad \text{(Eq. 5-5)}$$

The numerator in equation 5-5 describes the inclination of the curve at the initial yield stress value.

5.2.2. Behaviour in tension

In general when using the CDP material model, the concrete behaviour in tension is defined as the relation between postfailure stress and either of cracking strain $\tilde{\varepsilon}_t^{ck}$, cracking displacement u_t^{ck} or fracture energy G_f. In the work carried out within current report the tension behaviour is given as relation between postfailure stress and cracking displacement as seen in figure 5-2. This is due to the fact that non-reinforced structures are unreasonable mesh sensitive when using the cracking strain definition.

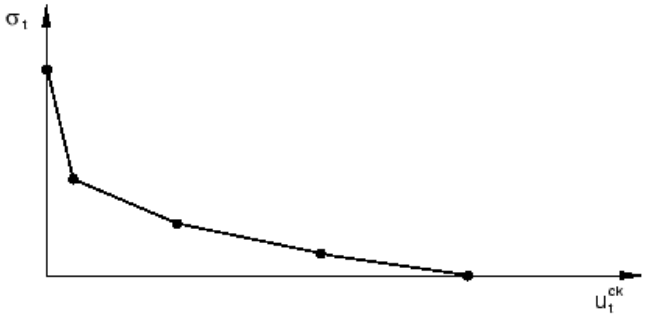

Figure 5-2: Stress displacement relation after tensile failure [Dassault Systémes 2010].

The relation between the postfailure stress and the cracking displacement has been calculated according to [Cornelissen et al. 1986] in the following manner:

$$\frac{\sigma_t}{f_{ctm}} = f(u_t^{ck}) - \frac{u_t^{ck}}{u_{t0}^{ck}}\cdot f(u_t^{ck} = u_{t0}^{ck}) \qquad \text{(Eq. 5-6)}$$

Where:

$$f(u_t^{ck}) = \left(1 + \left(\frac{C_1\cdot u_t^{ck}}{u_{t0}^{ck}}\right)^3\right)\cdot e^{-C_2\cdot u_t^{ck}/u_{t0}^{ck}} \qquad \text{(Eq. 5-7)}$$

For a normalweight concrete the constants C_1 and C_2 given in equation 5-7 are 3 and 6.93 respectively. The concrete fracture energy is defined as the area underneath the

graph seen in figure 5-2. The cracking displacement at which complete loss of strength takes place u_{t0}^{ck}, may be determined by first establish a reasonable concrete fracture energy G_F and then integrate the combined expression of equation 5-6 and 5-7. For a normalweight concrete this gives following relation

$$u_{t0}^{ck} = \frac{G_F}{0.195 \cdot f_{ctm}}$$

When using the CDP material model, the damage caused by strains is measured with a damage tension parameter denoted "concrete tension damage" d_t. The parameter may be visualized during post processing and indicates the status of the concrete after cracking has occurred, i.e. grade of impaired stiffness. In the work carried out within this report the concrete tension damage is linearly defined with a maximum of 0.9. This means that an element gets inactive when the cracking displacement u_{t0}^{ck} is reached and at this point the damage tension parameter has the value of 0.9.

6. Anchors loaded in tension

6.1. General

For an anchor in tension, the concrete in the vicinity of the anchor is subjected to both a global stress field as a result of global deformation of the structure and a local stress field caused by interaction between the anchor and the concrete. The global stress field caused by the transverse tension load is for most concrete structures dominated by global bending stresses. These bending stresses are tensile at the face where the anchor is located. The local stress field caused by the anchor-concrete interaction is thus located in a global stress field that is in tension. As the concrete strength is strongly limited in tension, the global stress field in the vicinity of the anchor can be detrimental for the tension breakout capacity.

Global bending of a concrete structure caused by a transverse load is influenced by a number of different parameters. In general, the curvature of the concrete structure increases linearly with load level, decreases with the square of the thickness, increases with the square of the structure width, decreases with stiffness in boundary conditions of the structure and decreases with the amount of reinforcement. Corresponding global bending stresses in the concrete are directly related to the curvature of the concrete structure. These bending stresses are essential in determining the concrete breakout strength.

Presence of reinforcement in the vicinity of the anchor also has a local impact on the anchor behaviour and anchor capacity. If potential concrete failure surfaces are crossed by reinforcement, the potential concrete failure prism can be tied to the concrete structure and the concrete breakout strength can increase. If the reinforcement loaded in tension starts to yield in the anchor region, however, increased concrete cracking can result in reduced anchor capacity.

As the character of the concrete material is strongly nonlinear, determination of the concrete breakout capacity is best done either by testing or numerical simulation. The presence of reinforcement complicates the response of the anchor in tension even more and necessitates one of these two methods in determining its capacity. In the following, the possibility with the numerical approach is investigated.

Cracks in the concrete reduce the anchor capacity. In the following simulations of anchors in tension, it is assumed that the concrete structure is without initial cracks if not otherwise stated.

6.2. Physical tests of single anchors in tension

6.2.1. Single anchor in non-reinforced concrete slab

The concrete cone capacity of headed anchor bolts in non-reinforced and non-cracked concrete slabs was experimentally investigated [Eligehausen et al. 1992]. Both square specimens (small and medium sizes of series I to III) and octagon specimens (all other specimens) were tested. Three different embedment depths (h_{ef} = 50, 150 and 450 mm) and three different sizes of non-reinforced concrete slabs (small, medium and large) were tested, see figure 6-1 and table 6-1.

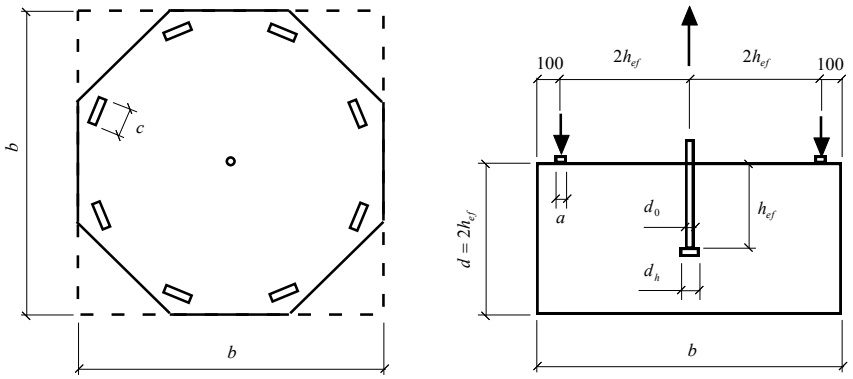

Figure 6-1: Geometry of test specimen [Eligehausen et al. 1992].

Table 6-1: Dimension of anchor, specimen and support in mm [Eligehausen et al. 1992].

Size	Anchor			Specimen		Support	
	h_{ef}	d_0	d_h	*b*	*d*	*a*	*c*
Small	50	8	12.7	400	100	10	40
Medium	150	24	32.9	800	300	30	100
Large	450	72	88.5	2000	900	100	180

In order to avoid splitting failure, the specimens of series I to III were reinforced by an orthogonal ribbed reinforcement placed near the top surface and anchored by hooks. In series IV to VI, the specimens were constrained by a welded orthogonal steel frame which was placed around the top of the specimens. The concrete breakout cones were in no case intersected by reinforcement. The concrete had an average compressive cube strength of $f_{cm,cube} = 31.3$ MPa. The tension load was applied under displacement control. Measured failure loads are given in table 6-2.

Table 6-2: Failure loads N_u and normalized failure loads $N_u^{norm} = N_u \cdot \sqrt{31.3/f_{c,cube}}$ of anchors. Results given in italic font correspond to square specimens while results given in normal font correspond to octagon specimens [Eligehausen et al. 1992].

Series	$f_{c,cube}$	N_u [kN] for h_{ef} in [mm]			N_u^{norm} [kN] for h_{ef} in [mm]		
	MPa	50	150	450	50	150	450
I	32.6	*25.8*	*150.0*	1087	*25.3*	*147.0*	1065
II	29.7	-	*161.7*	1108	-	*166.0*	1137
III	33.2	*35.6*	*131.4*	1162	*34.6*	*127.6*	1128
IV	29.3	27.2	133.3	937.2	28.1	137.8	968.7
		26.1	181.7		27.0	187.8	
V	28.3	21.5	160.7	989.0	22.6	169.0	1040
		30.2	165.7		31.8	174.3	
VI	34.4	29.3	151.5	1221	27.9	144.5	1165
		33.2	167.7		31.6	160.0	
		29.6			28.2		
		35.6			33.9		
Average	31.3	29.4	156.0	1084	29.1	157.1	1084

6.2.2. Single anchor in reinforced concrete slab

In order to investigate the effect of surface reinforcement on the capacity of cast-in headed anchor bolts in tension, a number of tests with different configuration of the concrete slab was conducted [Nilsson and Elfgren 2009]. As anchor bolt, a threaded rod with diameter Ø30 mm and an end nut with diameter Ø45 were used. Embedment depth was 220 mm in all tests and the dimension of the concrete slab varied from 1.2x1.2x0.3 m up to 2.2x2.2x0.6 m. The amount of reinforcement was varied from no reinforcement to Ø16cc100. The depth of the concrete cover was 30 mm. A support ring with a diameter almost as large as the width of the slab was put on top of the slab in order to apply tension load on the anchor bolt. Figure 6-2 shows the test setup schematically where reaction forces between the slab and the support ring as well as the tension load on the anchor bolt are shown.

A concrete quality C25/30 was used in manufacturing the concrete tests slabs. In total, 66 tests were conducted.

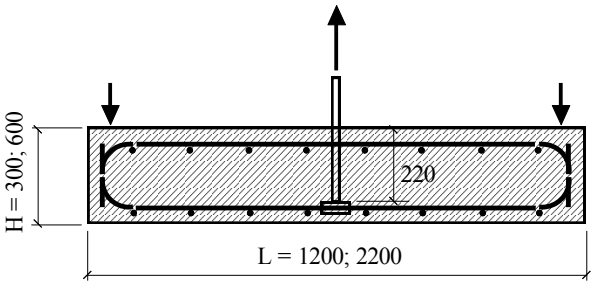

Figure 6-2: Concrete slab with cast-in threaded rod and nut, top and bottom reinforcement. Reaction forces at the top of the concrete slab indicate location of support ring [Nilsson and Elfgren 2009].

The geometry of the slab, the amount of reinforcement and the pre-crack width are given in table 6-3. The pre-crack was introduced by bending the slab in three-point-bend. The width of the pre-crack was kept by spacers that were put in the pre-crack intersecting the anchor bolt. Table 6-3 also gives the averaged maximum tension load $\bar{P}_{test}$ for each test configuration and corresponding averaged displacement $\bar{\delta}_{test}$ at maximum tension load.

Table 6-3: Summary of test data and test results for the different configurations. *L* is the width and *H* is the thickness of the slab, $\bar{N}_{u,test}$ is the averaged failure load, and $\bar{\delta}_{test}$ is the averaged displacement at maximum tension load. The amount of top reinforcement and width of the pre-crack are also given. For further information see [Nilsson and Elfgren 2009].

No.	*L* [m]	*H* [m]	Top rein-forcement	Pre-crack [mm]	$\bar{N}_{u,test}$ [kN]	$\bar{\delta}_{test}$ [mm]
1	1.2	0.3	-	0	196	10.4
2	1.2	0.3	Ø12cc300	0	280	9.2
3	1.2	0.3	Ø16cc150	0	319	7.6
4	1.2	0.3	Ø16cc100	0	317	2.4
5	1.2	0.6	Ø12cc300	0	357	9.6
6	2.2	0.3	Ø12cc400	0	241	8.8
7	2.2	0.3	Ø12cc150	0	262	8.0
8	2.2	0.6	Ø12cc150	0	327	8.7
9	1.2	0.3	-	0.5	144	9.5
10	1.2	0.3	Ø12cc300	0.5	292	9.2
11	1.2	0.3	Ø16cc150	0.5	303	6.7
12	1.2	0.3	Ø16cc100	0.5	256	2.1
13	2.2	0.3	Ø12cc500	0.5	217	6.8

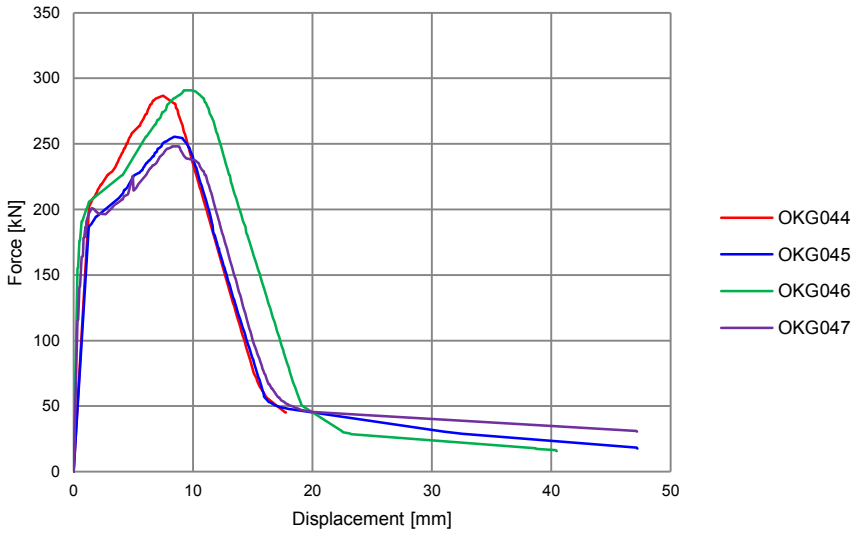

Figure 6-3: Force-displacement curves for tests conducted on configuration 2 test specimens [Nilsson and Elfgren 2009].

In the test, the tension load on the anchor bolt was applied by moving the upper part of the anchor bolt relative to the top surface of the concrete slab at a constant displacement rate. The tension force and the relative displacement are measured during the test. As an example, force-displacement curves for configuration 2 test specimens are shown in figure 6-3. Up to a force of about 190 kN, the overall structural response is essentially elastic for the specimens. Thereafter an inelastic behaviour is seen and the curves start to deviate from each other. At a displacement of about 9 mm maximum load is reached, see figure 6-3.

Table 6-4: Comparison of failure loads for non-cracked and pre-cracked concrete slabs with different amount of reinforcement. Data is taken from [Nilsson and Elfgren 2009].

No. in table 6-3	Top reinforcement	$\bar{N}_{u,test}$ [kN]		Ratio
		No pre-crack	Pre-crack 0.5 mm	
1, 9	-	196	144	1.36
2, 10	ø12cc300	280	292	0.96
3, 11	ø16cc150	319	303	1.05
4, 12	ø16cc100	317	256	1.24

In table 6-4, failure loads for non-cracked and pre-cracked concrete slabs with different amount of reinforcement are compared. For the non-reinforced slabs, the failure load is a factor 1.36 higher for that without pre-crack. This corresponds rather well with CEN/TS 1992-4-2 section 6.2.5.1 [CEN/TS 1992-4-2 2009] where corresponding ratio is 11.9/8.5=1.4. For the slabs with reinforcement amount ø12cc300 and ø16cc150, the failure load ratio is close to 1. For these slabs, a pre-crack of 0.5 mm does not seem to significantly influence the concrete breakout failure load. One explanation might be that the confinement remains in the anchor bolt region as a result of existing reinforcement. The higher failure load for the pre-cracked than for the non-cracked ø12cc300 specimens is in [Nilsson and Elfgren 2009] explained by natural variations in the concrete properties. As the amount of reinforcement is further increased to ø16cc100, the ratio again deviates from 1 and pre-cracking reduces the failure load. This is a somewhat unexpected result. One explanation might be an effect of how the pre-crack was introduced by three-point-bending as discussed in [Nilsson and Elfgren 2009]. As the amount of reinforcement was increased, the load used in three-point-bending was also increased. This loading might have had a detrimental impact on the concrete in the vicinity of the anchor bolt.

6.3. Numerical simulations of single anchor in tension

Numerical simulations of physical tests are of importance in validating the numerical approach. In the following two sections, tests of single anchor in non-reinforced and in reinforced concrete slabs are simulated. The concrete damaged plasticity model described in chapter 4 and 5 together with the Abaqus/Explicit solver is utilized in the simulations. Modelling is done with solid element C3D8R with reduced integration. Beam element B31 is used for modelling the rebars. Elastic response is assumed for steel material in the models. This assumption has been checked after all simulations and found correct.

The simulations presented in this chapter were preceded by a parametric study where the influence of a number of parameters was investigated. Part of this parametric study is discussed in this chapter and in the following chapter 7.

6.3.1. Single anchor in non-reinforced concrete slab

The physical tests described in section 6.2.1 are numerically simulated. Figure 6-4 shows one of the finite element models used. In the simulation, the concrete specimen is restricted to move in the vertical direction at the red marked nodes corresponding to the location of the support in the experiment. Due to symmetry, one fourth of the specimen is modelled and symmetric boundary conditions are utilized. In order to avoid splitting failure, a steel frame is modelled around the top of the specimen in accordance with the testing. Tension load is applied by moving the upper part of the headed bolt in the vertical direction at a constant displacement rate of 30 mm/s. Element size in the vicinity of the anchor bolt is about 10 mm. The material parameters used in the simulation are shown in table 6-5. The concrete compressive strength is measured on cubes with an average value of $f_{cm,cube} = 31.3$ MPa [Eligehausen et al. 1992]. For the numerical analyses, the cube compressive strength is converted to cylindrical compressive strength according to $f_{cm} = 0.76 \cdot f_{cm,cube} = 23.8$ MPa [Betonghandbok- Material 2008].

Table 6-5: Concrete material parameters utilized in the analyses.

Parameter	Description	Value (20 °C)
Ψ	Dilation angle	35 degrees
ε	Flow potential eccentricity	0.1 (default value)
σ_{b0}/σ_{c0}	Ratio of initial equibiaxial compressive yield stress to initial uniaxial compressive yield stress	1.16 (default value)
K_c	Ratio of the second stress invariant on the tensile meridian to that on the compressive meridian at initial yield for any given value of the pressure invariant such that the maximum principal stress is negative	0.667 (default value)
E	Modulus of elasticity	31.0 GPa
σ_{cu}	Ultimate compressive stress	23.8 MPa
σ_{t0}	Failure tensile stress	2.38 MPa
ν	Poisson's ratio	0.2
ρ	Density	2400 kg/m^3

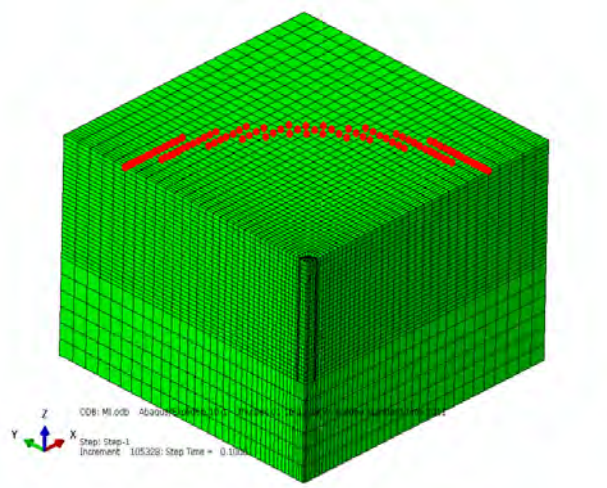

Figure 6-4: Finite element model for simulation of anchor in tension. Due to symmetry, one fourth of the specimen is modelled.

For comparison with a design code, the concrete breakout failure load is predicted for non-cracked concrete based on [CEN/TS 1992-4-2 2009]. According to CEN/TS, the characteristic resistance load $N^0_{Rk,c}$ given in N is calculated as

$$N^0_{Rk,c} = 11.9 \cdot \sqrt{f_{ck,cube}} \cdot h_{ef}^{1.5} \qquad \text{(Eq. 6-1)}$$

where $f_{ck,cube}$ is the characteristic cube strength of the concrete strength class given in MPa and h_{ef} is the embedment depth given in mm. The characteristic resistance load $N^0_{Rk,c}$ in CEN/TS corresponds to the 5% fractile of the physical resistance load why the value calculated with equation 6-1 has to be multiplied with 1.33 to get the mean value before it is compared with simulated and tested failure loads. Furthermore, the characteristic compressive cube strength $f_{ck,cube}$ in equation 6-1 is replaced by the mean compressive cube strength $f_{cm,cube}$ for the comparison. The predicted failure load based on CEN/TS is designated $N_{u,CEN/TS}$.

In table 6-6 and figure 6-5, failure loads from testing described in section 6.2.1 [Eligehausen et al. 1992], simulations and predictions based on CEN/TS are compared. A concrete compressive strength of $f_{cm,cube} = 31.3$ MPa is used in equation 6-1. For $h_{ef} = 50$ mm, the failure load is similar for the three approaches. As the embedment depth increases, simulation predicts somewhat higher values than the other two. For $h_{ef} = 450$ mm, the prediction based on CEN/TS results in a lower failure load than testing and simulation. An explanation for this deviation might be that equation 6-1 cannot fully capture the mechanics of anchor bolts in tension for larger embedment depths.

Table 6-6: Comparison of failure loads from testing in section 6.2.1 [Eligehausen et al. 1992], simulations and predictions based on [CEN/TS 1992-4-2 2009].

h_{ef} (mm)	$\bar{N}_u^{norm}$ (kN) [Eligehausen et al. 1992]	$N_{u,simulation}$ (kN)	$N_{u,CEN/TS}$ (kN)
50	29.1	30	31.3
150	157.1	190	162.7
450	1084	1190	845.3

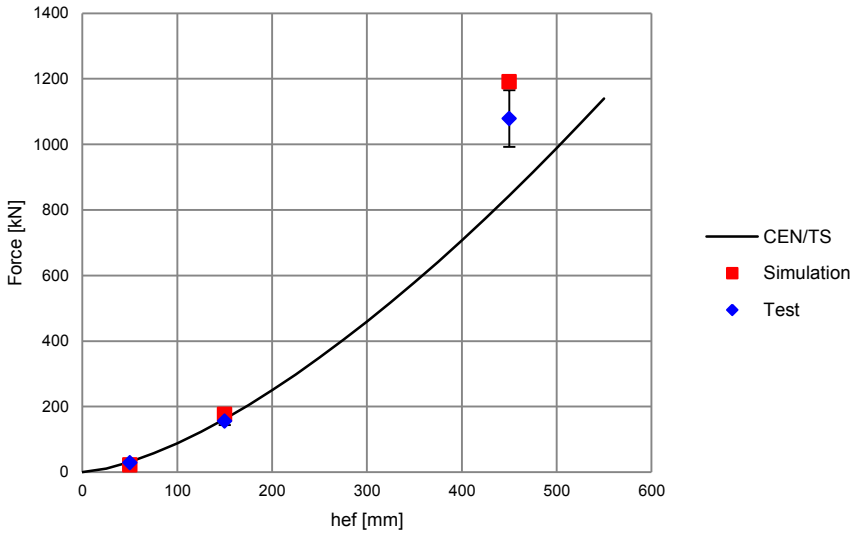

Figure 6-5: Failure load as a function of embedment depth for headed anchor bolts in non-reinforced non-cracked concrete slabs.

The results of this section show that the numerical approach used rather well can predict the failure load of tested headed anchor bolts subjected to tension in non-reinforced concrete. The global stiffness of the concrete structure has not been discussed so far. The present test specimens must be regarded as relatively stiff. This means that concrete cone breakout controls the failure. In the following sections, the effect of reducing the global stiffness will be investigated.

6.3.2. Single anchor in reinforced concrete slab

The physical tests of single anchors in reinforced concrete slabs summarised in section 6.2.2 are numerically simulated. One of the finite element models used is shown in figure 6-6 and 6-7. Due to symmetry, one fourth of the specimen is modelled and symmetric boundary conditions are utilized. The support ring is modelled and contact conditions are introduced between the concrete slab and the support ring. Pre-cracked specimens are modelled in a simplistic way. For these specimens, the upper half of the concrete slab along one symmetry plane is free to move perpendicular to the pre-crack. The reinforcement perpendicular to the pre-crack can still carry load. Element size in the vicinity of the anchor bolt is about 10 mm. Tension load is applied by moving the upper part of the headed bolt in the vertical direction at a constant displacement rate of 30 mm/s. The material parameters used in the simulations are given in table 6-7.

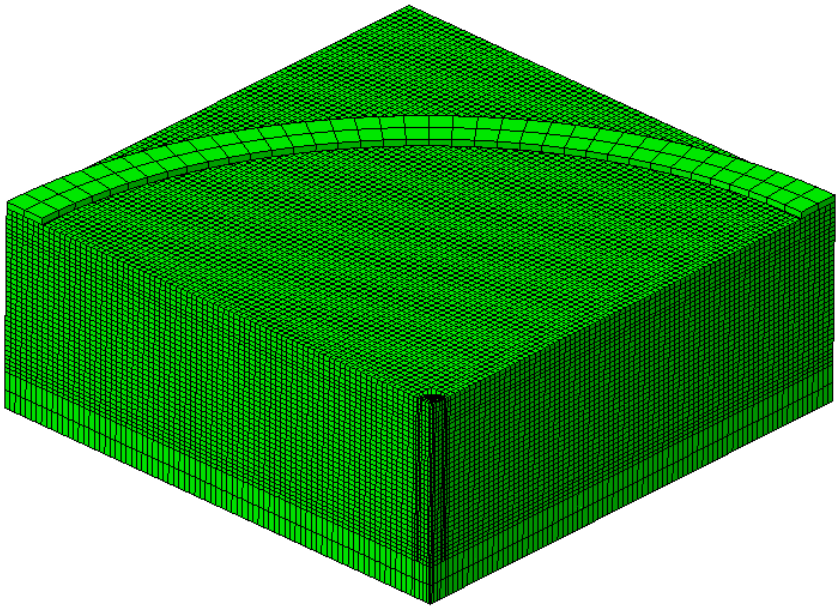

Figure 6-6: Finite element model used for simulation of single anchor in reinforced concrete. One fourth of the test specimen is modelled due to symmetry.

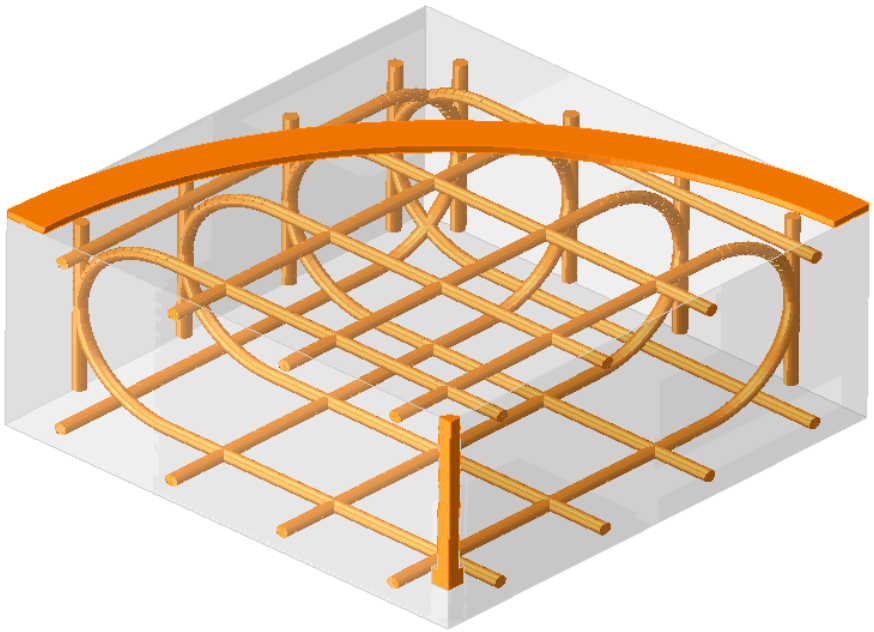

Figure 6-7: Transparent perspective view of the different parts constituting the reinforced concrete model.

Table 6-7: Concrete damage plasticity parameters utilized in analyses.

Parameter	Description	Value (20 °C)
Ψ	Dilation angle	35 degrees
ε	Flow potential eccentricity	0.1 (default value)
σ_{b0}/σ_{c0}	Ratio of initial equibiaxial compressive yield stress to initial uniaxial compressive yield stress	1.16 (default value)
K_c	Ratio of the second stress invariant on the tensile meridian to that on the compressive meridian at initial yield for any given value of the pressure invariant such that the maximum principal stress is negative	0.667 (default value)
E	Modulus of elasticity	31.0 GPa
σ_{cu}	Ultimate compressive stress	25.0 MPa
σ_{t0}	Failure tensile stress	2.46 MPa
ν	Poisson's ratio	0.2
ρ	Density	2400 kg/m^3

Table 6-8: Steel material values used in analyses.

Symbol	Description	Value (20°C)
E	Modulus of elasticity	200.0 GPa
ν	Poisson's ratio	0.3
ρ	Density	7850 kg/m^3

In figure 6-8 and table 6-9 a summary of results from physical tests and corresponding numerical results are shown for all configurations investigated, see table 6-3 and [Nilsson and Elfgren 2009].

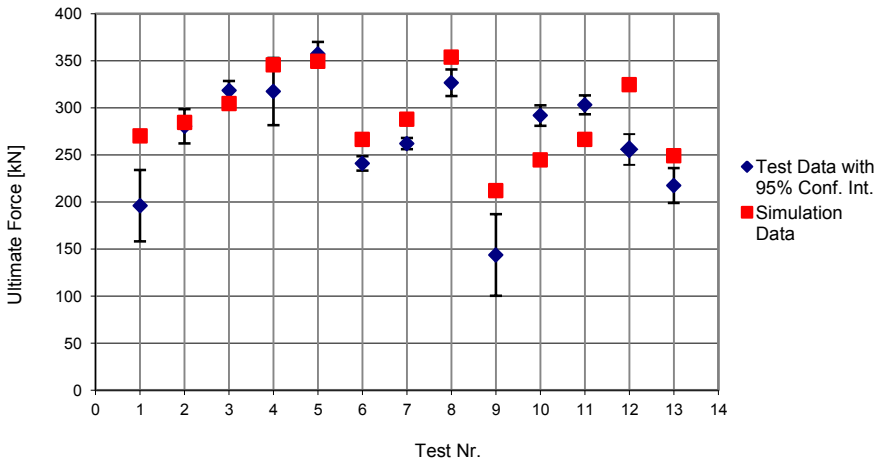

Figure 6-8: Summary of failure loads from physical tests [Nilsson and Elfgren 2009] and corresponding simulation results.

Table 6-9: Summary of results from physical tests [Nilsson and Elfgren 2009] and corresponding simulation results.

No.	*L* [m]	*H* [m]	Top reinforce-ment	Pre-crack [mm]	$\bar{N}_{u,test}$ [kN]	$N_{u,simulation}$ [kN]	$\frac{N_{u,simulation}}{\bar{N}_{u,test}}$ [-]
1	1.2	0.3	-	0	196	270	1.38
2	1.2	0.3	ø12cc300	0	280	284	1.01
3	1.2	0.3	ø16cc150	0	319	305	0.96
4	1.2	0.3	ø16cc100	0	317	346	1.09
5	1.2	0.6	ø12cc300	0	357	349	0.98
6	2.2	0.3	ø12cc400	0	241	267	1.11
7	2.2	0.3	ø12cc150	0	262	288	1.10
8	2.2	0.6	ø12cc150	0	327	354	1.08
9	1.2	0.3	-	0.5	144	212	1.47
10	1.2	0.3	ø12cc300	0.5	292	245	0.84
11	1.2	0.3	ø16cc150	0.5	303	266	0.88
12	1.2	0.3	ø16cc100	0.5	256	325	1.27
13	2.2	0.3	ø12cc500	0.5	217	249	1.15

For the non-reinforced concrete slabs in table 6-9, simulated failure loads are higher than those attained from testing. The ratio is about 1.43. Corresponding ratio from the simulations in section 6.3.1 is about 1.10. One important difference between the two types of specimens used in section 6.2.1 and section 6.2.2 is the global stiffness. The ratios in table 6-10 show that the specimen used by [Eligehausen et al. 1992] is considerably stiffer than that used by [Nilsson and Elfgren 2009]. A consequence of this is that the non-reinforced concrete specimen in [Nilsson and Elfgren 2009] is more prone to splitting compared to that in [Eligehausen et al. 1992]. Figure A1-1 in Appendix 1 indicates the splitting failure mode. Concerning the numerical simulation of anchor bolts subjected to tension in non-reinforced concrete slabs, the failure load is better predicted if the splitting mode has a minor impact compared to that of the concrete cone breakout.

Table 6-10: Comparison of global stiffness of non-reinforced concrete specimens in section 6.2.1 [Eligehausen et al. 1992] and section 6.2.2 [Nilsson and Elfgren 2009].

	[Eligehausen et al. 1992]	[Nilsson and Elfgren 2009]
$\frac{\text{Width of slab}}{h_{ef}}$	$\frac{4 \cdot h_{ef}}{h_{ef}} = 4$	$\frac{1200 - 100}{220} = 5$
$\frac{\text{Thickness of slab}}{h_{ef}}$	$\frac{2 \cdot h_{ef}}{h_{ef}} = 2$	$\frac{300}{220} = 1.36$
$\frac{\text{Width of slab}}{\text{Thickness of slab}}$	2	3.7

Predicted failure load for non-reinforced concrete based on CEN/TS 1992-4-2 with $h_{ef} = 220$ mm and a mean compressive cube strength $f_{cm,cube} = f_{cm}/0.76 = 25/0.76 = 32.9$ MPa is

$$N_{u,non-cracked} = 1.33 \cdot \left(11.9\sqrt{32.9} \cdot 220^{1.5}\right) = 296 \text{ kN}$$

$$N_{u,cracked} = 1.33 \cdot \left(8.5\sqrt{32.9} \cdot 220^{1.5}\right) = 212 \text{ kN}$$

where the factor 1.33 adjusts the CEN/TS 5% fractile value of the failure load to the mean value. Predicted failure loads based on CEN/TS correspond well with simulated failure loads in table 6-9. The relation $f_{cm,cube} = f_{cm}/0.76$ is given by [Betonghandbok- Material 2008].

One conclusion of these results for anchor bolts subjected to tension in non-reinforced concrete is that both simulations and predictions based on CEN/TS might overestimate the capacity if the global stiffness of the concrete structure is not sufficiently high. In most cases, however, concrete structures are reinforced why this is not a problem in practice.

Table 6-11: Comparison of tested and simulated failure loads for non-cracked and pre-cracked concrete slabs with different amount of reinforcement. *LxLxH* is 1.2x1.2x0.3 m. Test data is taken from [Nilsson and Elfgren 2009].

Top rein-forcement	No pre-crack			Pre-crack 0.5 mm		
	$\bar{N}_{u,test}$ (kN)	$N_{u,simulation}$ (kN)	$\frac{N_{u,simulation}}{\bar{N}_{u,test}}$	$\bar{N}_{u,test}$ (kN)	$N_{u,simulation}$ (kN)	$\frac{N_{u,simulation}}{\bar{N}_{u,test}}$
Ø12cc300	280	284	1.01	292	245	0.84
Ø16cc150	319	305	0.96	303	266	0.88
Ø16cc100	317	346	1.09	256	325	1.27

Tested and simulated failure loads for non-cracked and pre-cracked concrete slabs with different amount of reinforcement are compared in table 6-11. The dimension of all slabs in the table is 1.2x1.2x0.3 m. Simulated failure loads increase with the amount of reinforcement both for non-cracked and pre-cracked slabs. This is not the case for the tested specimens with pre-crack as already discussed in section 6.2.2. As the pre-crack is introduced differently in the physical specimen and in the simulation, it can be expected that deviations between testing and simulation are biggest for pre-cracked slabs. This is also seen in table 6-11. For reinforced slabs with no pre-crack, simulated failure loads agree rather well with test results. Introduction of pre-cracks slightly increases the deviation between tested and simulated failure loads. The maximum deviation is 27%.

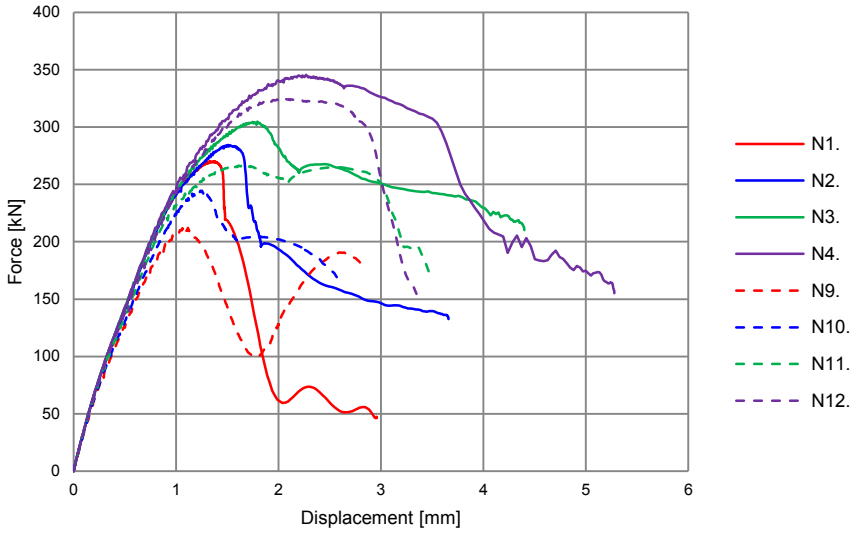

Figure 6-9: Simulated force-displacement curves for configurations 1 to 4 with no pre-crack and 9 to 12 with pre-crack 0.5 mm in table 6-9.

In figure 6-9, simulated force-displacement curves for some of the non-cracked and corresponding pre-cracked slabs in table 6-9 are shown. A comparison of the force displacement curves of the non-reinforced and the reinforced slabs shows a more ductile response for the reinforced ones. Furthermore, the non-cracked slabs show a higher failure load and somewhat more ductile response than the pre-cracked.

In order to investigate the impact of slab thickness, specimen configuration 2 in table 6-9 was modified by increasing the thickness from 0.3 to 0.6 m. The new specimen configuration is called 5. As expected, the test failure load increased. Simulated failure load for configuration 5 agrees well with test result. As the thickness is increased, the global stiffness also increases. In Appendix 1, figure A1-2 and A1-5 show the damage parameter at failure load and at end of simulation. As seen, the damage evolution differs between the two configurations. The figures reveal that failure is caused by splitting in the thinner slab and by concrete cone breakout in the thicker slab. The dissimilar failure mode is a result of difference in global stiffness. Type of failure mode also explains the difference in level of failure load.

Specimens with a width of 2.2 m were also tested in [Nilsson and Elfgren 2009]. Results for specimen configuration 6, 7, 8 and 13 are shown in table 6-9. Configuration 6 has a thickness of 0.3 m and reinforcement Ø12cc400. Compared to configuration 2, the global stiffness is lower and the amount of reinforcement is less. As a result, the tested failure load is also lower. The only difference between configuration 7 and 8 is the thickness. An increase of thickness increases the global stiffness and thereby also the failure load as seen in table 6-9. Figure A1-6 and A1-7 in Appendix 1 show the different damage evolution in the two specimens which also explains the difference in failure load. Configuration 6, 7 and 8 have no pre-cracks while configuration 13 is pre-cracked. The latter configuration has a thickness of 0.3 m and reinforcement Ø12cc500. Among the reinforced test specimens, configuration 13 has the lowest global stiffness and least reinforcement. Hence, tested failure load for configuration 13 is also the lowest among the reinforced slabs as seen in table 6-9.

Simulated failure loads for specimens with a width of 2.2 m agree rather well with corresponding test results as seen in table 6-9 and figure 6-8. Simulations overestimate failure load compared with test results with a maximum deviation of 15%.

Comparison of force-displacement curves

In figure 6-10, 6-11 and 6-12, force-displacement curves from testing [Nilsson and Elfgren 2009] and simulations are shown for specimen configuration 2, 3 and 4, respectively. Tested failure loads for these configurations are fairly well predicted with simulations. However, the shape of the curves from testing and simulation deviates. Simulated displacement at failure load is underestimated for specimen configuration 2 and 3. For specimen configuration 4, displacement at failure load correlates well with two of the tests but not with the third one.

Test results from [Nilsson and Elfgren 2009] show a variety of different force-displacement curves. Testing such a complex material as concrete in combination with reinforcement explains this variety. The difficulty to simulate the different shapes of the force-displacement curves from the physical tests is obvious. Before a refinement of the modelling is done, the way the displacement is measured in the tests needs to be more known in detail.

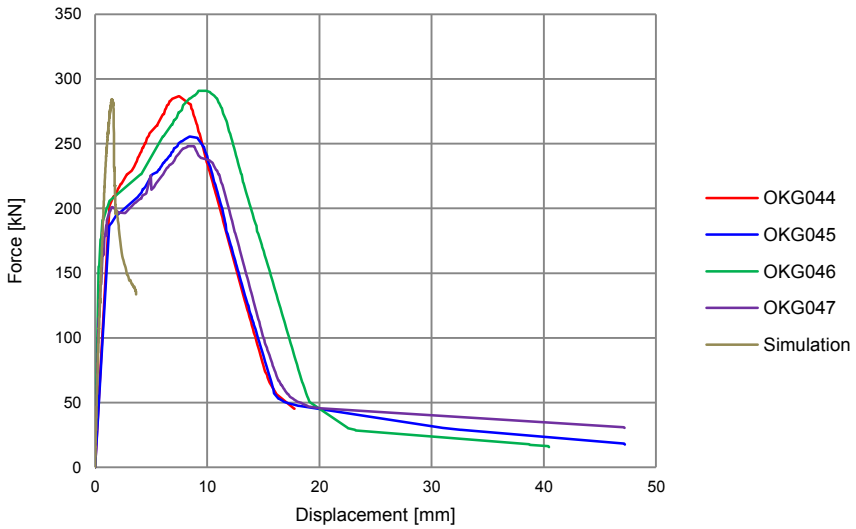

Figure 6-10: Force-displacement curves from four tests [Nilsson and Elfgren 2009] and simulation for specimen configuration 2 in table 6-9.

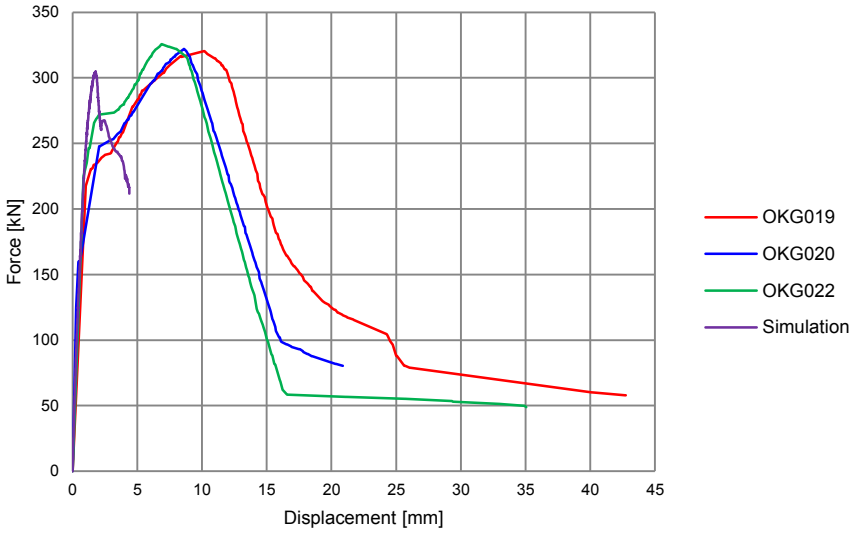

Figure 6-11: Force-displacement curves from four tests [Nilsson and Elfgren 2009] and simulation for specimen configuration 3 in table 6-9.

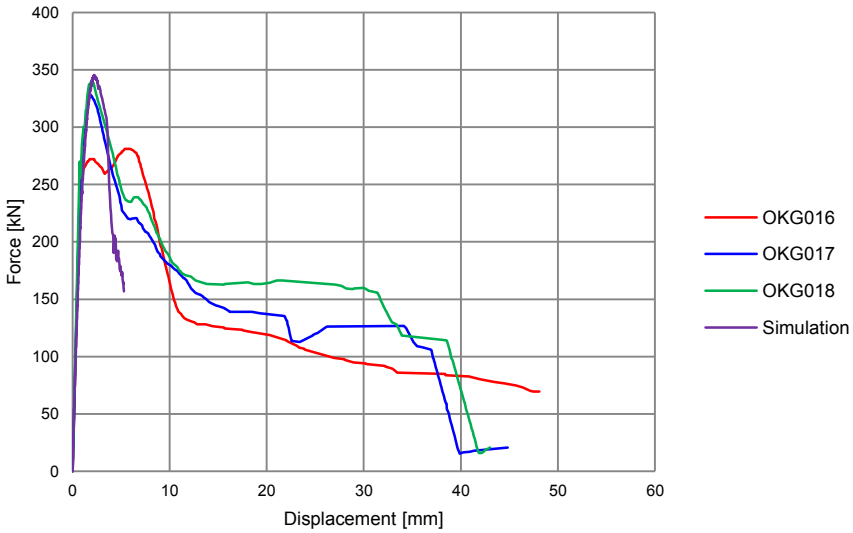

Figure 6-12: Force-displacement curves from four tests [Nilsson and Elfgren 2009] and simulation for specimen configuration 4 in table 6-9.

Influence of boundary conditions

Boundary conditions are of importance in simulations. In the numerical investigation presented above, the support ring is modelled and contact conditions are introduced between the concrete slab and the support ring. As an alternative, the nodes on the concrete slab that are in contact with the support ring can be restricted to move in the vertical direction. In the following, both ways of modelling the interaction between the slab and the support ring is compared.

Figure 6-13 shows simulated force-displacement curves for some of the configurations in table 6-9 with the two different ways of modelling the interaction

between the support ring and the slab. As seen, simulated failure loads are lower if the support ring is included in the model. Also the shape of the force-displacement curves differs. Different degree of restraint introduced by the two types of boundary conditions explains the differences in response. Including the support ring in the model best reflects the physics of the tests.

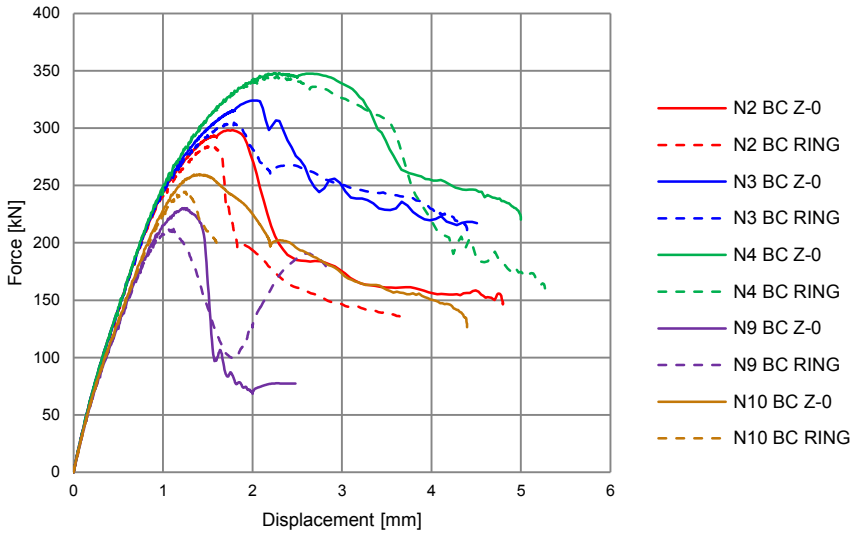

Figure 6-13: Simulated force-displacement curves for models with (BC RING) and without (BC Z-0) support ring modelled.

Influence of finite element size

For the numerical investigation presented above in this section, a finite element size of about 10 mm in the anchor bolt region was chosen. This choice of element size was based on a number of simulation tests that shown what was required to sufficiently well capture the response of anchor bolts in tension.

In order to show some effects of mesh density, the influence of different element size (5, 7.5, 10, 15 and 20 mm) is investigated for the specimen configuration 3 in table 6-9. Figure 6-14 shows simulated force-displacement curves for the different element sizes. The first thing to notice is that failure loads are similar for the five cases. The shape of the force-displacement curves differs however. Particularly that for the case with an element size of 5 mm deviates from the others. An explanation for this change in response for the smallest element size might be the way the rebar elements are connected to the concrete elements in the finite element model. As the concrete elements get smaller, the volume of concrete elements that interacts mechanically with the rebar elements also gets smaller. A comparison with test results in figure 6-11 also indicates that the model with the smallest elements deviates the most.

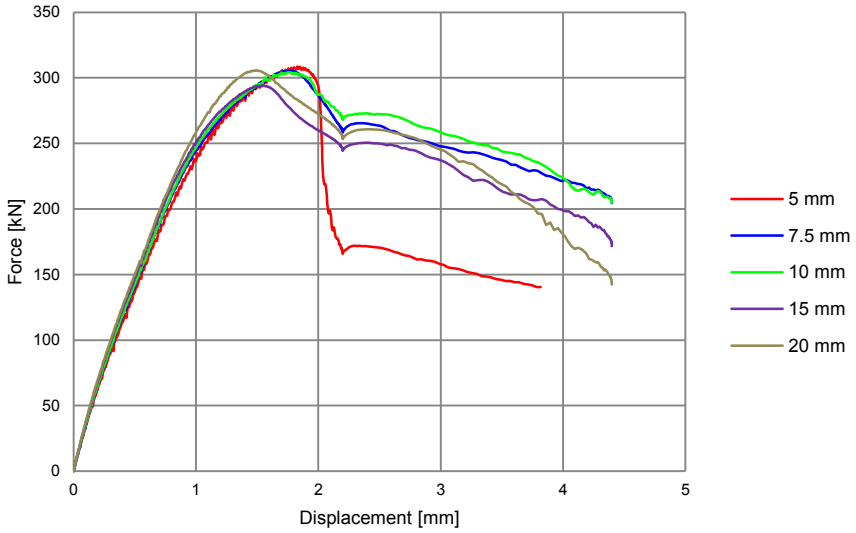

Figure 6-14: Force-displacement curves for different finite element size. Specimen configuration 3 in table 6-9 is used.

6.3.3. Single anchor in reinforced concrete wall

Global stiffness of the concrete structure influences the capacity of anchor bolts in tension as already discussed. In general, an increase of global stiffness increases the failure load. Width and thickness of the structure, boundary conditions and the amount of reinforcement are all important factors in this context.

In this section, a single anchor bolt in tension located in the centre of a reinforced wall is investigated numerically. The size of the wall (*LxLxH*) is 3x3x0.3 m, 3x3x0.6 m and 2.2x2.2x0.3 m. Two different boundary conditions are used, i.e. simply supported or clamped at all four edges. The embedment depth is $h_{ef} = 220$ mm and the mean compressive cylinder strength is $f_{cm} = 25$ MPa. Input data is summarised in table 6-12. The material constants used in the simulations are found in table 6-7 and table 6-8.

Table 6-12: Input data and results for simulation of single anchor subjected to tension load in different reinforced walls.

	L [m]	*H* [m]	Top reinforce-ment	Boundary conditions	$N_{u,simulation}$ [kN]
Wall 1	3	0.3	Ø12cc150	clamped	366
Wall 2	3	0.3	Ø12cc150	simply supported	304
Wall 3	3	0.6	Ø12cc150	simply supported	379
Wall 4	2.2	0.3	Ø12cc150	simply supported	312

Results are found in table 6-12 and figure 6-15. A comparison of wall 1 and 2 shows that correct boundary conditions are essential when simulating anchors in tension located in concrete walls. If the wall is clamped instead of simply supported, the failure load increases 20%. Results for the simply supported wall 2 and 3 show that an increase of wall thickness from 0.3 to 0.6 m increases the failure load by 25%.

Wall 2 and 4, both simply supported, show that a reduction of width from 3 to 2.2 m increases the failure load not more than about 3%.

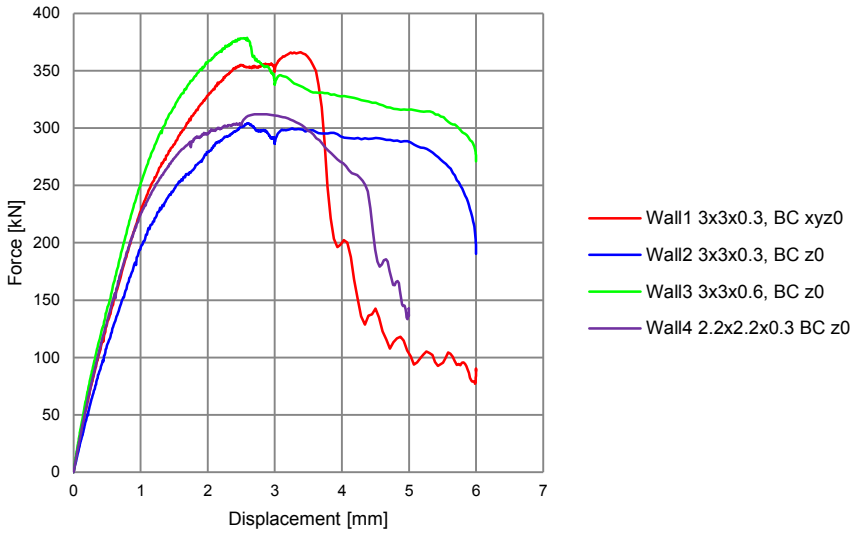

Figure 6-15: Force-displacement curves for a single anchor in a reinforced concrete wall with different boundary conditions and different wall thickness.

Analysed walls in this section all show different global stiffness and thereby also different failure load. The global stiffness increases if the boundary conditions go from simply supported to clamped, if the thickness of the wall increases and if the width of the wall decreases. An increase of the amount of reinforcement would also increase the global stiffness. The initial slope of the force-displacement curves in figure 6-15 gives an indication of the global stiffness of the walls. The correlation between initial slope and failure load is obvious.

6.3.4. Influence of tensile strength of concrete

For concrete, tensile strength and compressive strength are related. In [Betonghandbok- Material 2008] the relation is expressed as

$$f_{ct} = 0.24 \cdot (f_{cm,cube})^{2/3} \qquad \text{(Eq. 6-2)}$$

where f_{ct} is the tensile strength and $f_{cm,cube}$ is the mean compressive cube strength for the concrete. In Eurocode 2 [EC2 2005] the relation is expressed as

$$f_{ctm} = 0.3 \cdot (f_{ck})^{2/3} \qquad \text{(Eq. 6-3)}$$

where f_{ctm} is the mean value of axial tensile strength and f_{ck} is the characteristic compressive cylinder strength of concrete at 28 days. A comparison of the two expressions gives that

$$f_{ctm} = 0.3 \cdot (f_{ck})^{2/3} = 0.3 \cdot (f_{cm}/1.33)^{2/3} =$$

$$= 0.3 \cdot \left(0.76 \cdot f_{cm,cube}/1.33\right)^{2/3} = 0.207 \cdot \left(f_{cm,cube}\right)^{2/3} = \qquad \text{(Eq. 6-4)}$$

$$= 0.86 \cdot f_{ct}$$

where f_{cm} is the mean compressive cylinder strength. As seen from equation 6-4, f_{ctm} is about 14% lower than f_{ct}. The relation $f_{cm} = 0.76 \cdot f_{cm,cube}$ is given by [Betonghandbok- Material 2008].

In all simulations of anchors in tension, a tensile strength calculated with equation 6-2 is used in the concrete constitutive model. In order to see the effect of lowering the tensile strength, some of the analyses in section 6.3 have been done with the value of f_{ctm} instead of f_{ct}. The concrete compressive strength is kept unchanged.

Table 6-13: Simulated failure load for some of the analyses reported in table 6-6 and table 6-9 with lowered failure stress in tension σ_{t0}in the constitutive model. The ultimate compressive stress σ_{cu} is kept unchanged.

Table	Slab dimension [m]	Top rein-forcement	h_{ef} [mm]	σ_{t0} [MPa]	N_u [kN]	$\sigma_{t0,alt}$ [MPa]	$N_{u,alt}$ [kN]	$\frac{N_{u,alt}}{N_u}$ [-]
6-6	1.2x1.2x0.6	-	450	2.38	1188	2.05	1140	0.96
6-9	1.2x1.2x0.3	ø12cc300	220	2.46	284	2.12	272	0.96
6-9	1.2x1.2x0.3	ø16cc100	220	2.46	346	2.12	322	0.93

For the investigated cases, the 14% reduction of tensile strength in the constitutive model reduces the failure load between 4 to 7%. The reduction is higher for the slab with the higher amount of reinforcement as seen in table 6-13.

6.4. Numerical simulations of anchor groups in tension

Tension capacity of anchor groups in concrete structures with and without reinforcement is investigated numerically. Spacing of anchors, number of anchors, amount of reinforcement, type of concrete structure and boundary conditions for the concrete structure are parameters of interest. A comparison with CEN/TS 1992-4-2 is also made.

6.4.1. Anchor group in non-reinforced concrete slab

In this section, an anchor group subjected to tension is investigated numerically and the result is compared with predictions based on CEN/TS 1992-4-2. The anchor group is located in a non-reinforced concrete slab and the spacing of anchors is used as a parameter.

The finite element model used is shown in figure 6-16. The symmetric anchor group with four anchors is located in a non-reinforced symmetric concrete slab with thickness $H = 4 \cdot h_{ef}$, width $L = 4 \cdot h_{ef} + \sqrt{2} \cdot s$ and embedment depth of anchors $h_{ef} = 179$ mm. s is the spacing of anchors. A support ring is modelled and contact conditions are introduced between the concrete slab and the support ring. The concrete element size in the vicinity of the anchor bolts is about 10 mm. Tension load is applied by moving the top area of the steel plate between the anchor bolts in the vertical direction at a constant displacement rate of 30 mm/s. The material parameters used in the simulations are given in table 6-7.

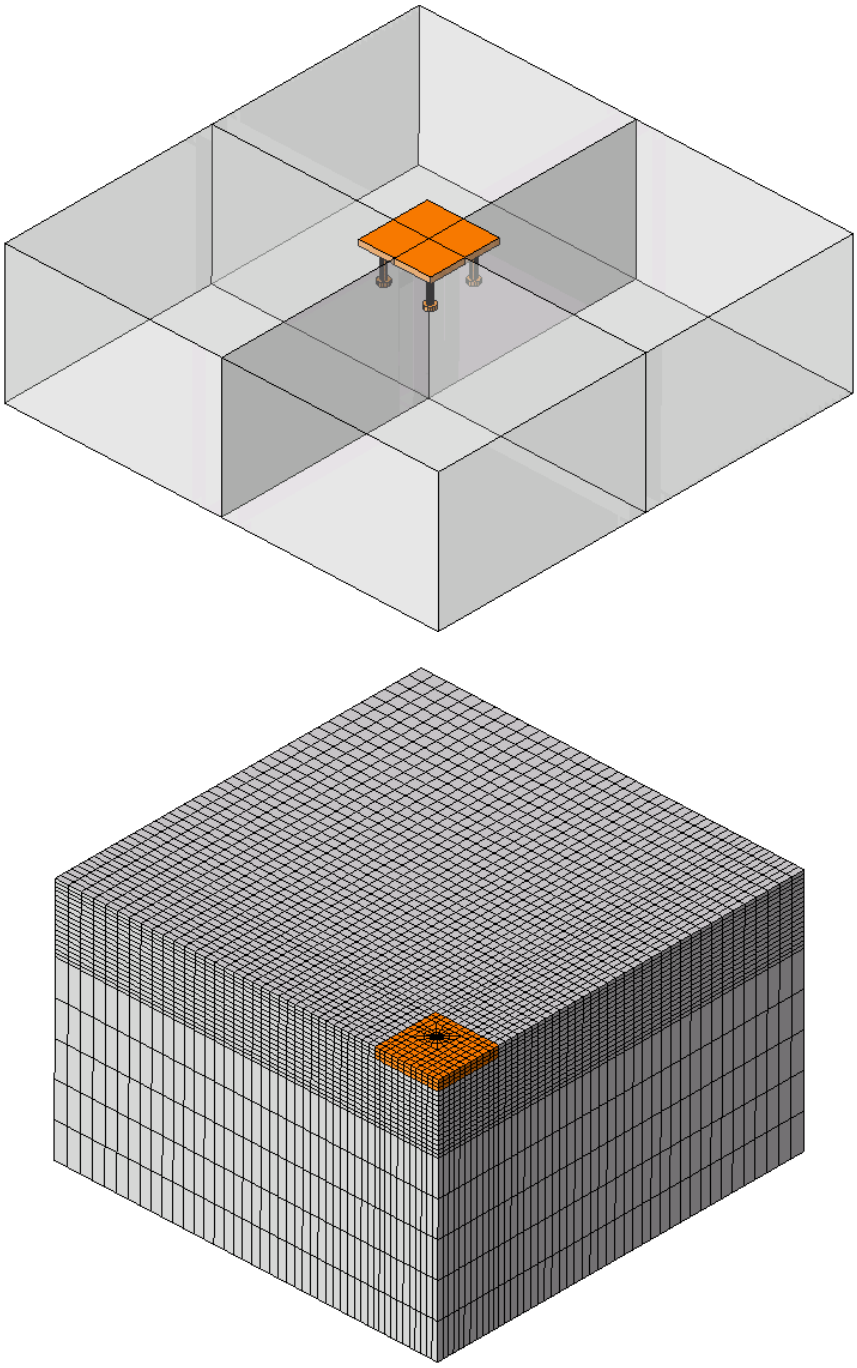

Figure 6-16: Finite element model of anchor group with four anchors. One fourth of the specimen is modelled due to symmetry.

According to CEN/TS 1992-4-2, the characteristic concrete breakout cone capacity of an anchor group in tension is expressed as

$$N_{Rk,c} = N^0_{Rk,c} \cdot \frac{A_{c,N}}{A^0_{c,N}} \cdot \psi_{s,N} \cdot \psi_{re,N} \cdot \psi_{ec,N} \qquad \text{(Eq. 6-5)}$$

where $N^0_{Rk,c}$ is the characteristic concrete breakout cone capacity of a single anchor in the group, $A_{c,N}$ is the actual projected concrete failure area of the group, $A^0_{c,N}$ is the reference projected concrete failure area of a single anchor, $\psi_{s,N}$ is a factor taking account for edge effects, $\psi_{re,N}$ is a factor taking account for shell spalling and $\psi_{ec,N}$ is a factor taking account for the effect of the eccentricity of the load.

In the following comparison, all ψ -constants in equation 6-5 are set equal to one. This can be done if there are no concrete edges located in the vicinity of the anchor group, if the anchor plate is centrically loaded and if $h_{ef} \geq 100$ mm. A further general requirement for equation 6-5 to be valid is that the global stiffness of the concrete structure is sufficiently high. With all ψ -constants equal to one, the relation between the anchor group capacity and the single anchor capacity is equal to $A_{c,N}/A^0_{c,N}$. Spacing of anchors influences $A_{c,N}$ and thereby also the capacity of the anchor group. For centre to centre spacing not exceeding $3 \cdot h_{ef}$, the capacity increases as the spacing increases. As the spacing exceeds $3 \cdot h_{ef}$, the capacity remains constant provided the anchor plate is sufficiently stiff.

Comparison of results from simulations and predictions based on CEN/TS 1992-4-2 is shown in figure 6-17. The ratio between the concrete cone capacity of the group and a single anchor is given as a function of the ratio between the anchor spacing *s* and the anchor embedment depth h_{ef}. As can be seen, the numerical results correspond rather well with that of CEN/TS 1992-4-2. Together with the numerical result for the single anchor in section 6.3.1, it is shown that the failure load for an anchor group subjected to tension in non-reinforced concrete can be predicted by numerical simulation provided the global stiffness of the concrete slab is sufficiently stiff. The influence of global stiffness on group capacity will be discussed more later on.

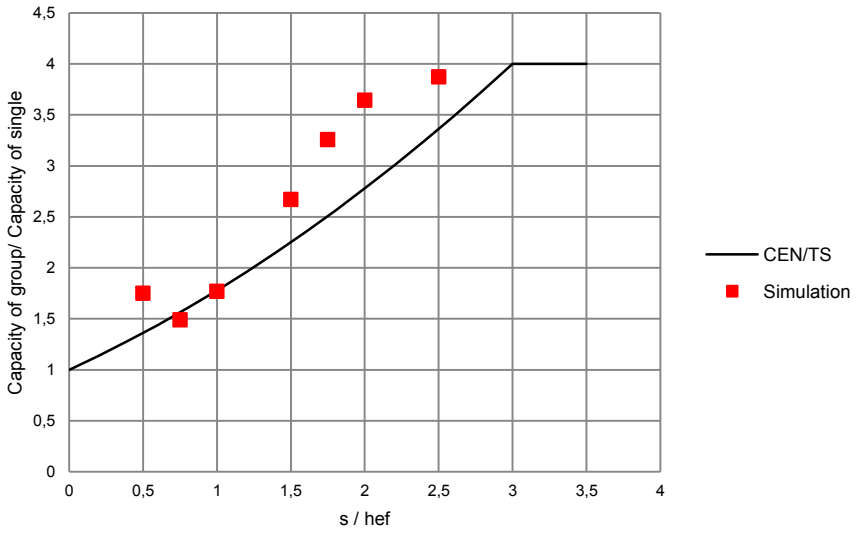

Figure 6-17: Ratio between concrete cone capacity of a symmetric anchor group with four anchors and concrete cone capacity of a single anchor in the group as a function of the distance *s* between anchors in the group divided by embedment depth h_{ef}.

Figure 6-18 shows an example of developed damage in the concrete (DAMAGET) at maximum tension load. Due to symmetry only one fourth of the concrete slab is shown. The shape of the concrete cone of the anchor group is indicated by the damage.

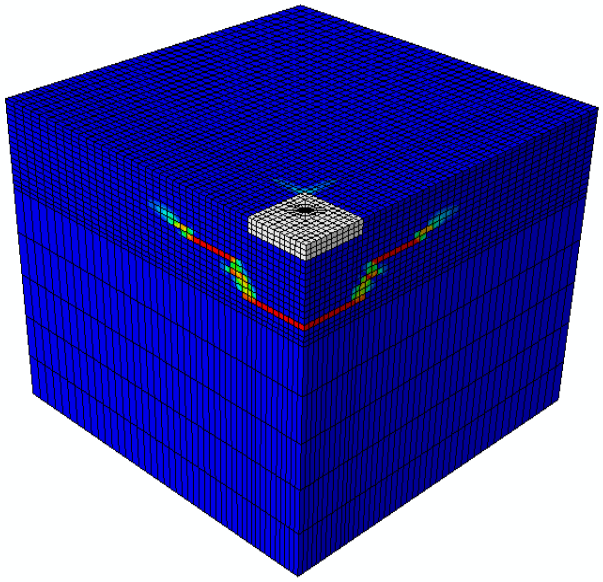

Figure 6-18: Example of developed damage in the concrete (DAMAGET) at maximum tension load. Due to symmetry only one fourth of the concrete slab is shown.

6.4.2. Anchor group in reinforced concrete slab

The response of anchor groups in tension located in reinforced concrete slabs is numerically simulated. Three geometries of slabs are investigated, i.e. 2.2x2.2x0.3 m, 2.2x2.2x0.6 m and 3x3x0.6 m. The amount of reinforcement varies from ∅12cc300 to ∅12cc100. The anchor groups are symmetric with four or six anchors. The embedment depth is $h_{ef} = 220$ mm and the anchor spacing is $s = 220$ mm between outside anchors. The size of the anchor plate is 320x320x20 mm, see figure 6-19.

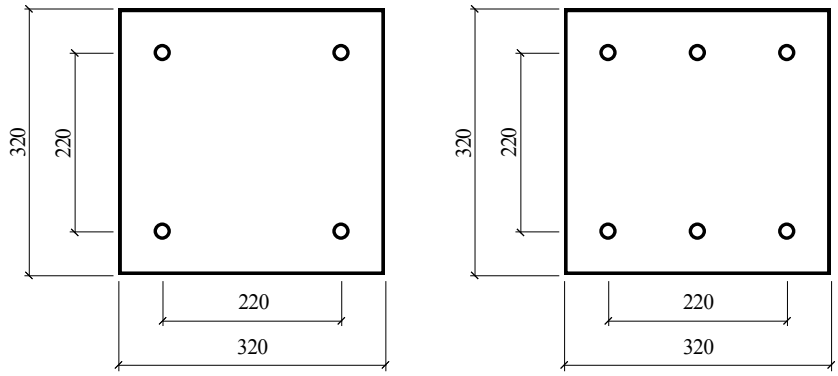

Figure 6-19: Dimension of anchor plates with four and six anchors, respectively. Thickness of anchor plate is 20 mm and embedment depth is $h_{ef} = 220$ mm.

For all but two slabs, a support ring is modelled and contact conditions are introduced between the concrete slab and the support ring. The largest slabs are instead simply supported or clamped at the slab boundaries. The concrete element size in the vicinity of the anchor bolts is about 10 mm. Tension load is applied by moving the top area of the anchor plate where the profile is attached at a constant displacement rate of 30 mm/s perpendicular to the anchor plate. All configurations investigated are summarised in table 6-14. The material parameters used in the simulations are given in table 6-7 and table 6-8. One of the finite element models used is shown in figure 6-20 and 6-21.

Table 6-14: Investigated configurations of anchor groups in reinforced concrete slabs. $N_{u,group}$ is the failure load of the group.

Slab	Slab dimension [m]	Top rein-forcement	Support	Anchor group	Cross-section of profile [mm]	$N_{u,group}$ [kN]
1	2.2x2.2x0.3	ø12cc300	Ring	2x2	120x120	341
2	2.2x2.2x0.3	ø12cc150	Ring	2x2	120x120	464
3	2.2x2.2x0.3	ø12cc100	Ring	2x2	120x120	492
4	2.2x2.2x0.3	ø12cc150	Ring	2x2	220x220	461
5	2.2x2.2x0.3	ø12cc300	Ring	2x3	120x120	340
6	2.2x2.2x0.3	ø12cc150	Ring	2x3	120x120	443
7	2.2x2.2x0.3	ø12cc100	Ring	2x3	120x120	502
8	2.2x2.2x0.6	ø12cc150	Ring	2x2	120x120	612
9	2.2x2.2x0.6	ø12cc150	Ring	2x2	220x220	622
10	3x3x0.6	ø12cc300	Simply supported	2x2	220x220	600
11	3x3x0.6	ø12cc300	Clamped	2x2	220x220	618

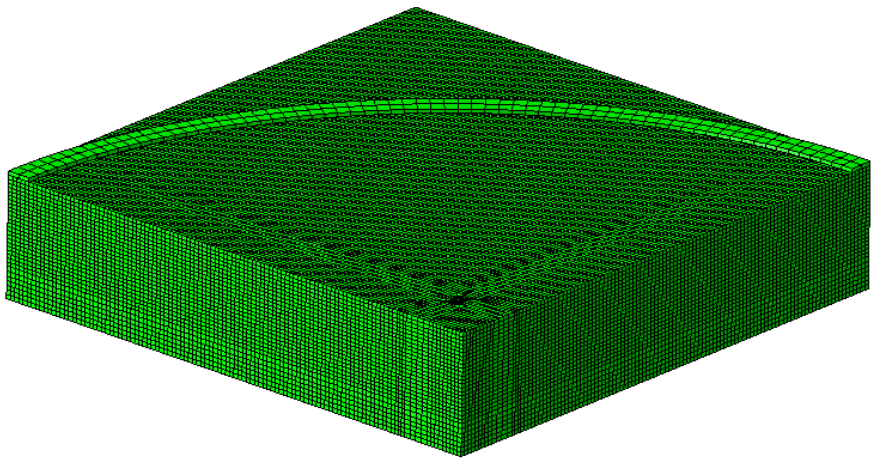

Figure 6-20: Finite element model used for simulation of anchor group in reinforced concrete.

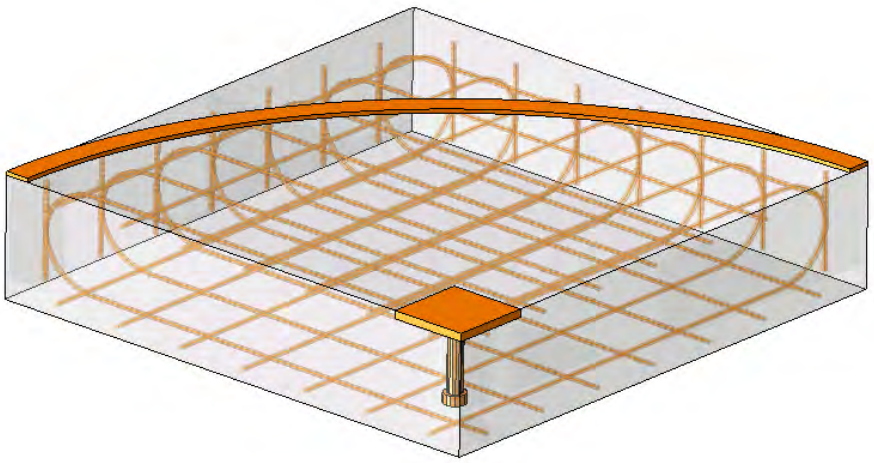

Figure 6-21: Transparent perspective view of the different parts constituting the reinforced concrete model.

The characteristic capacity of the anchor groups in figure 6-19 in non-reinforced non-cracked concrete is according to CEN/TS equal to

$$N_{Rk,c} = N^0_{Rk,c} \cdot \frac{A_{c,N}}{A^0_{c,N}} \cdot \psi_{s,N} \cdot \psi_{re,N} \cdot \psi_{ec,N} \qquad \text{(Eq. 6-6)}$$

where

$$\psi_{s,N} = \psi_{re,N} = \psi_{ec,N} = 1$$
$$A^0_{c,N} = 9 \cdot h_{ef}^2 = 4.36 \cdot 10^5 \text{ mm}^2$$
$$A_{c,N} = (3 \cdot h_{ef} + s)^2 = 7.74 \cdot 10^5 \text{ mm}^2$$
$$N^0_{Rk,c} = 11.9 \cdot \sqrt{f_{cm,cube}} \cdot h_{ef}^{1.5} = 223 \text{ kN}$$

For comparison with simulations, $N^0_{Rk,c}$ is calculated with $f_{cm,cube}$ instead of $f_{ck,cube}$ under the square root. Furthermore, $N_{Rk,c}$ is multiplied with 1.33 to get the mean value, i.e.

$$N_{u,CEN/TS} = 1.33 \cdot N_{Rk,c} = 526 \text{ kN}$$

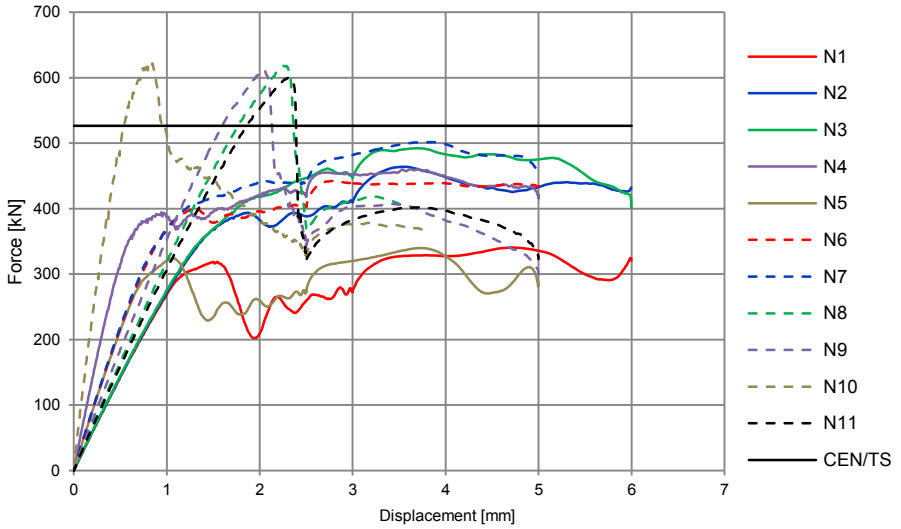

Figure 6-22: Force-displacement curves for the anchor groups in table 6-14. CEN/TS prediction of failure load for anchor group without considering the reinforcement is included for comparison.

Figure 6-22 shows force-displacement curves for investigated anchor groups in table 6-14. The thickness of the slab has a major impact on the capacity and the shape of the curve. Only those slabs with a thickness of 0.6 m show a failure load larger than that predicted with CEN/TS without considering the reinforcement.

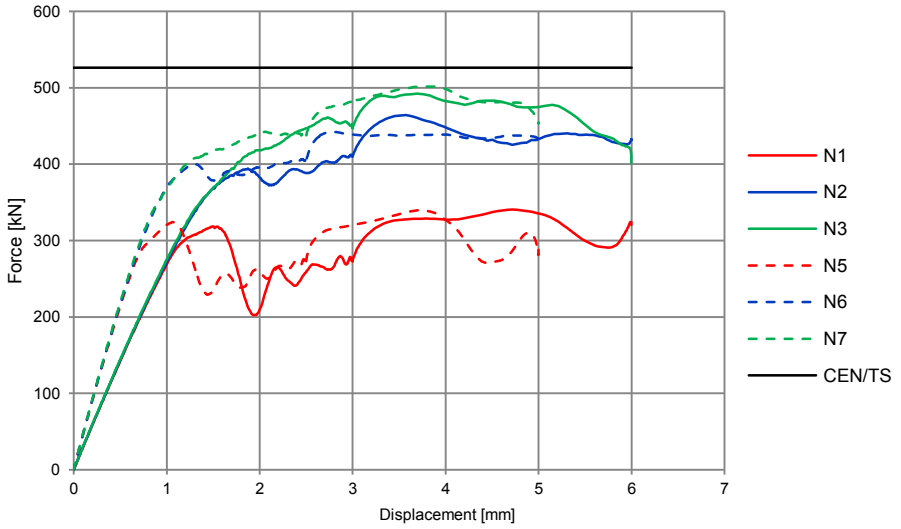

Figure 6-23: Simulated force-displacement curves for the anchor group configuration 1, 2, 3, 5, 6 and 7 in table 6-14. Comparison of anchor groups with four and six anchors. CEN/TS prediction of failure load for anchor group without considering the reinforcement is included for comparison.

In figure 6-23, force-displacement curves for anchor groups with four and six anchors are compared. The amount of reinforcement is varied from Ø12cc300 to Ø12cc100. The anchor groups are designated 1, 2, 3, 5, 6 and 7 in table 6-14. Corresponding CEN/TS capacity for the anchor groups without considering the

reinforcement is also included in figure 6-23. CEN/TS predicts the same capacity for all groups as spacing between outside anchors is the same.

Figure 6-23 shows that failure load increases with the amount of reinforcement. An increase from Ø12cc300 to Ø12cc100 increases the failure load about 45%. For the same amount of reinforcement, the response of the anchor groups with four and six anchors is similar.

In non-reinforced non-cracked concrete, CEN/TS predicts a failure load of 526 kN for investigated anchor groups. All simulations with a slab thickness of 0.3 m show lower failure loads despite the fact that simulated anchor groups are located in reinforced slabs. The discrepancy is explained by the global stiffness of the concrete slab. CEN/TS assumes a stiff concrete structure while simulated concrete slabs are not as stiff. For simulated cases, a tendency of splitting reduces the capacity. Instead of assuming non-cracked concrete in doing the CEN/TS prediction, it might be more correct to assume cracked concrete for those slabs where the global stiffness is insufficient. The reason for changing condition would be that pre-cracking caused by splitting precedes the concrete cone failure and thereby reduces the failure load. In doing so, $N_{u,CEN/TS}$ is reduced to $526/1.4 = 376$ kN which better corresponds with simulated failure loads. Figure A1-9, A1-10 and A1-11 in Appendix 1 confirm the splitting tendency for slab configurations 1, 2 and 6, respectively.

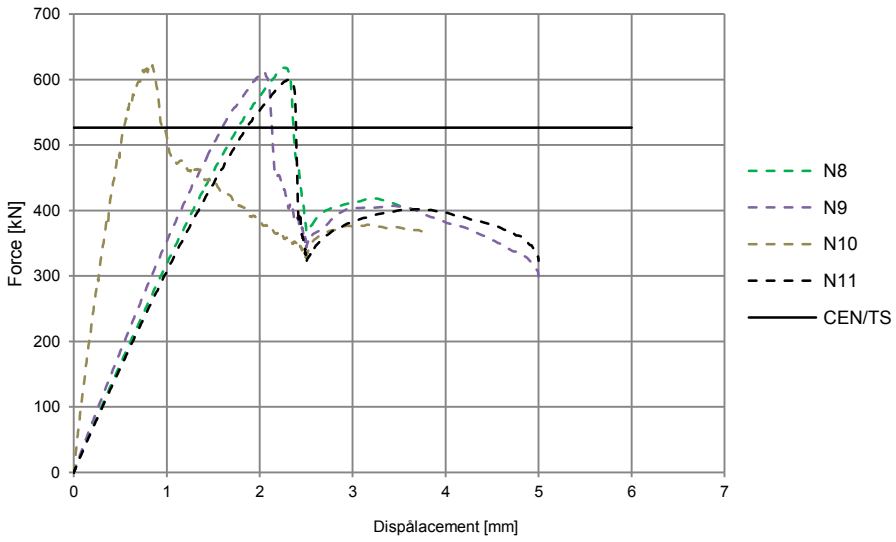

Figure 6-24: Simulated force-displacement curves for the anchor group configuration 8, 9, 10 and 11 in table 6-14. CEN/TS prediction of failure load for anchor group without considering the reinforcement is included for comparison.

Simulated force-displacement curves for the anchor group configuration 8, 9, 10 and 11 in table 6-14 are shown in figure 6-24. All slabs have a thickness of 0.6 m. Configuration 10 and 11 have a larger width than configuration 8 and 9. Slab 10 is simply supported and slab 11 clamped at the boundaries.

In contrast to the other slabs in table 6-14, these four slabs show a higher failure load than that predicted based on CEN/TS. Besides the fact that these slabs are reinforced, the increase in slab thickness from 0.3 to 0.6 m results in a higher global stiffness. The tendency for splitting of the concrete structure is thereby avoided. The difference in initial slope of the curves between anchor group configurations 8 and 9

is explained by the cross-section size of the attached profile. The flexibility of the anchor plate increases as the cross-section gets smaller. Regarding slab 10 and 11, the size of the slab and the boundary conditions influence the initial slope of the curves. Figure A1-12 in Appendix 1 show the damage evolution in slab 8 where the failure mode is concrete cone breakout.

Table 6-15: Comparison of simulated failure load for some of the anchor groups in table 6-14 and corresponding single anchor in table 6-9.

Slab	Slab dimension [m]	Top rein-forcement	Anchor group	Cross-section of profile [mm]	$N_{u,group}$ [kN]	$N_{u,single}$ (table 6-9) [kN]	$\frac{N_{u,group}}{N_{u,single}}$ [-]
2	2.2x2.2x0.3	ø12cc150	2x2	120x120	464	288	1.61
4	2.2x2.2x0.3	ø12cc150	2x2	220x220	461	288	1.60
6	2.2x2.2x0.3	ø12cc150	2x3	120x120	443	288	1.54
8	2.2x2.2x0.6	ø12cc150	2x2	120x120	612	354	1.73
9	2.2x2.2x0.6	ø12cc150	2x2	220x220	622	354	1.76

Table 6-15 compares simulated failure load for some of the anchor groups in table 6-14 and corresponding single anchor in table 6-9. The ratio is smaller for slabs with a thickness of 0.3 m compared to that with a thickness of 0.6 m. The explanation is that a tendency of splitting limits the failure loads for the anchor groups in the thinner slabs. According to CEN/TS, the ratio between failure load for the anchor group and corresponding single anchor is 1.78 for investigated configurations. The higher global stiffness of the thicker slab explains why slab 8 and 9 agree better with CEN/TS.

7. Anchors loaded in shear

7.1. General

There is not much public information available regarding studies on the behaviour of bolts anchored in concrete and subjected to shear. However, section 7.2 describes part of a testing program that was carried out in the year of 2001 at the University of Texas in which near-edge single anchor bolts in non-reinforced concrete were forced towards the concrete edge. Necessary information such as geometries, materials, loading rate and results from the physical tests are presented in section 7.2.

The objective has been to achieve numerical simulation results in compliance with mentioned physical test results by using the constitutive material model described in chapter 5. The methodology has thenceforth been to use the established model for further numerical simulations of other similar problems. Single anchor bolts in reinforced concrete and group of anchors in both non-reinforced and reinforced concrete has been investigated by means of finite element analyses.

Within the scope of this project regarding anchors loaded in shear, numerical simulations have been performed based on the above mentioned physical tests. The finite element model, the constitutive material model and results from the numerical simulations as well as comparative physical test results are presented in section 7.3.1.

As the simulation results show good agreement with physical test results, the constitutive material model utilized in the simulations is considered appropriate for the task at hand. Nevertheless, different parameters defining the constitutive model have been examined in a parametric study with the objective to see what impact on analysis results different parameters may have. These studies are thoroughly described in section 7.3.2.

Section 7.3.3 and 7.4.2 present numerical simulation results of what impact different reinforcement setups have with respect to failure load magnitudes and concrete fracture surfaces for single anchor bolts and group of anchor bolts, respectively.

7.2. Physical tests of single anchors in shear

In the year of 2001 a research project at the University of Texas under the sponsorship of the U.S. Nuclear Regulatory Commission was carried out to obtain information to determine how the seismic behaviour and strength of anchors and their supporting concrete differ from the static behaviour [Hallowell Gross et al. 2001]. One task in this project was to test static and dynamic behaviour of near-edge anchors. 150 physical tests were carried out and the static results from these tests have been used for comparison with the numerical simulation results presented in section 7.3.1. The distance from the concrete edge to the anchor, i.e. the edge distance in both the physical tests and the analyses is consistently 100 mm.

7.2.1. Test setup and procedure

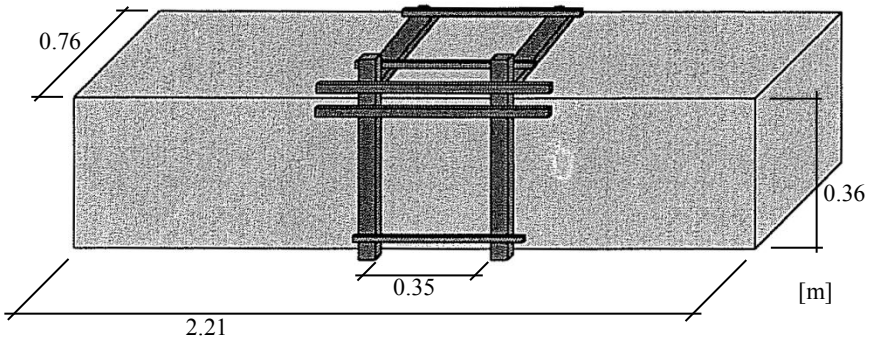

Figure 7-1: Dimensions of concrete specimens tested and schematic visualisation of test rig [Hallowell Gross et al. 2001].

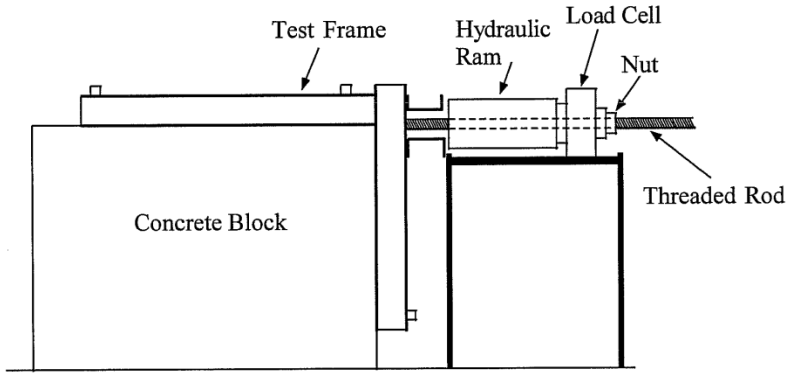

Figure 7-2: Side view of shear test setup [Hallowell Gross et al. 2001].

The test setup for the physical tests is visually described in figure 7-1 and figure 7-2. As seen in figure 7-2 the horizontal displacement was applied by a hydraulic ram. Centred in the test frame the hydraulic ram is connected to a steel plate in which the anchor bolt is attached. The magnitude of corresponding force caused by the applied displacement was measured in the load cell and the displacement was registered by a linear potentiometer at the back of the steel plate, see figure 7-3. For the static tests the displacement was applied in a monotonically increasing manner so that failure occurred in two to four minutes in order to avoid dynamic effects [Hallowell Gross et al. 2001]. Dimensions of the cast-in headed anchor bolt are shown in figure 7-4.

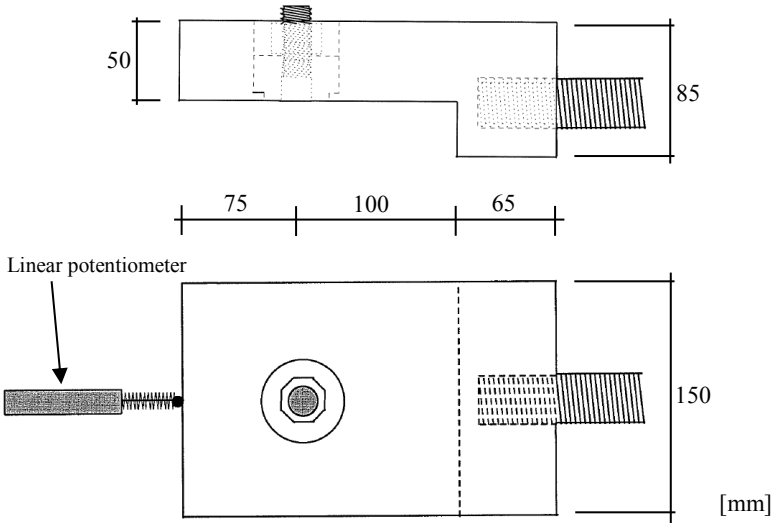

Figure 7-3: Dimensions of steel plate [Hallowell Gross et al. 2001].

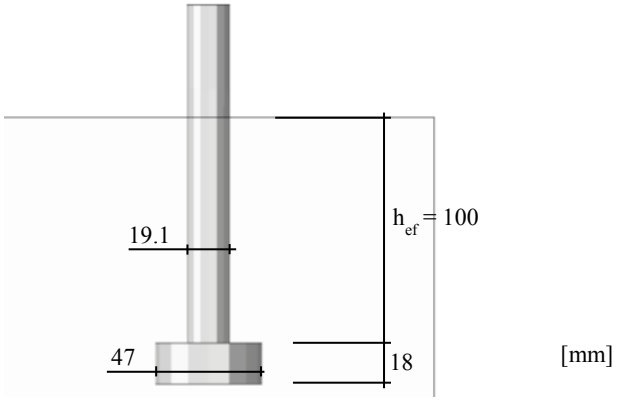

Figure 7-4: Dimensions of cast-in headed anchor bolt.

The concrete cylinder compressive strength for the ACI-testing program was 32.4 MPa with a permissible tolerance of ±3.45 MPa. The mixture used a local river-gravel aggregate [Hallowell Gross et al. 2001].

7.2.2. Results – A comparison with CEN/TS 1992-4-2

The characteristic capacity of a single anchor bolt close to an edge and subjected to shear is according to [CEN/TS 1992-4-2 2009] calculated in the following manner:

$$V_{Rk,c}^{0} = 1.6 \cdot d_{nom}^{\alpha} \cdot l_f^{\beta} \cdot \sqrt{f_{ck,cube}} \cdot c_1^{1.5} \qquad \text{[N]} \qquad \text{(Eq. 7-1)}$$

Where:

$l_f = h_{ef}$ in case of a uniform diameter of the shank of the headed fastener

$\alpha = 0.1 \cdot \left(\frac{l_f}{c_1}\right)^{0.5}$

$\beta = 0.1 \cdot \left(\frac{d_{nom}}{c_1}\right)^{0.2}$

By assuming the concrete strength class C25/30 according to table 3.1 in [EC2 2005], which have a mean cylindrical compressive strength f_{cm} = 33 MPa (≈ 32.4 MPa), following values is applicable for current case:

$$d_{nom} = 19.1 \quad \text{[mm]}$$
$$l_f = 100 \quad \text{[mm]}$$
$$f_{ck,cube} = 30 \quad \text{[MPa]}$$
$$c_1 = 100 \quad \text{[mm]}$$

The above stated values give a characteristic single anchor bolt capacity of 16.4 kN. In order to establish a normative mean capacity the characteristic compressive concrete strength is replaced by the mean compressive concrete strength f_{cm}, and equation 7-1 is multiplied with an uprating factor of 1.33 (see chapter 6). This gives a mean concrete edge capacity of $V^0_{Rm,c} = 22.9\ kN$. Representative results from the physical tests and the CEN/TS 1992-4-2 capacities are shown in figure 7-5.

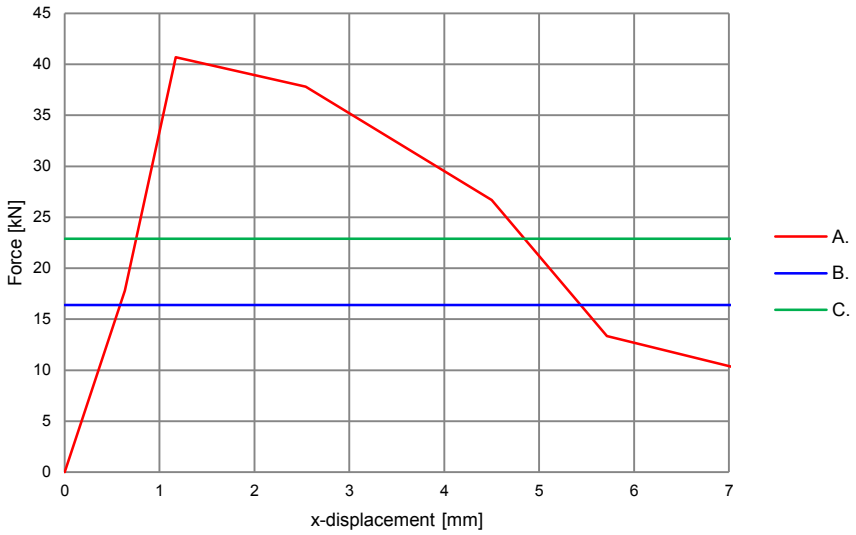

A. Physical test [Hallowell Gross et al. 2001]
B. Characteristic capacity of single anchor bolt according to [CEN/TS 1992-4-2 2009]
C. Predicted mean capacity of single anchor bolt based on [CEN/TS 1992-4-2 2009]

Figure 7-5: Relation between force and displacement for anchor in non-reinforced concrete for physical test and capacity according to CEN/TS 1992-4-2.

As seen in figure 7-5 the presented graph of the physical test behaves somewhat strange before failure load is reached. The structure is getting stiffer as the force increases. This ought to be explained by the flexibility in the test setup. When performing experimental tests the force will not be accurately transmitted until the test setup has completely got into equilibrium state meaning some deformation in the different contact areas of the test setup has to evolve before accurate results may be achieved. The physical test result graph shown in figure 7-5 is furthermore based on a few result points which especially during the phase up to failure mean that important information may be missing.

In figure 7-6 graph D, the graph A of figure 7-5 is modified, i.e. shifted to the left and has the same stiffness as graph A of figure 7-5 just before failure is reached. Hence, graph D in figure 7-6 presents a more credible relation between the force and the displacement in the physical test.

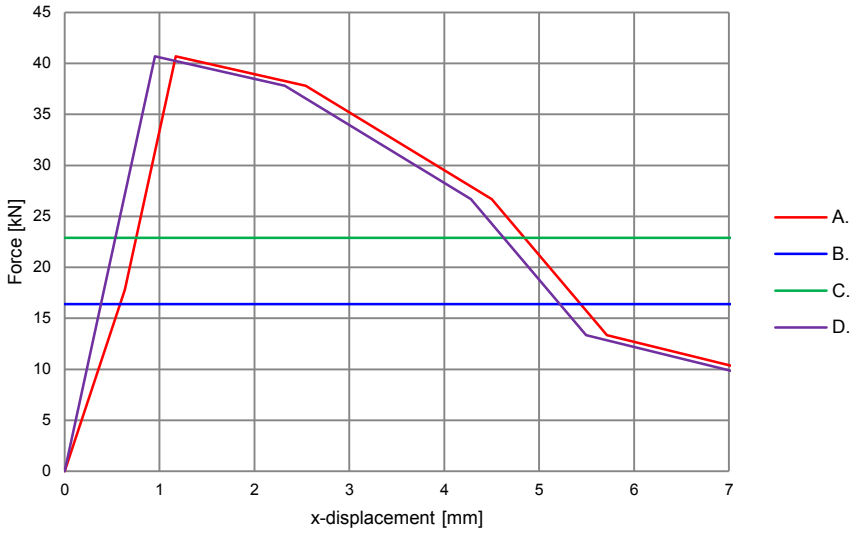

A. Physical test [Hallowell Gross et al. 2001]
B. Characteristic capacity of single anchor bolt according to [CEN/TS 1992-4-2 2009]
C. Predicted mean capacity of single anchor bolt based on [CEN/TS 1992-4-2 2009]
D. Modified force – displacement relation of physical test

Figure 7-6: Relation between force and displacement for anchor in non-reinforced concrete for physical test and capacities according to CEN/TS 1992-4-2.

A reasonable explanation to why the CEN/TS capacity is significantly lower than the physical test peak load is that the code does not consider global stiffness of the concrete as discussed in chapter 6. Due to the relatively small distance between the beams constituting the test frame (see figure 7-1), one may expect confinement effects that is not captured in the code.

The idealized concrete breakout cone surface according to CEN/TS 1992-4-2, section 6.3.5.2.2 in is shown in figure 7-7.

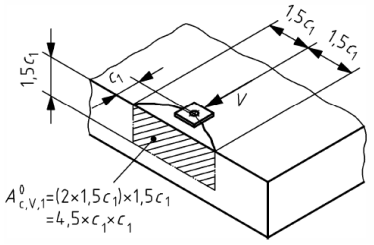

Figure 7-7: Idealized concrete edge breakout surface according to [CEN/TS 1992-4-2 2009].

Since the edge distance c_1 equals 100 mm the ideal width of the breakout surface should be 1.5·100·2=300 mm, and the height ought to be 150 mm. Fracture surfaces from the physical tests are however not available for comparison.

7.3. Numerical simulations of single anchors in shear

7.3.1. Single anchor in non-reinforced concrete

Finite element model

The finite element model comprises a concrete block, an anchor attached to a steel plate and a test frame (rig) as seen in figure 7-8.

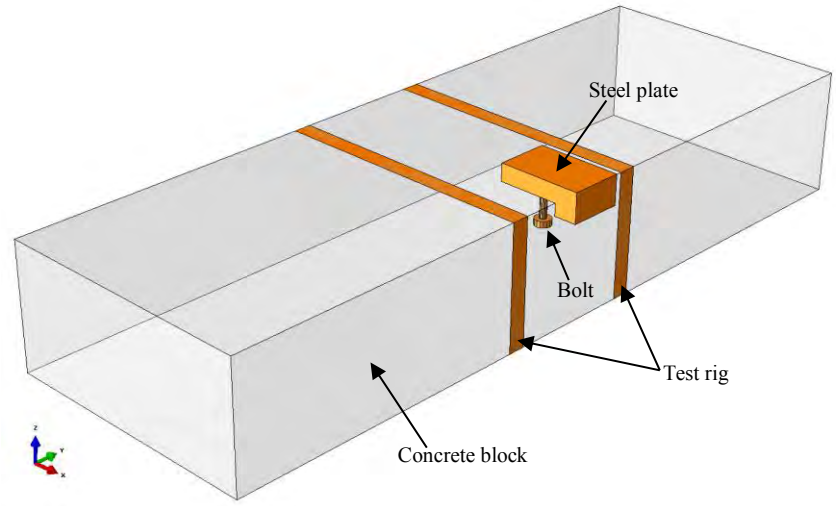

Figure 7-8: Transparent perspective view of the different parts constituting the model.

The concrete, anchor and the steel plate are modelled with 8-node (hexahedra) and 6-node (triangular prisms) solid elements with reduced integration, in Abaqus denominated C3D8R and C3D6R respectively [Dassault Systémes 2010]. The rig serves the purpose of holding the concrete block in place as the steel plate is forced towards the free edge and may be regarded as very stiff. Hence it is modelled with rigid elements, in Abaqus denominated R3D4. The model mesh is symmetrically shown in figure 7-9.

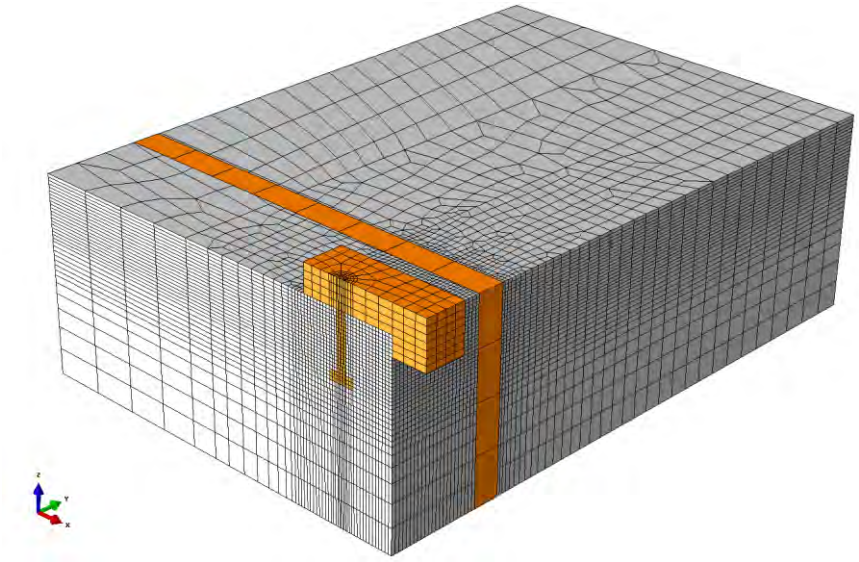

Figure 7-9: Symmetric view-cut of finite element model mesh.

The analyses are performed by applying a displacement rate on the steel plate in the positive x-direction (see figure 7-9). This is done at the level of the concrete upper surface to minimize eccentric effects in accordance with the physical tests. Since the analyses shall simulate a static loading scenario but in Abaqus/Explicit are performed dynamically, the displacement rate is consistently 30 mm/s throughout all numerical simulations. This rate keeps the analyses times to a minimum without adding dynamic effects. The displacement output information is registered throughout the analyses at the back of the steel plate, i.e. at the same location as the potentiometer in the physical test (see figure 7-3).

An element size convergence study has been performed in order to establish a sufficient finite element model mesh. The study resulted in an element size in the dense meshed part of the concrete, i.e. around the anchor bolt of approximately 7 mm. The size of the model that has been used in the analyses is shown in table 7-1.

Table 7-1: Size of non-reinforced FE-model.

Number of elements	Number of nodes	Number of degrees of freedom
~97 800	~104 600	~313 800

As earlier stated the finite element model is modelled with solid elements with reduced integration meaning there is one integration point in each element. When using reduced integration, element deformation modes may appear that causes no strain in the element, i.e. spurious zero energy modes or “hourglassing” [Dassault Systémes 2010]. These modes may lead to severe mesh distortion with no stresses resisting the deformation. In order to prevent hourglassing of elements, Abaqus provides several methods. The available methods in Abaqus/Explicit are divided into two categories named “Integral viscoelastic approach” and “Kelvin viscoelastic approach”. Some of these methods have been studied in order to see what type of hourglass control method best suits the topical numerical simulations. Table 7-2 gives a short description of the studied methods and results from the study are presented in Appendix 2.1.

Table 7-2: Studied Abaqus hourglass control methods.

Approach	Hourglass control method	Description [Dassault Systémes 2010]
Integral viscoelastic	Relax stiffness	Generates more resistance to hourglass forces early in the analysis step where sudden dynamic loading is more probable.
Kelvin viscoelastic	Stiffness	Acts to maintain a nominal resistance to hourglassing throughout the simulation. Recommended for both quasi-static and transient dynamic simulations.
	Enhanced	Represents a refinement of the stiffness method and provides increased resistance to hourglassing for nonlinear materials. May give overly stiff response in problems displaying plastic yielding under bending.
	Viscous	Effective for high-rate dynamic simulations. Is not recommended for low frequency dynamic or quasi-static problems since static loading in hourglass modes will result in excessive hourglass deformation due to the lack of any nominal stiffness.

The results presented in Appendix 2.1 are not based on the same concrete strength values as in the other analyses, i.e. the failure loads are not directly comparative to the physical test results. Anyhow, the intermutual relations between the results show that the pure stiffness and enhanced controls both lead to slightly high relative failure loads but more importantly result in fracture surfaces more like splitting failure rather than concrete edge failure. The conclusion is that the relax stiffness hourglass control method best suits the numerical simulation purpose at hand and is therefore used henceforth.

Boundary conditions
Nodes of the lower surface of the concrete block are restrained to move in vertical direction (z-direction) and in addition one low corner node is prevented from translating in the horizontal directions (x and y), see figure 7-10.

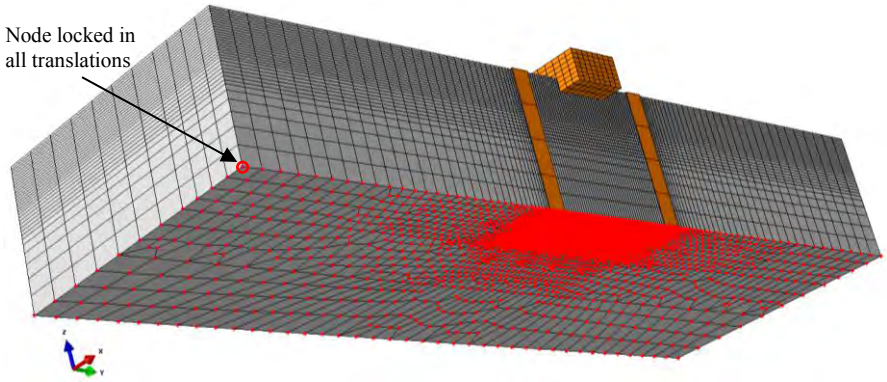

Figure 7-10: Boundary nodes at concrete bottom are highlighted in red.

Apart from the above mentioned boundary conditions the model constitutes some non-linear boundary conditions, i.e. contact definitions. A contact formulation is defined between the rig and the concrete block that prevents the different parts to pass each other's exterior surfaces but allows separation without any tensional stresses. The width of the rigid parts is 50 mm and the inner distance between the two parts is 350 mm. The contact formulation used in the model does not include any friction definition. The same contact behaviour is defined between the anchor bolt and the concrete as well as between the steel plate and the concrete.

Constitutive model

As stated in chapter 4 the finite element program Abaqus provides three different constitutive models for modelling non-linear concrete. The one used throughout this project is named "Concrete Damaged Plasticity" (CDP). The different parameters that need to be specified when using the CDP model and that have been used in the analyses are stated in table 7-3. Each parameter is explained in chapter 5.

Table 7-3: Concrete damaged plasticity parameters utilized in analyses.

Parameter	Description	Value
ψ	Dilation angle	35 degrees
ϵ	Flow potential eccentricity	0.1 (default value)
σ_{b0}/σ_{c0}	Ratio of initial equibiaxial compressive yield stress to initial uniaxial compressive yield stress	1.16 (default value)
K_c	Ratio of the second stress invariant on the tensile meridian to that on the compressive meridian at initial yield for any given value of the pressure invariant such that the maximum principal stress is negative	0.6667 (default value)
μ	Viscosity parameter	N/A in Abaqus/Explicit

Besides the above stated parameters the concrete behaviour is specified in compression and tension according to figure 7-11 and figure 7-12, respectively. For an explanation of these definitions see chapter 5.

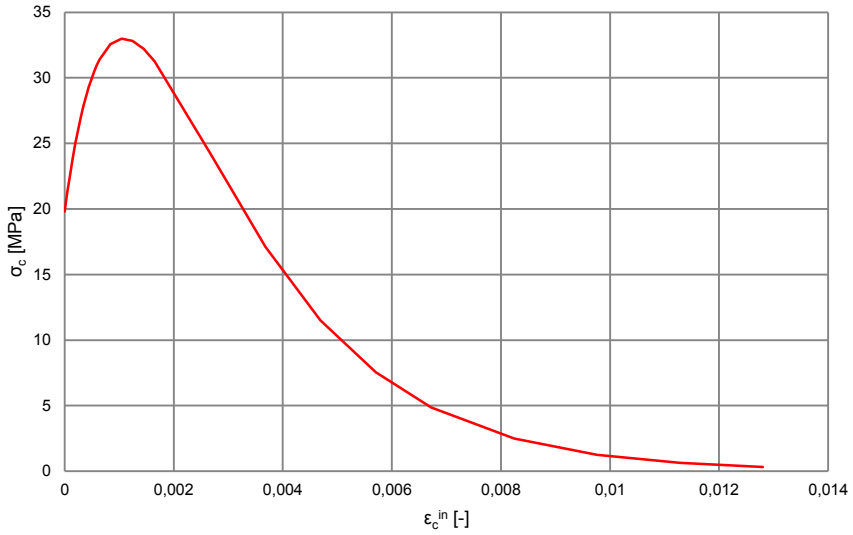

Figure 7-11: Concrete behaviour in compression.

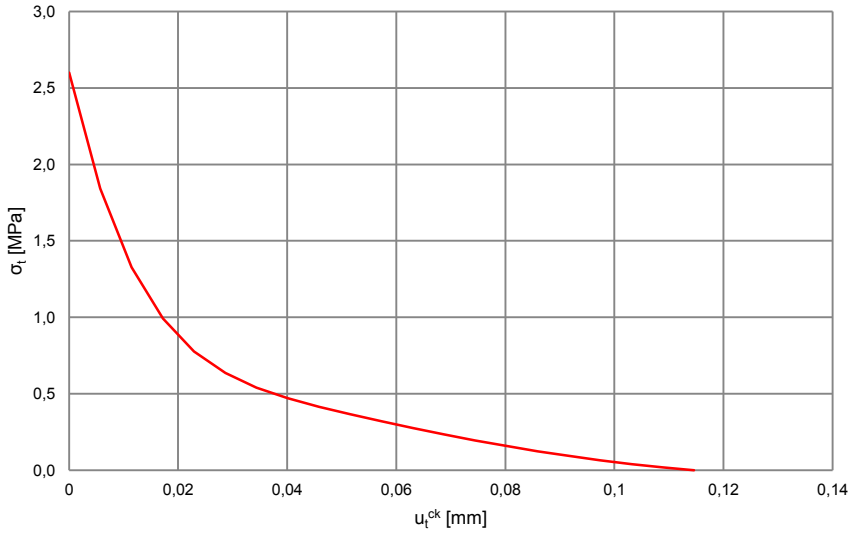

Figure 7-12: Concrete behaviour in tension.

As earlier stated the concrete cylinder compressive strength for the ACI-testing program was 32.4 MPa with a permissible tolerance of ±3.45 MPa [Hallowell Gross et al. 2001]. This is regarded as a mean value corresponding to the Eurocode value denominated f_{cm} [EC2 2005]. The Eurocode concrete class C25/30 has a mean cylindrical compressive strength of f_{cm} = 33 MPa. Equal C25/30 concrete material values used in the analyses are shown in table 7-4.

Table 7-4: Concrete material values used in analyses.

Symbol	Description	Value (20°C)
E	Modulus of elasticity	31.0 GPa
σ_{cu}	Ultimate compressive stress	33.0 MPa
σ_{t0}	Failure tensile stress	2.6 MPa
ν	Poisson's ratio	0.2
ρ	Density	2400 kg/m^3

The steel constituting the anchor bolt, the steel plate and the rebar reinforcement is modelled elastically with values according to table 7-5.

Table 7-5: Steel material values used in analyses.

Symbol	Description	Value (20°C)
E	Modulus of elasticity	210.0 GPa
ν	Poisson's ratio	0.3
ρ	Density	7800 kg/m^3

Results – A comparison with physical test results

Results in terms of force-displacement relations from analysis of the finite element model described in section 7.3.1 together with modified physical test results are shown in figure 7-13.

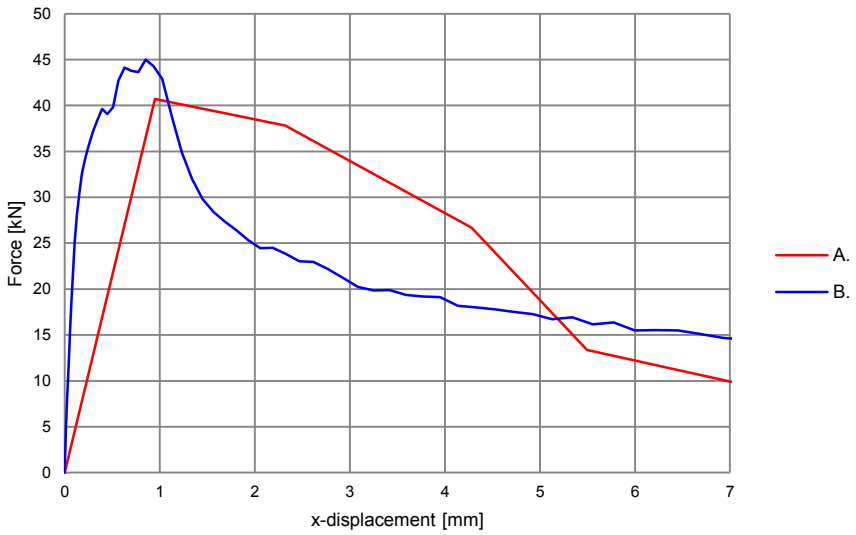

A. Modified force – displacement relation of physical test [Hallowell Gross et al. 2001]
B. Numerical simulation results with FE-model as described in section 7.3.1.

Figure 7-13: Relation between force and displacement for anchor in non-reinforced concrete for physical test and FE-analysis.

The idealized concrete breakout cone surface according to CEN/TS 1992-4-2, 6.3.5.2.2 is shown in figure 7-7 and corresponding breakout cone from the FE-analysis is shown in figure 7-14. Since the edge distance c_1 equals 100 mm the ideal width of the breakout surface should be $1.5 \cdot 100 \cdot 2 = 300$ mm, and the height ought to be 150 mm. Mentioned distances are shown together with FE-analysis fracture surface results in figure 7-14.

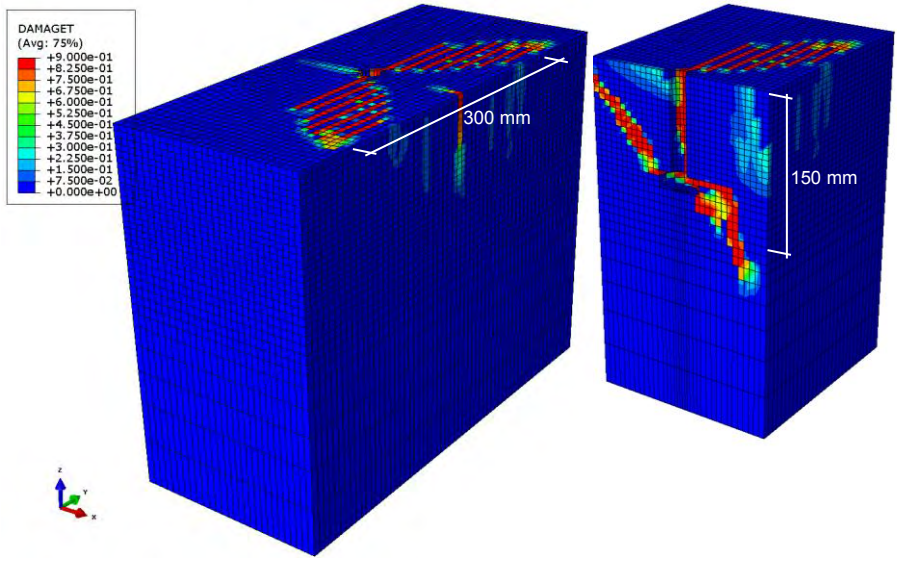

Figure 7-14: Damage tension parameter at 7 mm of x-displacement.

As seen in figure 7-13, the main difference between the results of the physical tests and the numerical simulation results is the initial stiffness. However, the failure load magnitude and the concrete fracture surface are in good compliance with expected results.

7.3.2. Parametric study of material properties

As the simulation results presented in section 7.3.1 show good agreement with physical test results, the constitutive material model utilized in the simulations is considered appropriate for the task at hand. Nevertheless, there are several important parameters that need to be specified when using the Abaqus - Concrete Damaged Plasticity model. Section 7.3.2 serves the purpose of confirming what impact some crucial parameters may have on the numerical simulation results. The constitutive model presented in chapter 5 together with the "best estimate" input values presented in section 7.3.1 is the material model setup that has been used in the main numerical simulations. Hence, the results presented within section 7.3.2, and the objective with the parametric study is mainly for comparative reasons and verification of the already established concrete material model.

In each and every study one parameter is changed at a time whereupon its impact on the results is noted. In the physical tests, the peak load was established to approximately 41 kN, see figure 7-13.

Dilation angle

The dilation angle is normally specified in the range $30 \leq \psi \leq 40$ degrees. In order to obtain a reasonable value three analyses have been run with three different dilation angles, viz. 28°, 35° and 40°.

Results in terms of force-displacement relations from the above mentioned analyses are shown in figure 7-15.

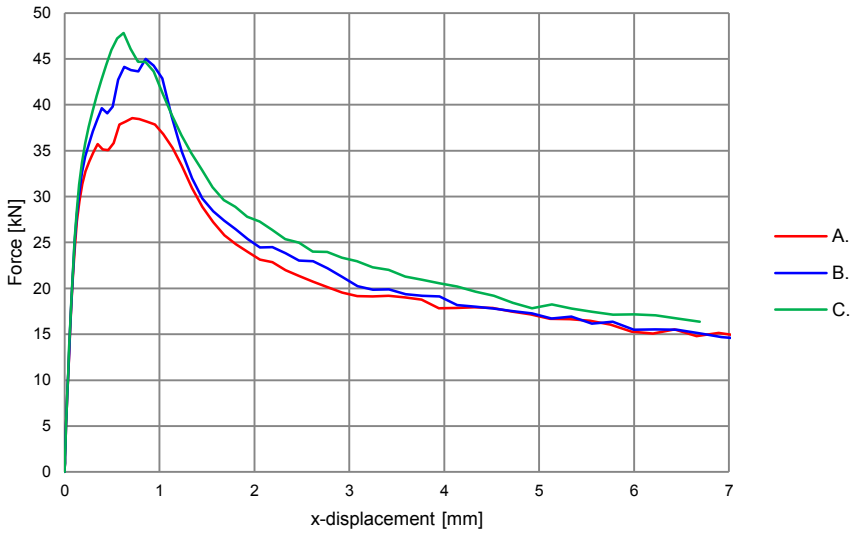

A. Dilation angle 28°
B. Dilation angle 35° (used in main analysis, described in section 7.3.1)
C. Dilation angle 40°

Figure 7-15: Relation between force and displacement for different dilation angles.

In table 7-6 the different failure loads for each dilation angle are presented. The figures referred to show fracture surfaces where part of the concrete block in the vicinity of the anchor bolt is visualized. Additional result plots are presented in Appendix 2.2.

Table 7-6: Dilation angle with corresponding failure load and fracture surface.

Dilation angle ψ	Failure load [kN]	Fracture surface
28	38.5	See figure 7-16
35	45.0	See figure 7-17
40	47.8	See figure 7-18

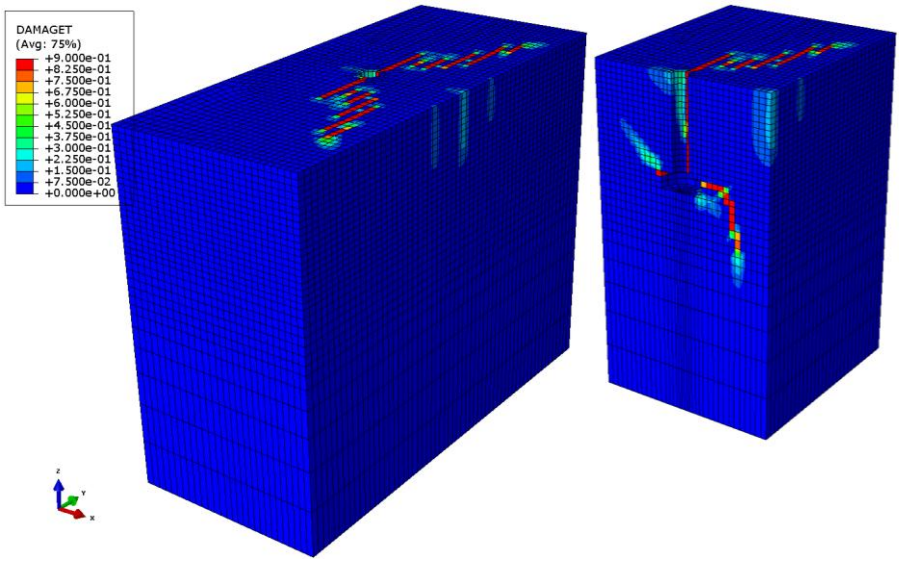

Figure 7-16: Dilation angle 28°. Damage tension parameter at the time of peak load (38.5kN).

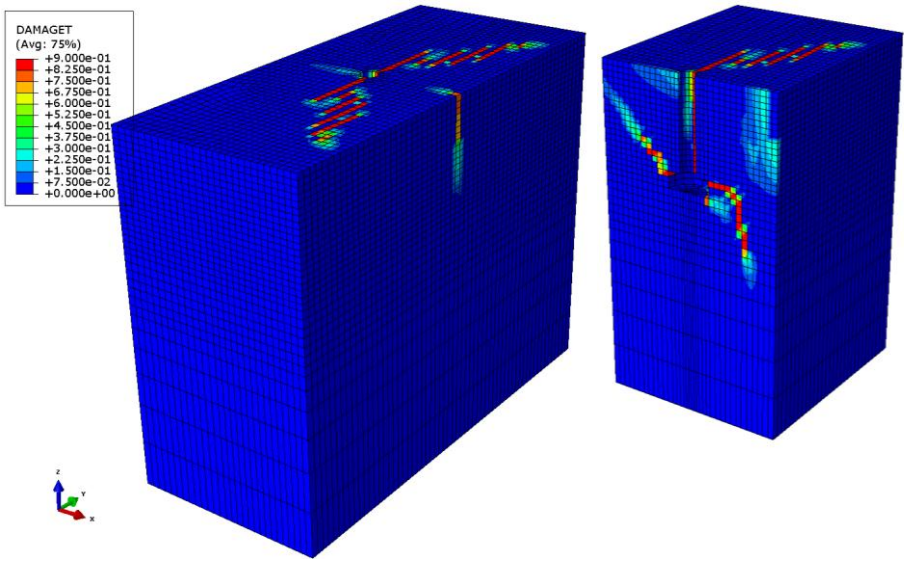

Figure 7-17: Dilation angle 35°. Damage tension parameter at the time of peak load (45.0kN).

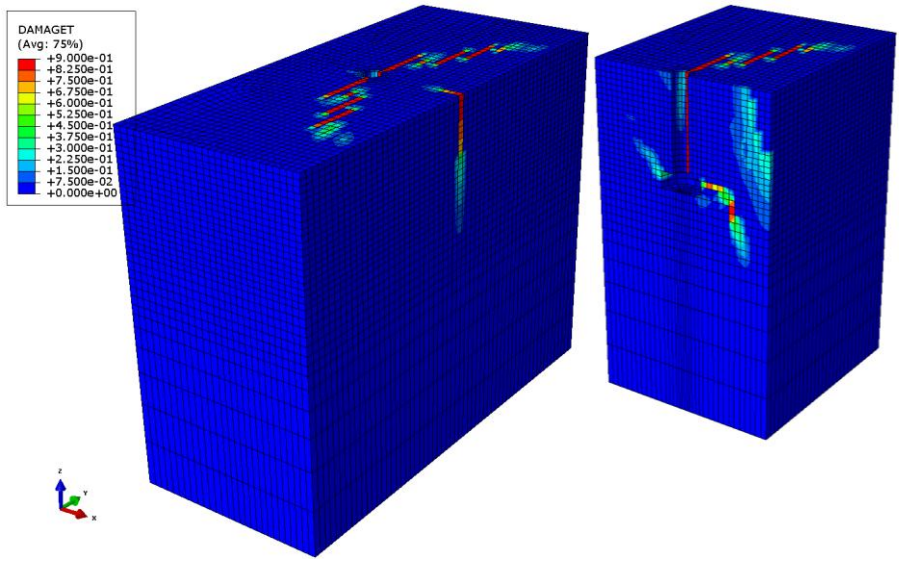

Figure 7-18: Dilation angle 40°. Damage tension parameter at the time of peak load (47.8kN).

Considering the three dilation angles that have been tried out there is no deviation of significant importance between the fracture surfaces. The failure load is however best captured when using dilation angle 35°, hence regarded as the more appropriate dilation angle value.

Fracture energy

The fracture energy may be calculated according to CEB-FIP model code 1990 [Comité Euro-International du Beton 1991] in the following manner:

$$G_F = G_{F0}\left(\frac{f_{cm}}{f_{cm0}}\right)^{0.7}$$

With f_{cm0} = 10 MPa and base value of fracture energy G_{F0} depending on maximum aggregate size according to table 7-7.

Table 7-7: Base values of fracture energy [Comité Euro-International du Beton 1991]

d_{max} [mm]	G_{F0} [Nm/m^2]
8	25
16	30
32	58

Three different maximum aggregate sizes have been tried, viz. 8, 20 and 32 mm. Based on these, corresponding fracture energies are calculated which below is exemplified for d_{max} = 20 mm. The value of f_{cm} is taken as 33 MPa since this was the approximate target compressive capacity in the physical tests made at the University of Texas, see section 7.2.1.

$$G_{F0} = \frac{(58-30)}{(32-16)} \cdot (20-16) + 30 = 37\ Nm/m^2$$

$$G_F = 37 \cdot \left(\frac{33}{10}\right)^{0.7} = 85\ Nm/m^2$$

Corresponding calculation for maximum aggregate sizes 8 and 32 mm gives fracture energies 58 Nm/m^2 and 134 Nm/m^2, respectively. The concrete tension behaviour for the different fracture energies investigated is presented in figure 7-19 and figure 7-20.

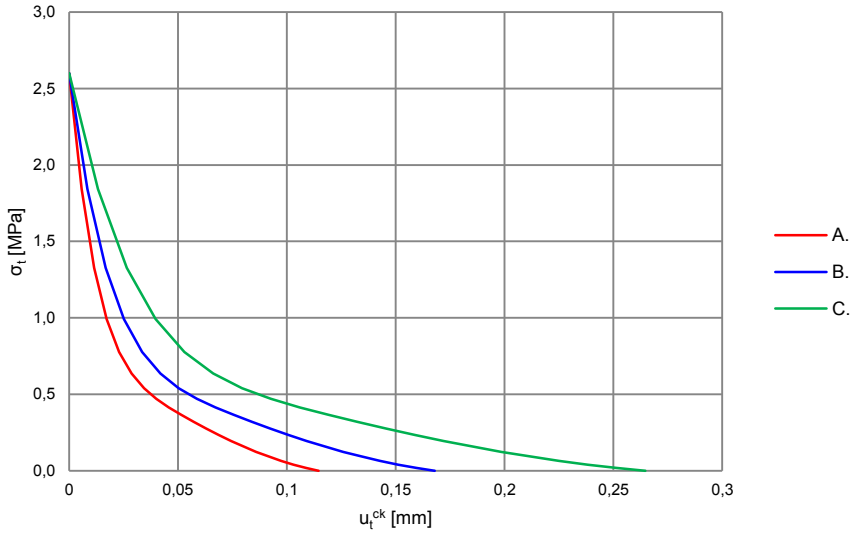

A. G_F = 58 Nm/m^2
B. G_F = 85 Nm/m^2
C. G_F = 134 Nm/m^2

Figure 7-19: Concrete behaviour in tension for different fracture energies.

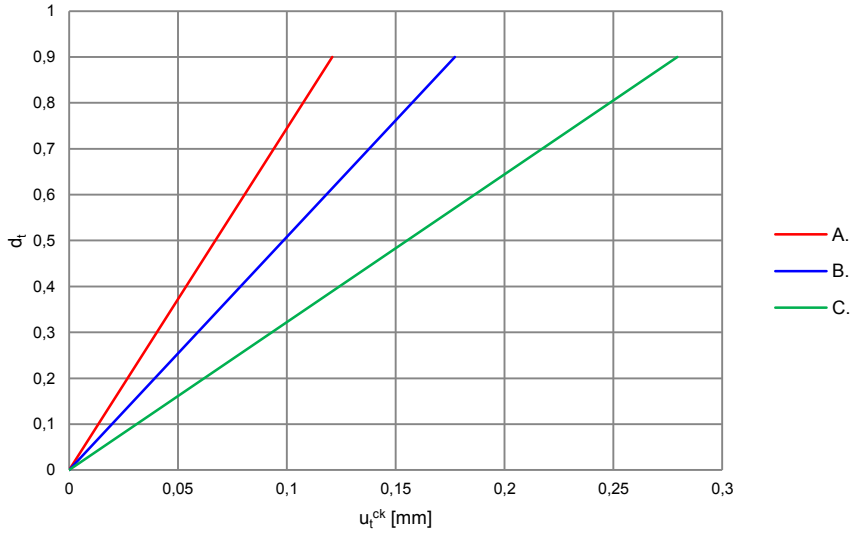

A. G_F = 58 Nm/m^2
B. G_F = 85 Nm/m^2
C. G_F = 134 Nm/m^2

Figure 7-20: Concrete tension damage parameter for different fracture energies.

Since the fracture energy only affects the tensional behaviour the compressive behaviour is equally defined for all three fracture energies, see figure 7-11. Results in terms of force-displacement relations for the three different fracture energies are shown in figure 7-21.

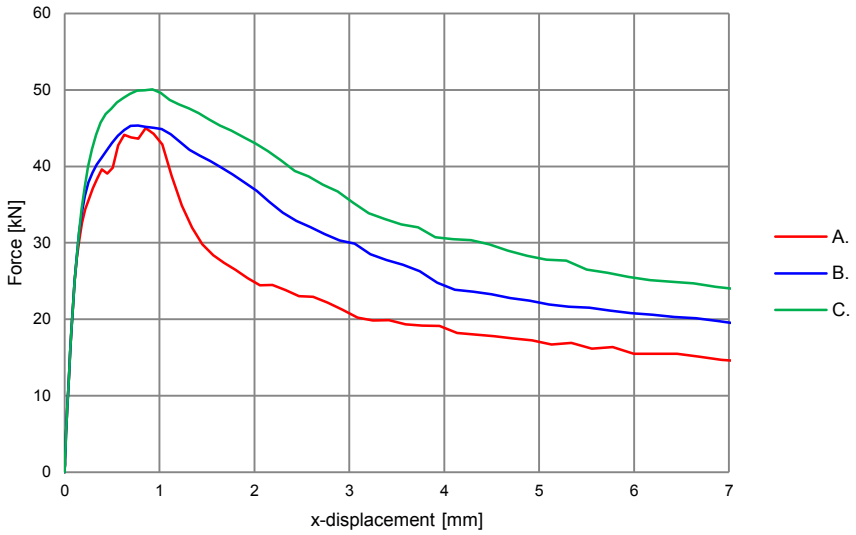

A. G_F = 58 Nm/m^2 (main analysis as described in section 7.3.1)
B. G_F = 85 Nm/m^2
C. G_F = 134 Nm/m^2

Figure 7-21: Relation between force and displacement for different fracture energies.

In table 7-8, the failure loads for each investigated fracture energy is presented. The figures referred to show fracture surfaces where part of the concrete block in the vicinity of the anchor bolt is visualized. Additional result plots are presented in Appendix 2.3.

Table 7-8: Maximum aggregate sizes and corresponding fracture energies.

d_{max} [mm]	G_F [Nm/m^2]	Failure load [kN]	Fracture surface
8	58	45.0	See figure 7-22
20	85	45.3	See figure 7-23
32	134	49.9	See figure 7-24

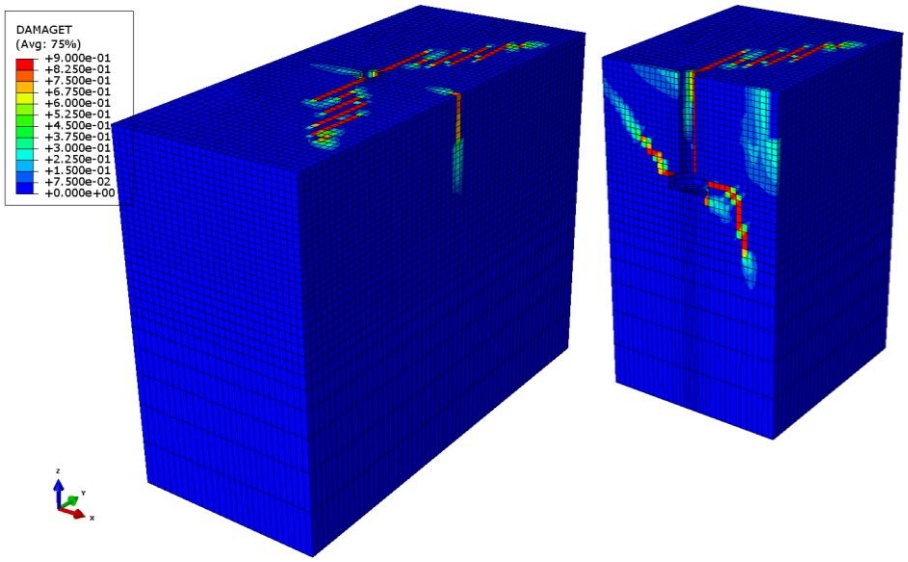

Figure 7-22: Damage tension parameter at the time of peak load for concrete with fracture energy 58 Nm/m^2 (dilation angle 35^o).

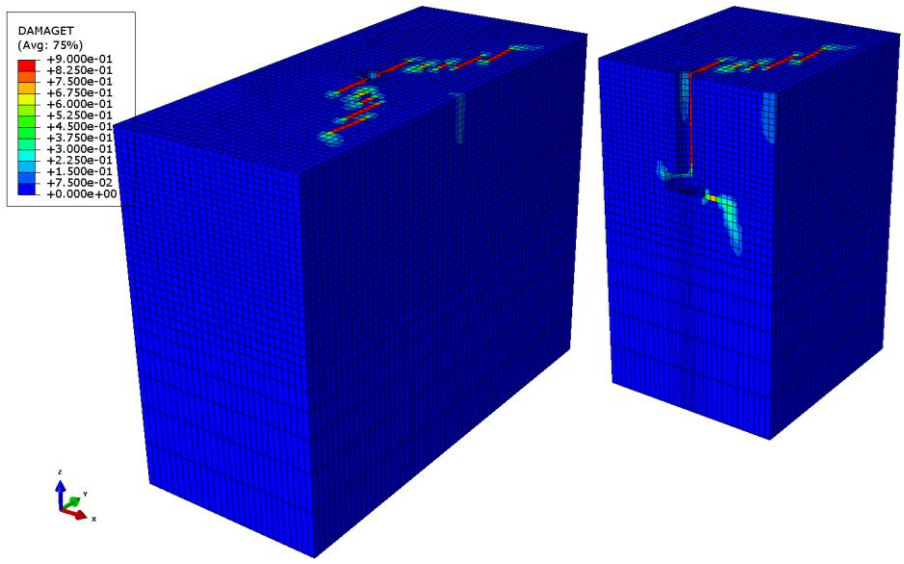

Figure 7-23: Damage tension parameter at the time of peak load for concrete with fracture energy 85 Nm/m^2 (dilation angle 35^o).

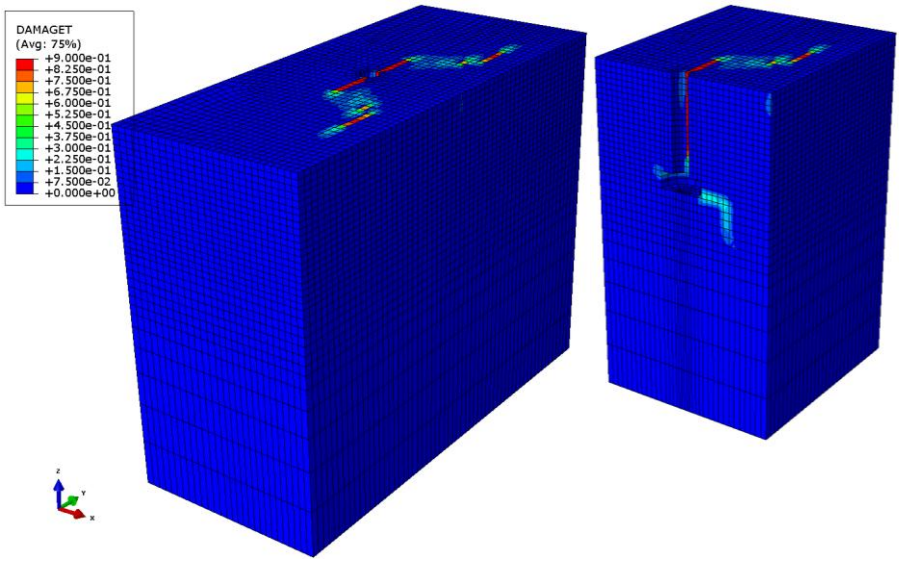

Figure 7-24: Damage tension parameter at the time of peak load for concrete with fracture energy 134 Nm/m^2 (dilation angle 35^o).

As stated in section 7.2.1, the concrete used in the physical tests was created with river-gravel. The report "*Dynamic Behavior of Single and Double Near-Edge Anchors Loaded in Shear*" does not however specify the aggregate size. According to the geological Wentworth scale, gravel may have aggregate sizes in the span from 2 to 64 mm [Gordon et al. 2004].

The analysis results regarding failure load magnitude show that fracture energies 58 Nm/m^2 and 85 Nm/m^2 conform to physical test results well. However, the fracture surface seen in figure 7-22 looks much like what to be expected. Based on these conclusions the fracture energy value of 58 Nm/m^2 (aggregate size 8 mm) is regarded as the appropriate choice.

Concrete crushing

The concrete behaviour in compression may be defined with crush meaning that when a certain maximum strain in an element have been reached, the element will collapse and not be active in the proceeding of the analysis. This behaviour is usually present in normative documents regarding concrete structures but may lead to convergence problems in numerical simulations. By instead define the concrete compressive behaviour without crushing as seen in figure 7-25, the analyses can be driven further and still conclude reliable results. The upper total compressive strain limit is commonly taken as 3.5 ‰. This is also the value that has been used in current study.

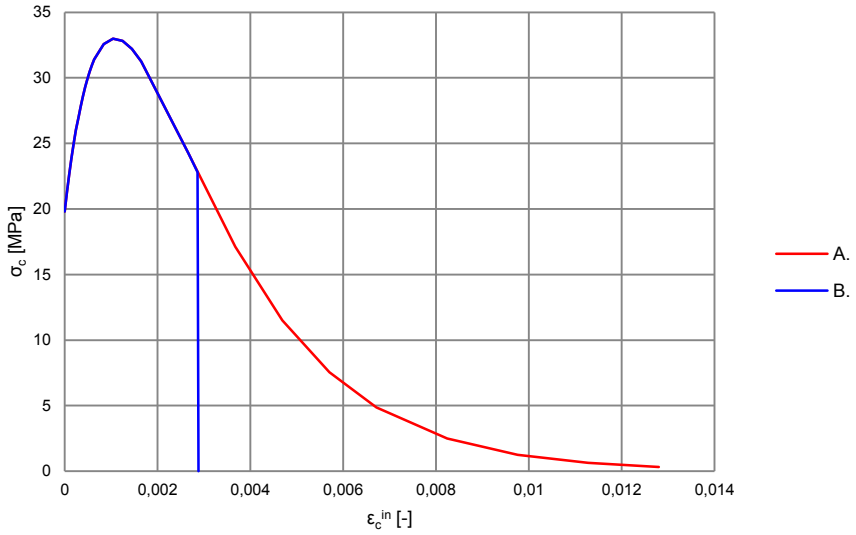

A. Concrete without crush (main analysis as described in section 7.3.1)
B. Concrete with crush

Figure 7-25: Definitions of concrete behaviour in compression.

Results in terms of force-displacement relations for the two different ways of defining the concrete compressive behaviour are shown in figure 7-26.

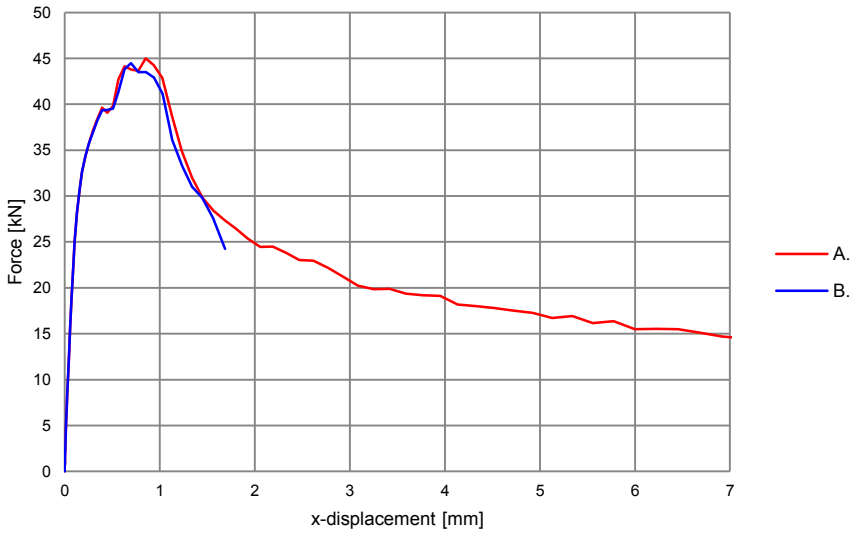

A. Concrete without crush (main analysis as described in section 7.3.1)
B. Concrete with crush

Figure 7-26: Relation between force and displacement for different concrete compressive behaviours.

Figure 7-27 and 7-28 show fracture surfaces for concrete without crush and with crush, respectively. Part of the concrete block in the vicinity of the anchor bolt is visualized.

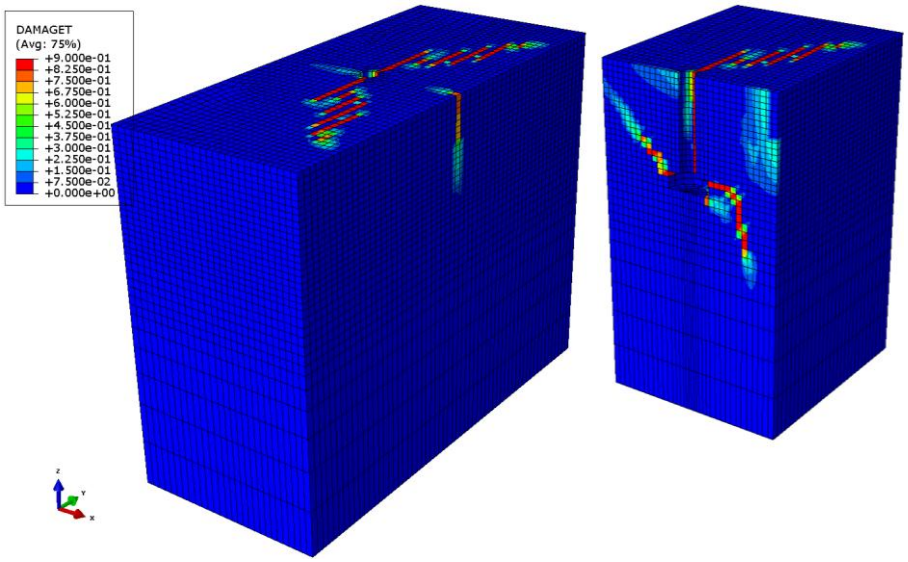

Figure 7-27: Concrete without crush. Damage tension parameter at the time of peak load (45.0kN).

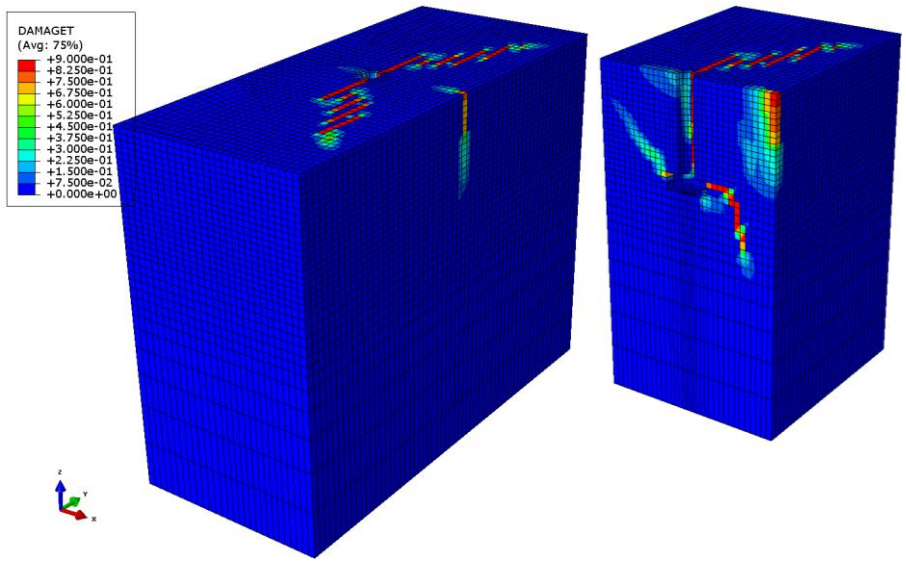

Figure 7-28: Concrete with crush. Damage tension parameter at the time of peak load (44.5kN).

The above presented results show that the difference between defining the concrete with or without crush is negligible. Since the analyses may be driven further without convergence problems when using the "Concrete without crush"-definition this is regarded as the more appropriate way of modelling the concrete compressive behaviour.

7.3.3. Single anchor in reinforced concrete

In analyses with reinforced concrete, the rebars are modelled with two-node beam elements. These beam elements are in Abaqus denominated B31 [Dassault Systémes 2010]. In order to captivate the physical interaction between the reinforcement and the concrete, the response of the surrounding concrete is used to constrain the translational degrees of freedom of the embedded beam element nodes (the rebar reinforcement).

Reinforcement in longitudinal direction

The diameter of the rebars is 12 mm and the spacing amounts to 150 mm. The concrete cover is 30 mm. Apart from the longitudinal reinforcement, the finite element model is the same as the model described in section 7.3.1. The different parts constituting the model are shown in figure 7-29.

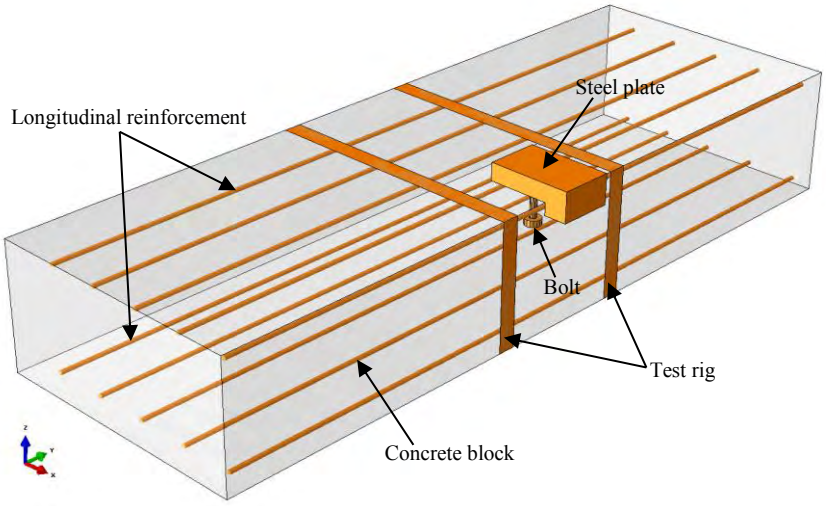

Figure 7-29: Transparent perspective view of the different parts constituting the longitudinally reinforced concrete model.

For further information on the finite element model and the constitutive material model see section 7.3.1. Results in terms of force-displacement relations for a non-reinforced concrete model and the FE-model including longitudinal reinforcement are shown in figure 7-30. Corresponding fracture surface is shown in figure 7-31. Additional result plots are presented in Appendix 2.4.

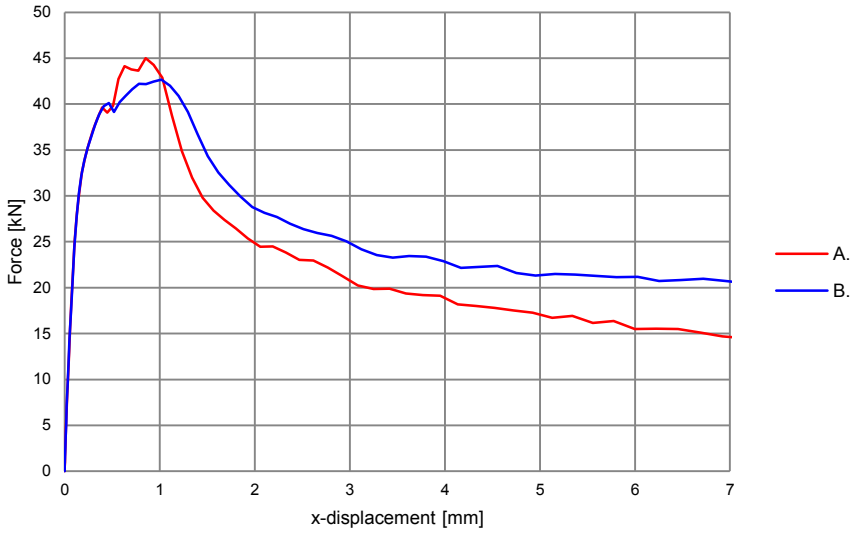

A. Non-reinforced concrete (main analysis as described in section 7.3.1)
B. Longitudinal reinforcement Φ12 cc 150 mm

Figure 7-30: Relation between force and displacement for single anchor in non-reinforced and longitudinally reinforced concrete.

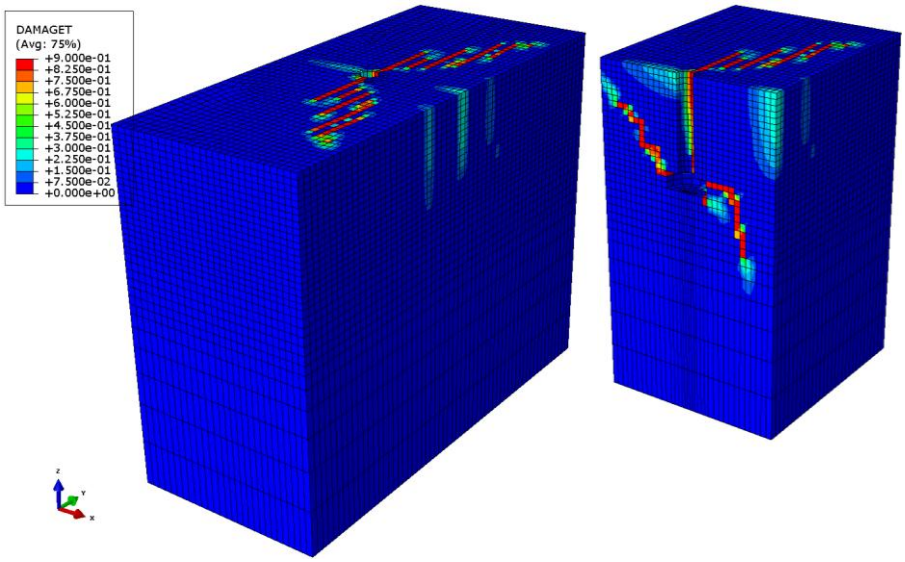

Figure 7-31: Damage tension parameter for longitudinally reinforced concrete at the time of peak load (42.6kN).

The maximum rebar normal force amount approximately 21.3kN (188 MPa) and occurs after the failure load has been reached, see figure 7-32. This means that after the concrete has failed and cracks have developed the reinforcement gets more utilized.

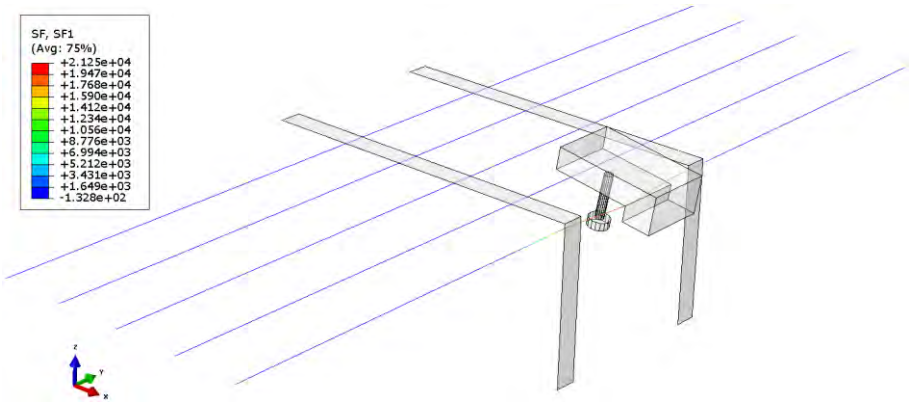

Figure 7-32: Maximum rebar normal force (21.3kN). Deformations are scaled by a factor 3.

Since there is only one rebar located between the anchor bolt and the concrete edge, this is the only one affecting the results for actuated shear loading scenario. As earlier stated the maximum rebar normal force is 21.3kN, resulting in a normal stress of 188 MPa. As stated in section 7.3.1 the steel is elastically modelled. By anyhow assuming a reasonable steel yield value of f_y = 450 MPa one can conclude that the rebar is moderately utilized. Since there is no reinforcement in the direction of the applied load the force will not be anchored more than for a non-reinforced concrete. This conclusion consorts with the results presented in figure 7-30 where the peak loads are much alike, whilst the reinforcement brings some ductile effect in relation to the non-reinforced concrete.

Shear reinforced concrete

The diameter of the rebars is consistently 12 mm but different reinforcement setups, e.g. spacing has been studied in different cases. For cases without shear reinforcement eccentricities, the anchor bolt is located between the rebars meaning the shear reinforcement is symmetrically placed around the anchor bolt. The concrete cover with respect to the longitudinal reinforcement is 30 mm and 18 mm to the shear reinforcement.

Apart from the reinforcement, the finite element model is the same as the model described in section 7.3.1. The different parts constituting the model are shown in figure 7-33.

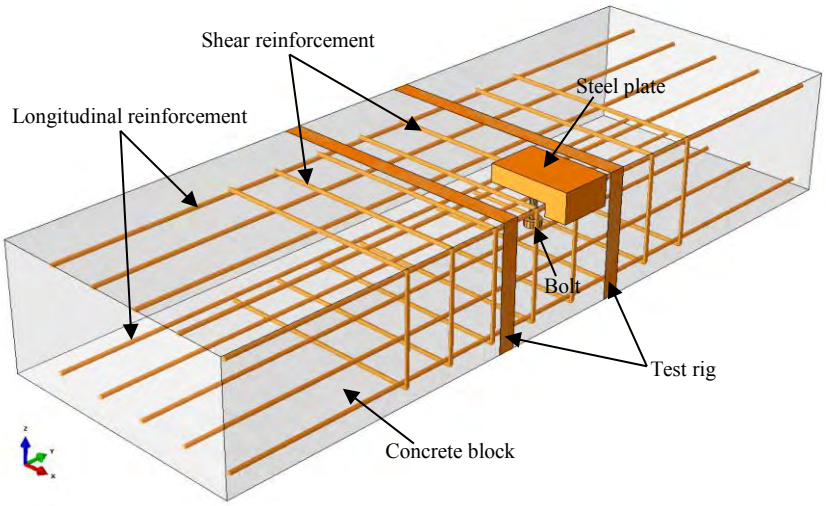

Figure 7-33: Transparent perspective view of the different parts constituting the shear reinforced concrete model.

For further information on the finite element model and the constitutive material model see section 7.3.1. Results in terms of force-displacement relations for non-reinforced concrete and different types of reinforcement setups are shown in figure 7-34. Figure 7-35 show the reinforcement placing around the anchor bolt with different shear reinforcement eccentricities.

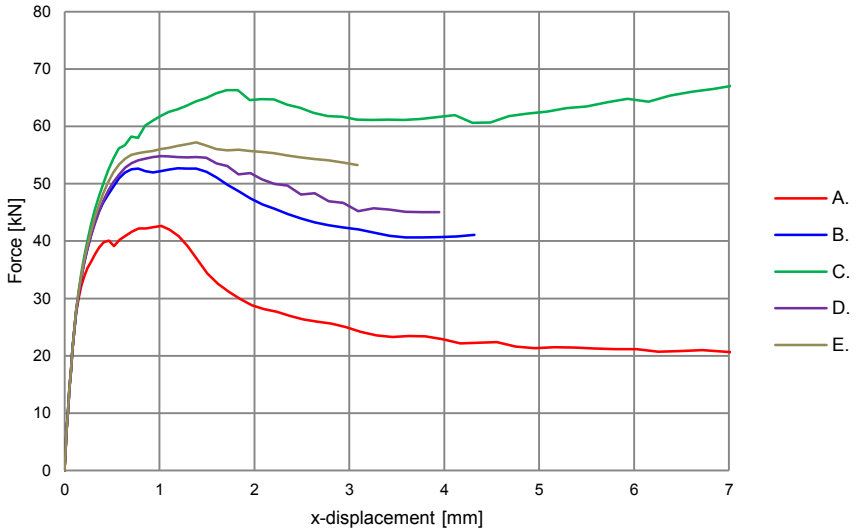

A. Longitudinal reinforcement Φ12cc150
B. Longitudinal reinforcement Φ12cc150 + shear reinforcement Φ12cc150
C. Longitudinal reinforcement Φ12cc150 + shear reinforcement Φ12cc100
D. Longitudinal reinforcement Φ12cc150 + 25 mm ecc. shear reinforcement Φ12cc150 (see figure 7-35 for description of reinforcement setup)
E. Longitudinal reinforcement Φ12cc150 + 40 mm ecc. shear reinforcement Φ12cc150 (see figure 7-35 for description of reinforcement setup)

Figure 7-34: Relation between force and displacement for different reinforcement setups.

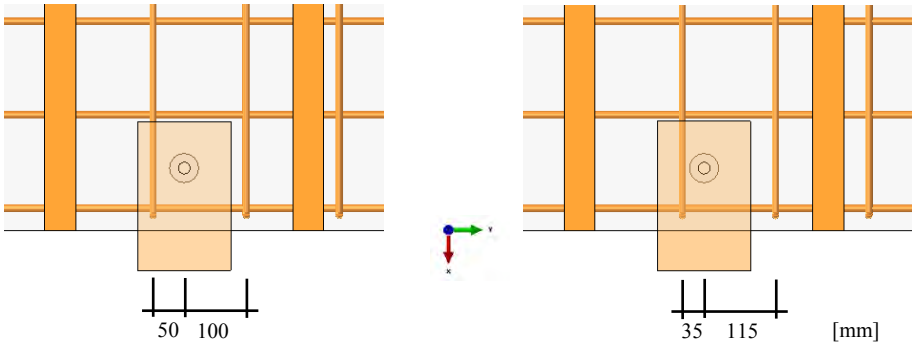

Figure 7-35: Top views showing reinforcement setups. To the left the shear reinforcement has a 25 mm eccentricity and to the right a 40 mm eccentricity.

In table 7-9 the failure load for the different reinforcement setups is presented. The figures referred to show fracture surfaces where part of the concrete block in the vicinity of the anchor bolt is visualized. Additional result plots are presented in Appendix 2.5-2.8.

Table 7-9: Failure load magnitudes and fracture surfaces for the different reinforcement setups presented in figure 7-34.

Reinforcement setup (see figure 7-34)	Failure load [kN]	Fracture surface
A	42.6	See figure 7-31
B	52.6	See figure 7-36 to 7-40
C	66.3	See figure 7-41 to 7-45
D	54.8	See figure 7-46 to 7-50
E	57.2	See figure 7-51 to 7-55

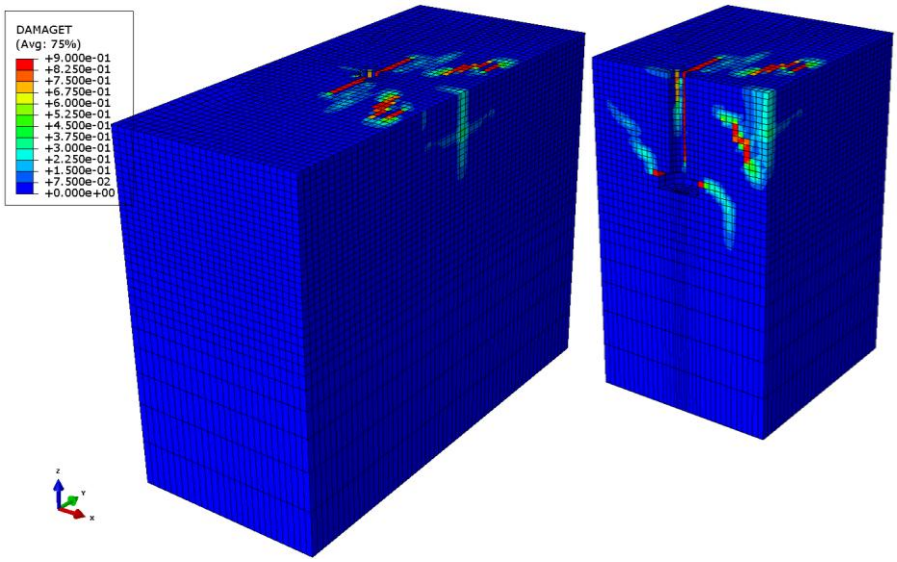

Figure 7-36: Reinforcement setup B. Damage tension parameter at the time of peak load (52.6 kN).

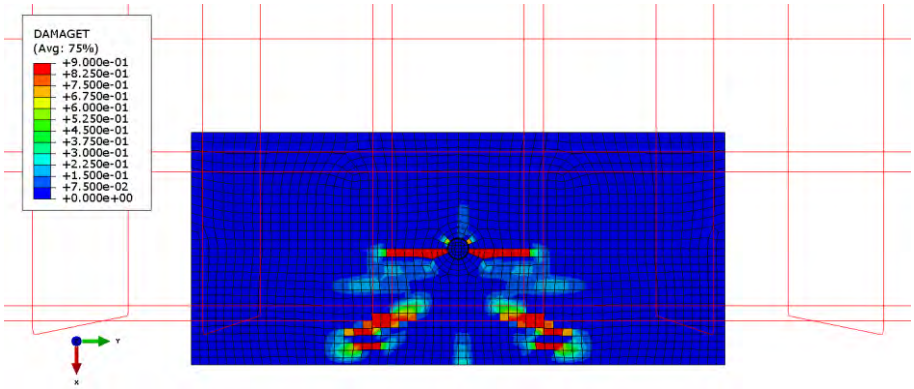

Figure 7-37: Reinforcement setup B. Top perspective view with highlighted reinforcement. Damage tension parameter at the time of peak load (52.6kN).

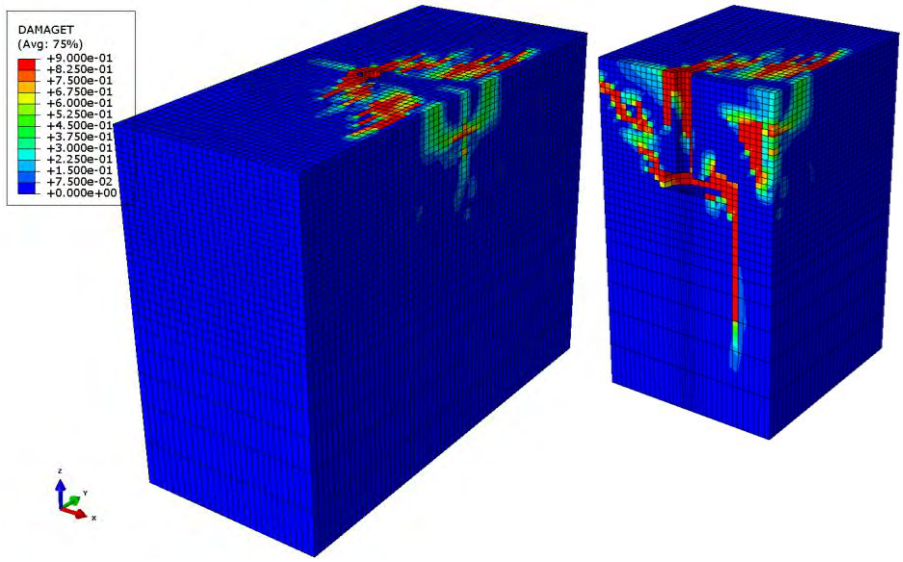

Figure 7-38: Reinforcement setup B. Damage tension parameter at the last increment.

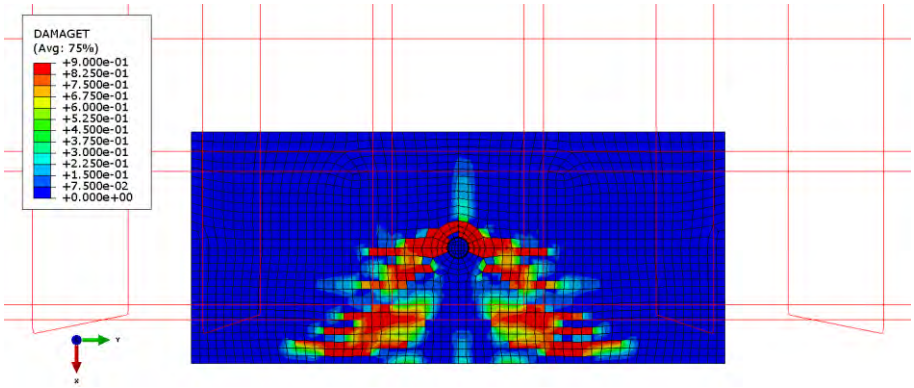

Figure 7-39: Reinforcement setup B. Top perspective view with highlighted reinforcement. Damage tension parameter at the last increment.

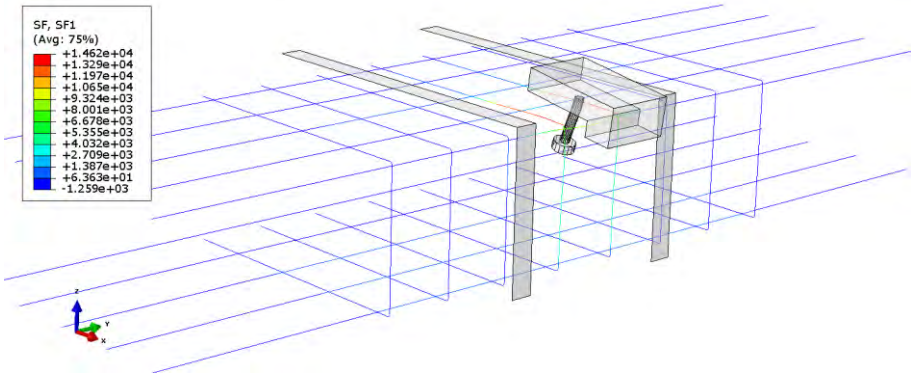

Figure 7-40: Reinforcement setup B. Maximum rebar normal force (14.6kN / 129 MPa). Deformations are scaled 10 times.

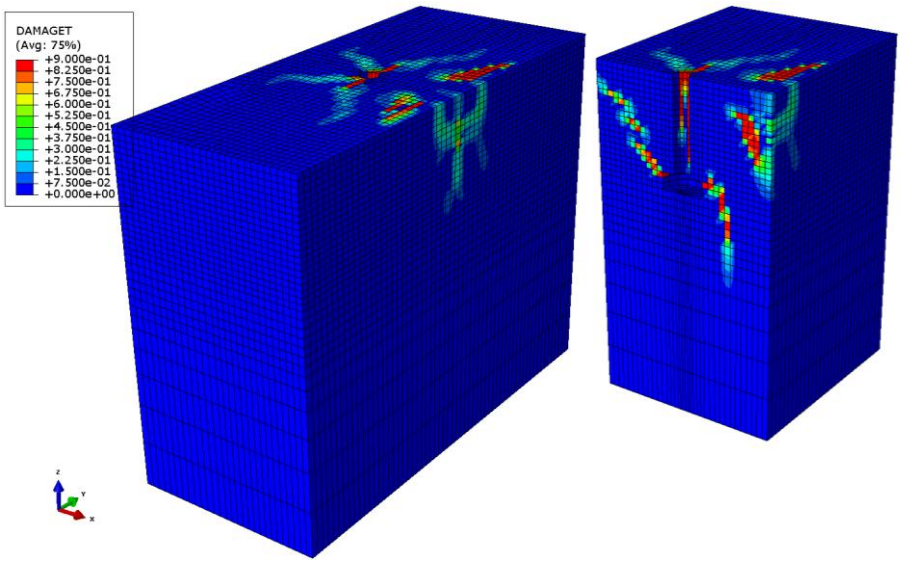

Figure 7-41: Reinforcement setup C. Damage tension parameter at the time of peak load (66.3kN).

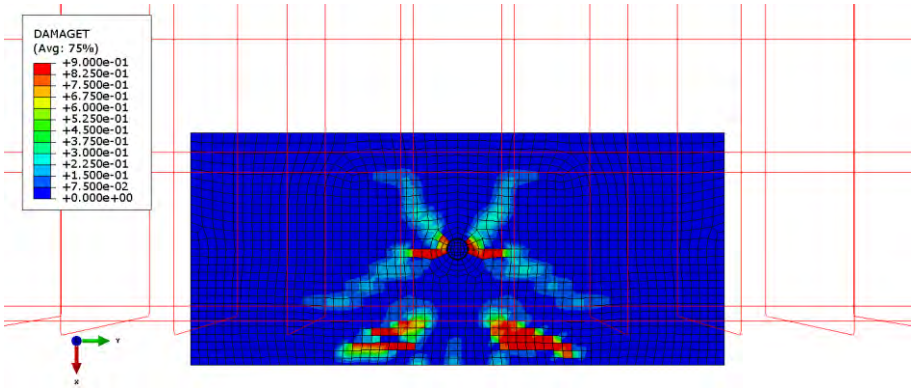

Figure 7-42: Reinforcement setup C. Top perspective view with highlighted reinforcement. Damage tension parameter at the time of peak load (66.3kN).

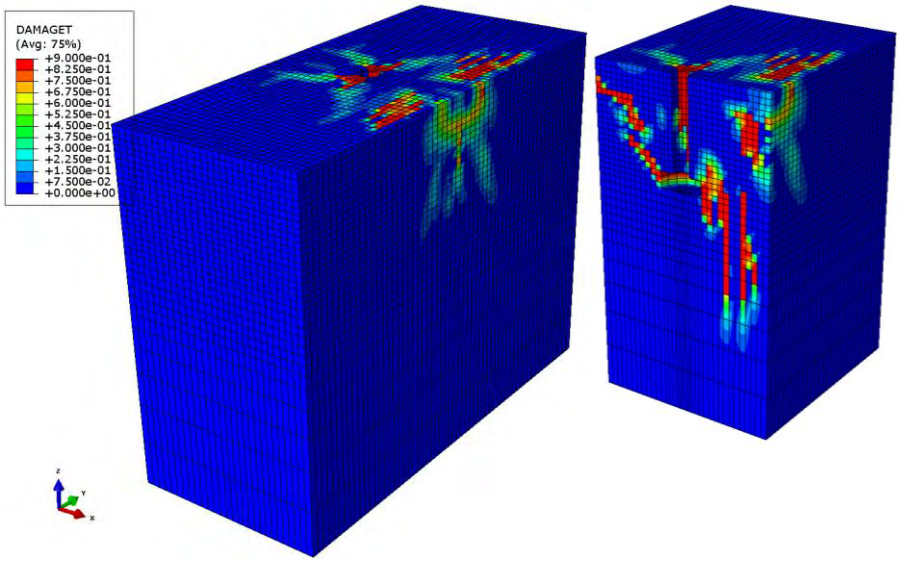

Figure 7-43: Reinforcement setup C. Damage tension parameter at the last increment.

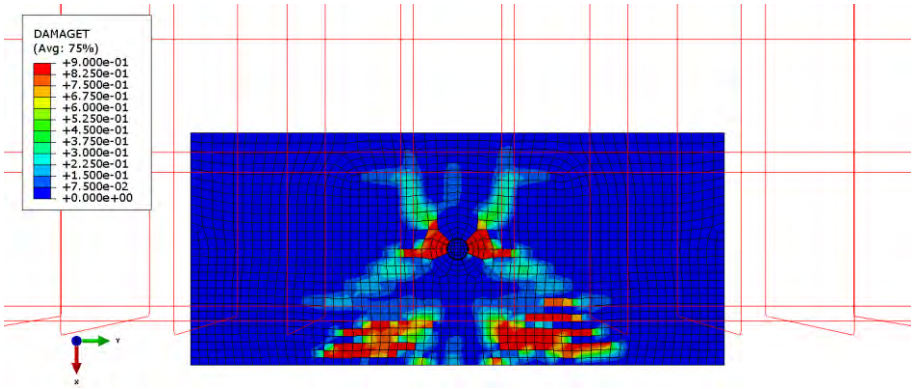

Figure 7-44: Reinforcement setup C. Top perspective view with highlighted reinforcement. Damage tension parameter at the last increment.

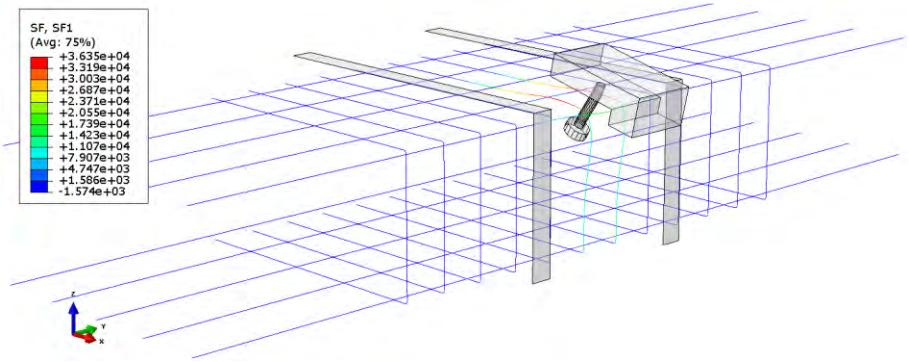

Figure 7-45: Reinforcement setup C. Maximum rebar normal force (36.4kN / 321 MPa). Deformations are scaled 10 times.

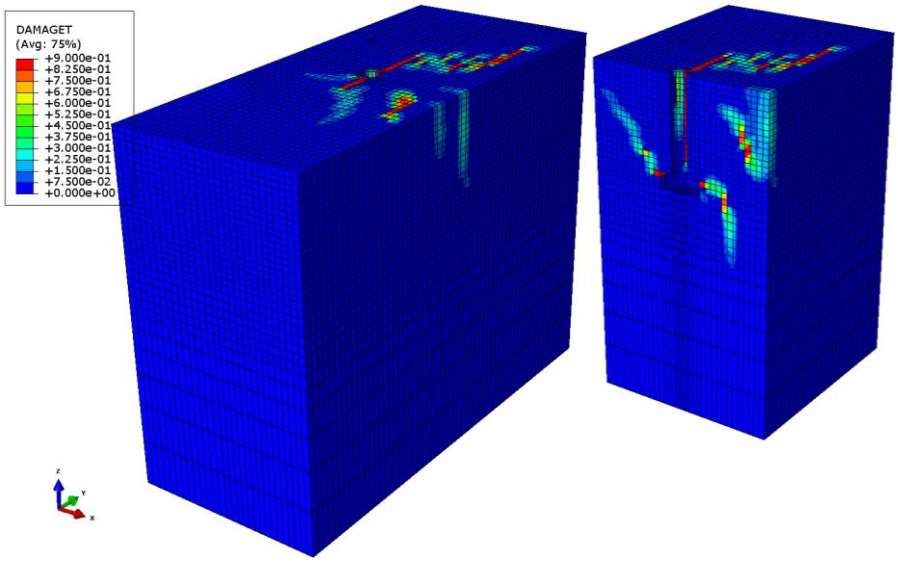

Figure 7-46: Reinforcement setup D. Damage tension parameter at the time of peak load (54.8kN).

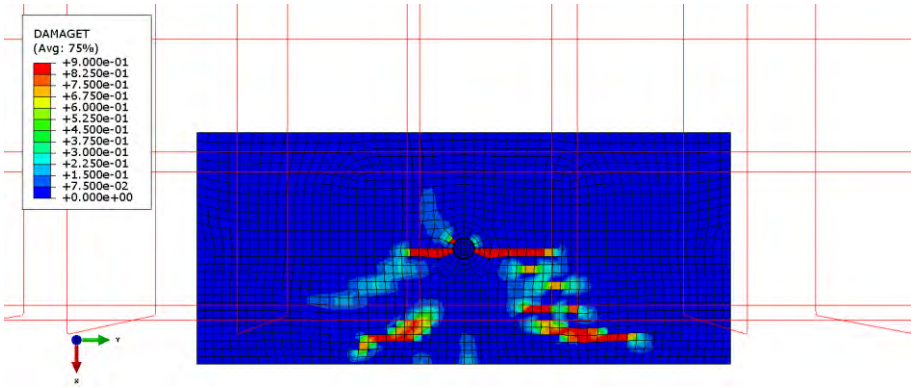

Figure 7-47: Reinforcement setup D. Top perspective view with highlighted reinforcement. Damage tension parameter at the time of peak load (54.8kN).

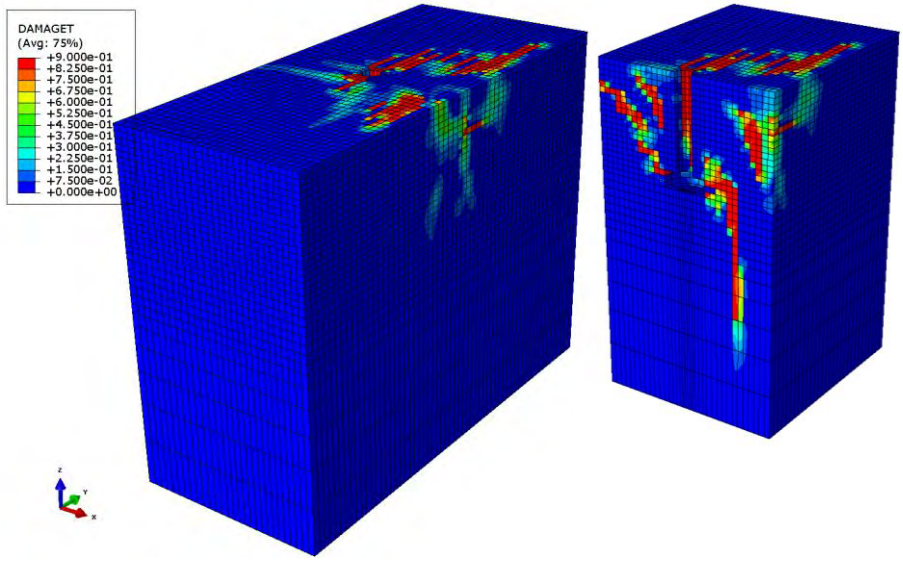

Figure 7-48: Reinforcement setup D. Damage tension parameter at the last increment.

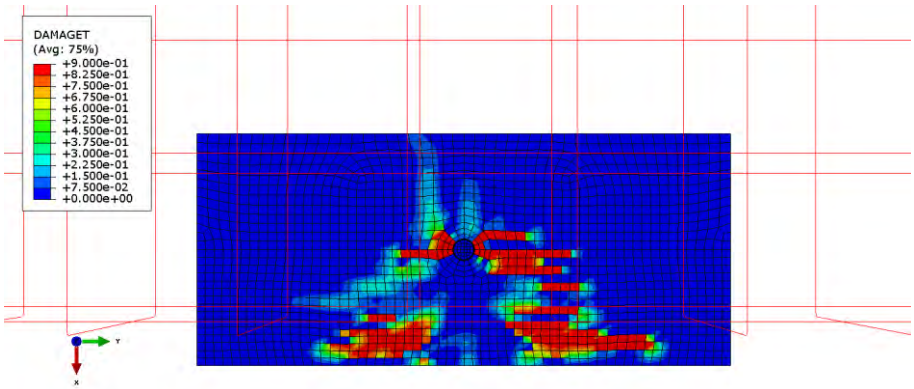

Figure 7-49: Reinforcement setup D. Top perspective view with highlighted reinforcement. Damage tension parameter at the last increment.

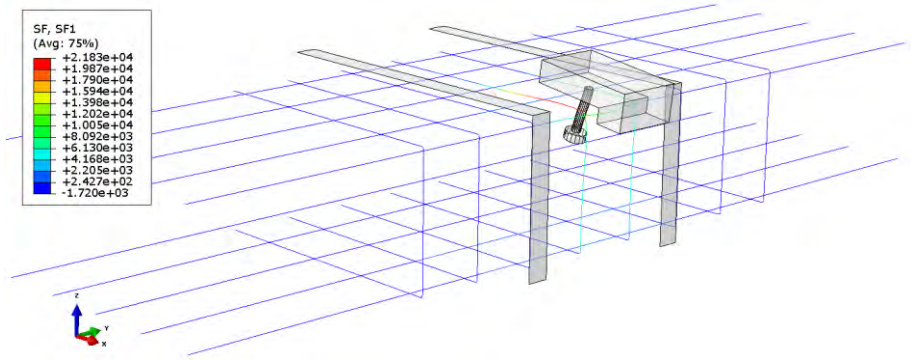

Figure 7-50: Reinforcement setup D. Maximum rebar normal force (21.8kN / 193 MPa). Deformations are scaled 10 times.

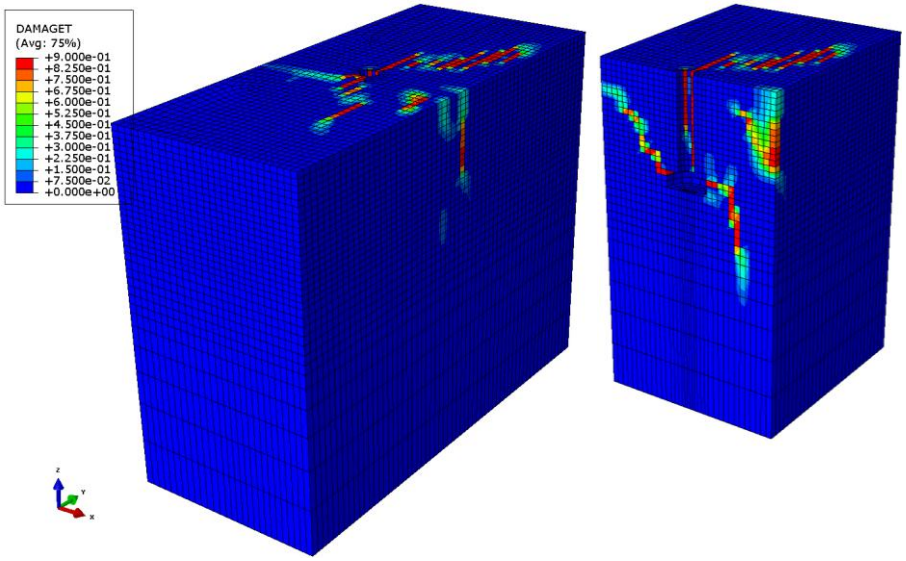

Figure 7-51: Reinforcement setup E. Damage tension parameter at the time of peak load (57.2kN).

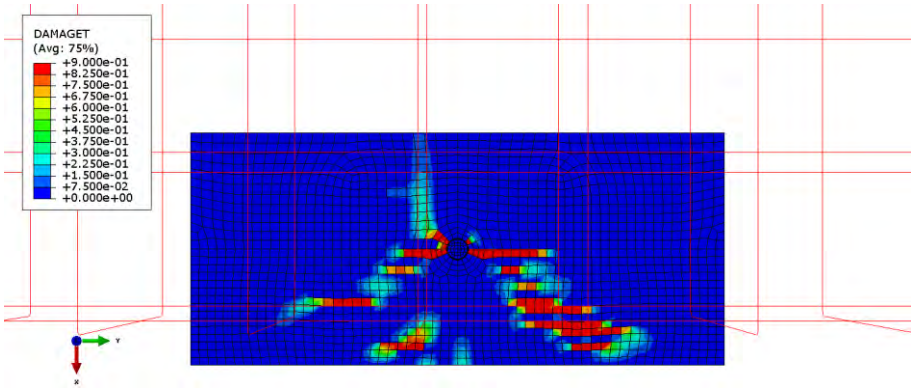

Figure 7-52: Reinforcement setup E. Top perspective view with highlighted reinforcement. Damage tension parameter at the time of peak load (57.2kN).

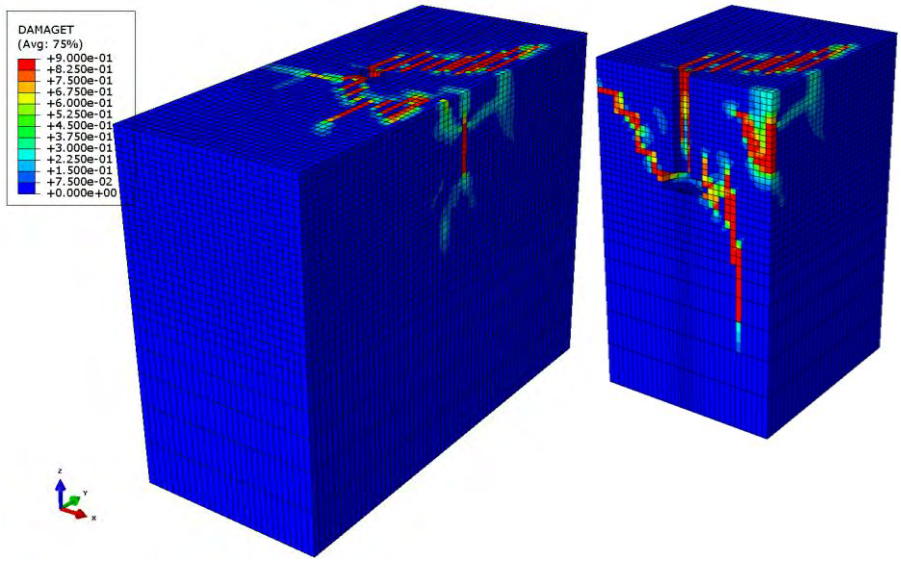

Figure 7-53: Reinforcement setup E. Damage tension parameter at the last increment.

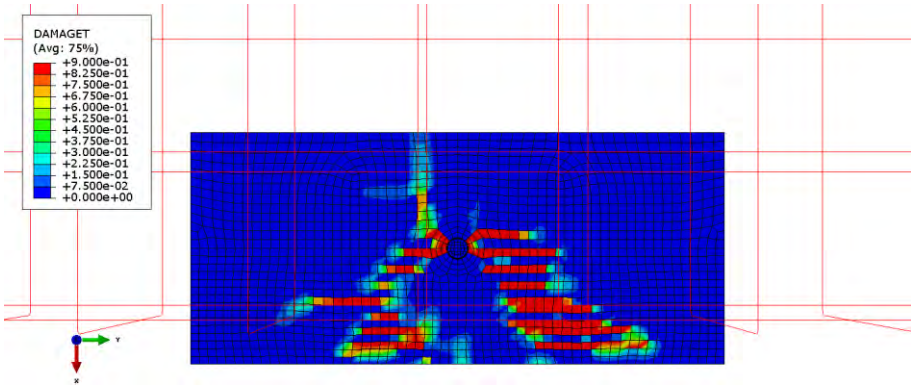

Figure 7-54: Reinforcement setup E. Top perspective view with highlighted reinforcement. Damage tension parameter at the last increment.

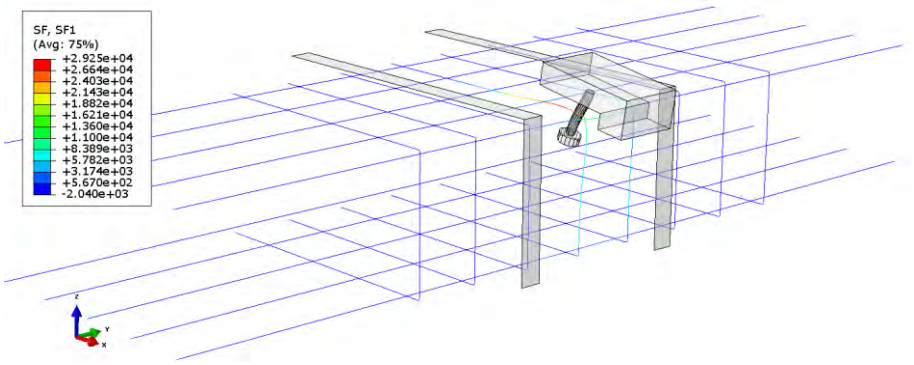

Figure 7-55: Reinforcement setup E. Maximum rebar normal force (29.3kN / 259 MPa). Deformations are scaled 20 times.

As expected the failure load magnitude increases with denser shear reinforcement and with the anchor bolt situated closer to a rebar. As the shear rebar is closer to the anchor bolt it will interfere with the concrete breakout cone at a higher extent leading to increased anchorage of the cone further back in the concrete structure. Particularly figure 7-44 and 7-54 show that with a well anchored shear rebar in the breakout cone, concrete cracks will propagate along the rebar behind the anchor.

An interesting observation is that all the rebars are moderately utilized, i.e. the stresses are well below the steel yield stress even though the analyses are driven past the time of the failure load.

The analyses are driven as long as possible but all of them were aborted due to excessive element distortion. This evidently means that the maximum reinforcement utilizations presented in contour plot figures within section 7.3.3 not necessarily are given in the same analysis time increment. Hence, the stresses are not directly comparable. Nevertheless, the stresses in all the rebars located within the failure breakout cone for each of the studied cases are presented in table 7-10 at the time of peak load. In addition, figure 7-56 presents the propagating rebar normal stresses in the most utilized elements for the different reinforcement setups.

Table 7-10: Stresses in shear reinforcement tying the failure prisms.

Reinforcement setup (see figure 7-56)	Failure load [kN]	Corresponding shear reinforcement stresses [MPa]
B	52.6	66.3; 66.3
C	66.3	15.9; 138.8; 141.5; 15.9
D	54.8	123.8; 49.5
E	57.2	184.0; 23.9

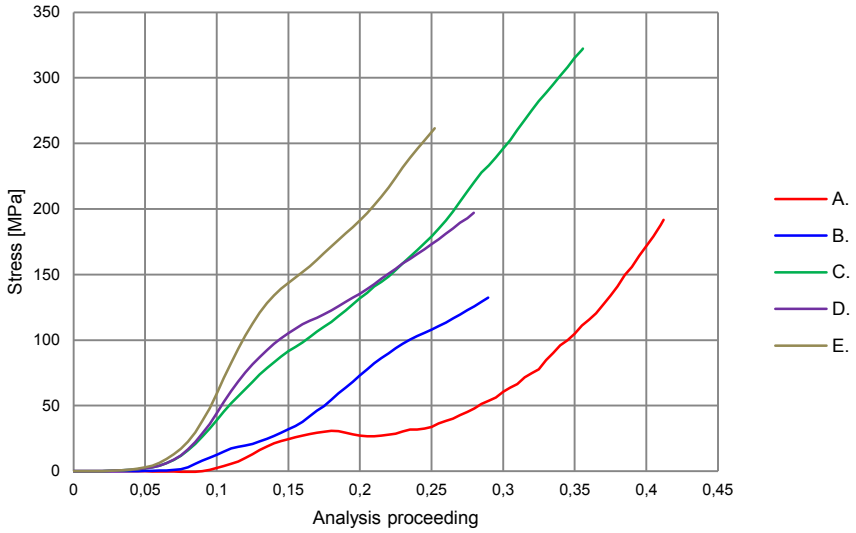

A. Longitudinal reinforcement Φ12cc150
B. Longitudinal reinforcement Φ12cc150 + shear reinforcement Φ12cc150
C. Longitudinal reinforcement Φ12cc150 + shear reinforcement Φ12cc100
D. Longitudinal reinforcement Φ12cc150 + 25 mm ecc. shear reinforcement Φ12cc150 (see figure 7-35 for description of reinforcement setup)
E. Longitudinal reinforcement Φ12cc150 + 40 mm ecc. shear reinforcement Φ12cc150 (see figure 7-35 for description of reinforcement setup)

Figure 7-56: Normal stress propagation in most utilized rebar for different reinforcement setups.

Strut and tie calculation

A comparative strut and tie calculation is performed below for reinforcement setup C. In figure 7-57 a schematic model is visualized that shows the anchor bolt and the reinforcing bars in the vicinity of the anchor. The dash dotted arrows show the pressed concrete braces and the other arrows show expected reaction force directions.

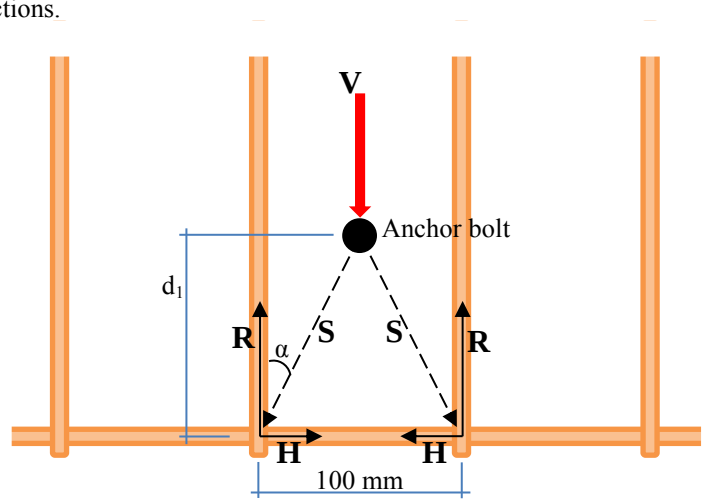

Figure 7-57: Strut and tie model of reinforcement setup C (presented in figure 7-34).

The failure load according to analysis results regarding reinforcement setup C is 66.3kN, hence this is the magnitude applied (V) in the calculation below. The concrete cover with respect to the longitudinal reinforcement is 30 mm which gives a distance d_1 = 100-30-12/2 = 64 mm and an angle α = 38°.

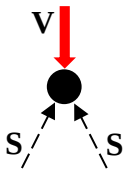

$$(\uparrow) \quad -V + 2 \cdot S \cdot \cos(\alpha) = 0$$
$$-66.3 + 2 \cdot S \cdot \cos(38) = 0$$
$$S = \frac{66.3}{2 \cdot \cos(38)}$$
$$S = 42.1\ kN$$

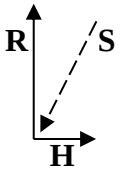

$$(\uparrow) \quad R - S \cdot \cos(\alpha) = 0$$
$$R = 33.2\ kN$$

$$(\rightarrow) \quad H - S \cdot \sin(\alpha) = 0$$
$$H = 25.9\ kN$$

As stated in figure 7-45, the maximum rebar normal force is 36.4kN. However, this force arouses in the last increment of the analysis after the concrete has failed. At the time of peak load corresponding rebar normal force is approximately 16kN which should be compared with the reaction force R calculated above.

The reason why the force R is twice the magnitude of the rebar normal force at the time of peak load is because of the simplicity in the two dimensional strut and tie calculation where the entire applied load is taken as tension in the reinforcement whilst the concrete is only assumed to transmit pressure. In the numerical simulation however, part of the applied force will be balanced by tensile stresses in the concrete and the force will not be transmitted in the same ideal manner, i.e. the three dimensional finite element model enables a more realistic load distribution through the structure.

Later on in the proceeding of the analysis, as the concrete gets more damaged, the applied force is in a greater extent taken by the reinforcement. Since the maximum rebar normal force amounts 36.4kN the corresponding applied force ought to be 36.4·2 = 72.8kN. This correlates well with graph C seen in figure 7-34.

7.4. Numerical simulations of anchor groups in shear

Unlike the performed analyses with respect to single anchors in non-reinforced concrete described in section 7.3.1, the finite element models and their associated analysis results presented for anchor groups loaded in shear are not compared to any physical test results. Nevertheless, since the derived material model described in section 7.3.1 has given analysis results that show good agreement to physical test results and the same material model is used for analyses of anchor groups, the numerical simulation results presented within this section may be regarded as realistic.

7.4.1. Group of anchors in non-reinforced concrete

Finite element model

The finite element model comprises a concrete block, two anchor bolts attached to a steel plate and a test frame (rig) as seen in figure 7-58.

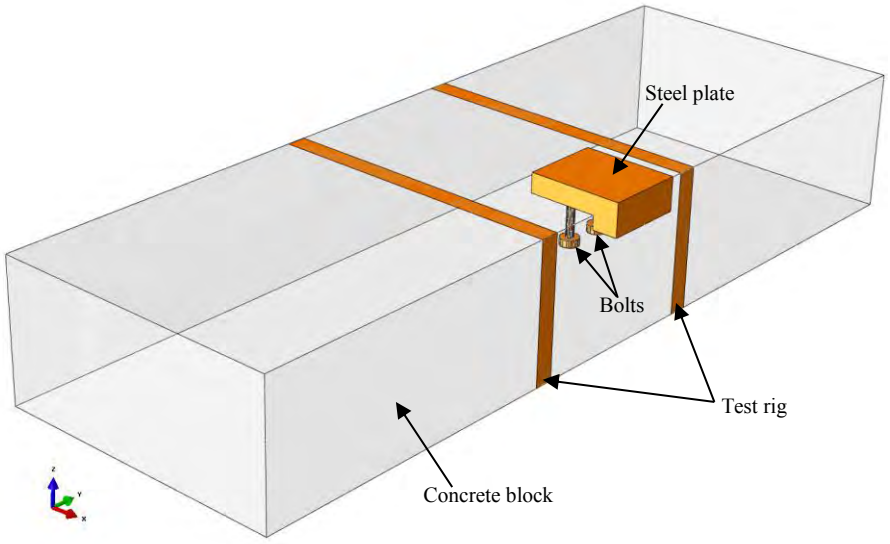

Figure 7-58: Transparent perspective view of the different parts constituting the model.

The distance between the bolts is 100 mm. Apart from the extra anchor bolt and hence the slightly different mesh, the finite element model of the anchor group is much like the model described in section 7.3.1. The concrete, anchor bolts and the steel plate are modelled with 8-node (hexahedra) and 6-node (triangular prisms) solid elements with reduced integration, in Abaqus denominated C3D8R and C3D6R respectively. The rig is modelled with rigid elements, in Abaqus denominated R3D4 [Dassault Systémes 2010].

Because of the extra anchor bolt the inner distance between the test rig frames is increased from earlier 350 mm to 450 mm. The model mesh is shown in figure 7-59.

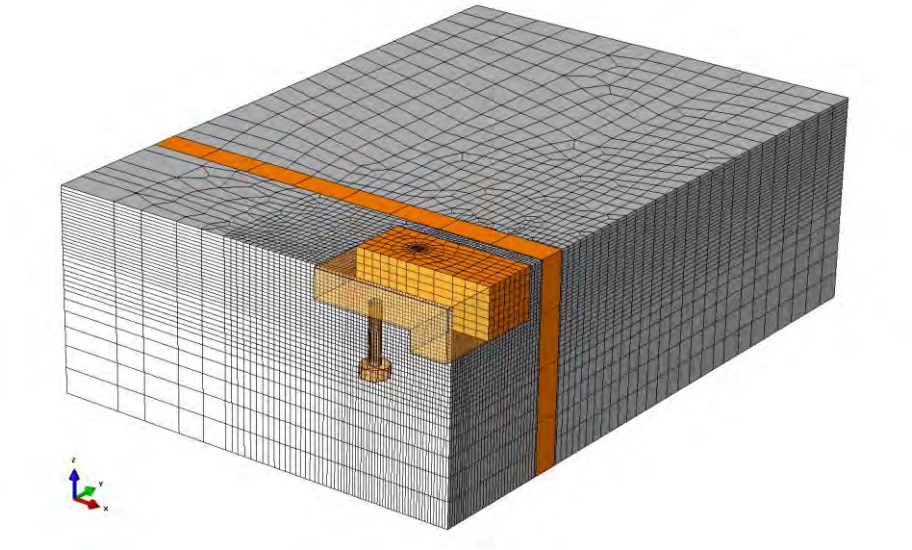

Figure 7-59: Symmetric view-cut of finite element model mesh.

The element size in the dense meshed part of the concrete, i.e. around the anchor bolt is approximately 7 mm. The size of the model is shown in table 7-11.

Table 7-11: Size of non-reinforced FE-model of anchor group.

Number of elements	Number of nodes	Number of degrees of freedom
145 500	154 600	464 000

For further information about the FE-model such as boundary conditions and materials see section 7.3.1.

Results

As stated in section 7.2.2, the characteristic single anchor bolt capacity is $V^0_{Rk,c}$ = 16.4 kN. According to [CEN/TS 1992-4-2 2009] the characteristic concrete edge capacity for a group of anchors in non-reinforced concrete is calculated accordingly:

$$V_{Rk,c} = V^0_{Rk,c} \cdot \frac{A_{c,V}}{A^0_{c,V}} \cdot \psi_{S,V} \cdot \psi_{h,V} \cdot \psi_{ec,V} \cdot \psi_{\alpha,V} \qquad [\text{N}]$$

With:

$$V^0_{Rk,c} = 16.4 \qquad [\text{kN}]$$
$$A_{c,V} = (150 + 100 + 150) \cdot 150 = 60\,000 \qquad [\text{mm}^2]$$
$$A^0_{c,V} = 4.5 \cdot c_1^2 = 4.5 \cdot 100^2 = 45\,000 \qquad [\text{mm}^2]$$
$$\psi_{S,V} = \psi_{h,V} = \psi_{ec,V} = \psi_{\alpha,V} = 1 \qquad [-]$$

The above stated values give a characteristic shear resistance of 21.8 kN. In order to establish a normative mean capacity of the anchor group the characteristic single anchor bolt capacity $V^0_{Rk,c}$ is replaced by the mean capacity of a single anchor bolt ($V^0_{Rm,c} = 22.9\ kN$, see section 7.2.2). This gives a mean capacity of the anchor group $V_{Rm,c} = 30.5\ kN$. Results from analysis of the finite element model described in section 7.4.1 together with the CEN/TS 1992-4-2 capacities and earlier presented results of single anchor in non-reinforced concrete are shown in figure 7-60.

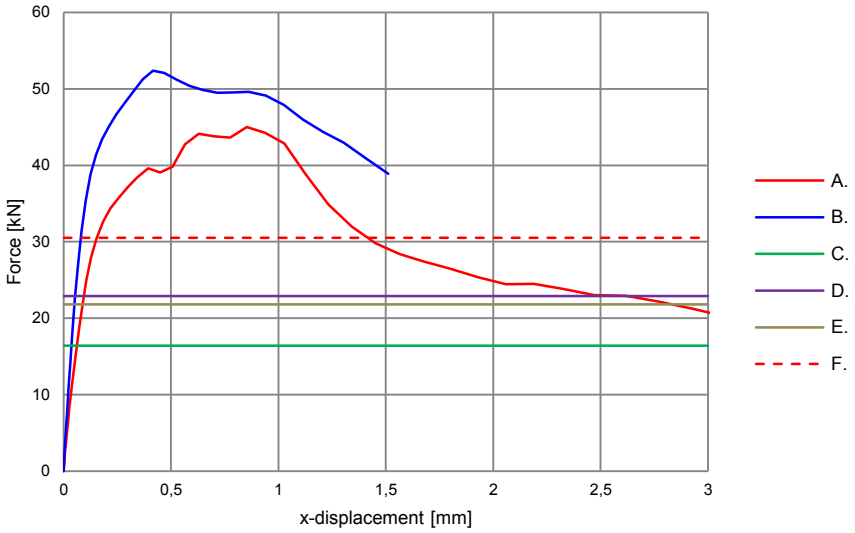

A. FEA-results for single anchor (failure load 45.0kN)
B. FEA-results for group of anchors (failure load 52.4kN)
C. Characteristic capacity of single anchor bolt according to [CEN/TS 1992-4-2 2009]
D. Predicted mean capacity of single anchor bolt based on [CEN/TS 1992-4-2 2009]
E. Characteristic capacity of group of anchor bolts according to [CEN/TS 1992-4-2 2009]
F. Predicted mean capacity of group of anchors based on [CEN/TS 1992-4-2 2009]

Figure 7-60: Relation between force and displacement for single anchor and group of anchors together with capacities according to CEN/TS 1992-4-2.

The idealized concrete breakout cone surface according to section 6.3.5.2.2 in [CEN/TS 1992-4-2 2009] is shown in figure 7-61 and corresponding breakout cone from the FE-analysis is shown in figure 7-62.

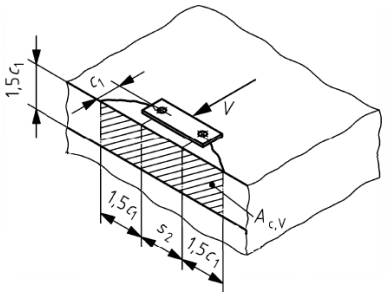

Figure 7-61: Idealized concrete edge breakout surface according to [CEN/TS 1992-4-2 2009].

Since the edge distance c_1 and distance between the anchor bolts s_2 equals 100 mm the ideal width of the breakout surface should be $(1.5+1.0+1.5)\cdot 100 = 400$ mm, and the height ought to be 150 mm. Mentioned distances are shown together with FE-analysis fracture surface results in figure 7-62.

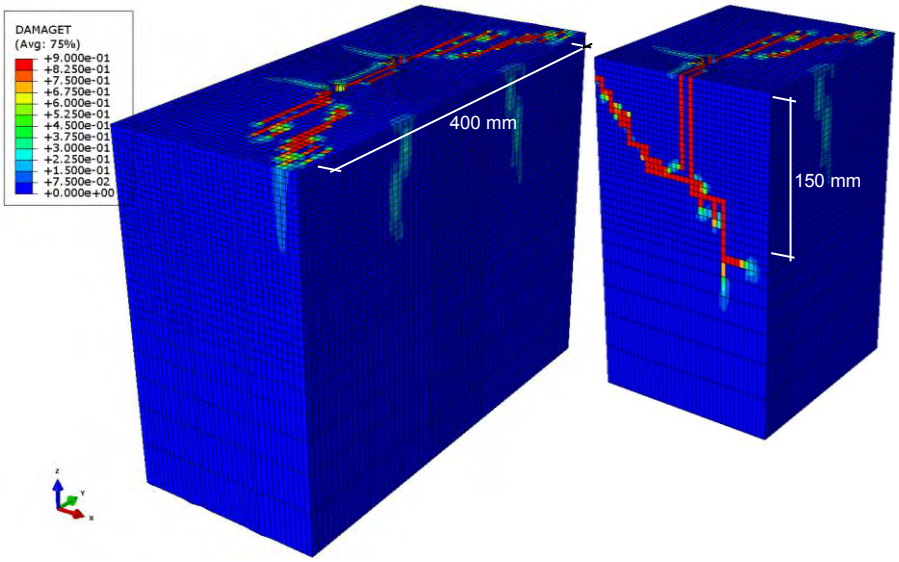

Figure 7-62: Damage tension parameter at last increment of FE-analysis.

7.4.2. Group of anchors in reinforced concrete

This section presents what impact on FEA-results different types of reinforcement setups may have for a group of anchors. The constitutive model used throughout the analyses is described in chapter 5 and material values are given in section 7.3.1. The reinforcement is modelled with two-node beam elements which in Abaqus are denominated B31 [Dassault Systémes 2010]. In order to captivate the physical interaction between the reinforcement and the concrete, the response of the surrounding concrete is used to constrain the translational degrees of freedom of the embedded beam element nodes (the rebar reinforcement).

Reinforcement in longitudinal direction

The diameter of the rebars is 12 mm and the spacing 150 mm. The concrete cover is 30 mm. Apart from the longitudinal reinforcement the finite element model is the same as the model described in section 7.4.1. The different parts constituting the model are shown in figure 7-63.

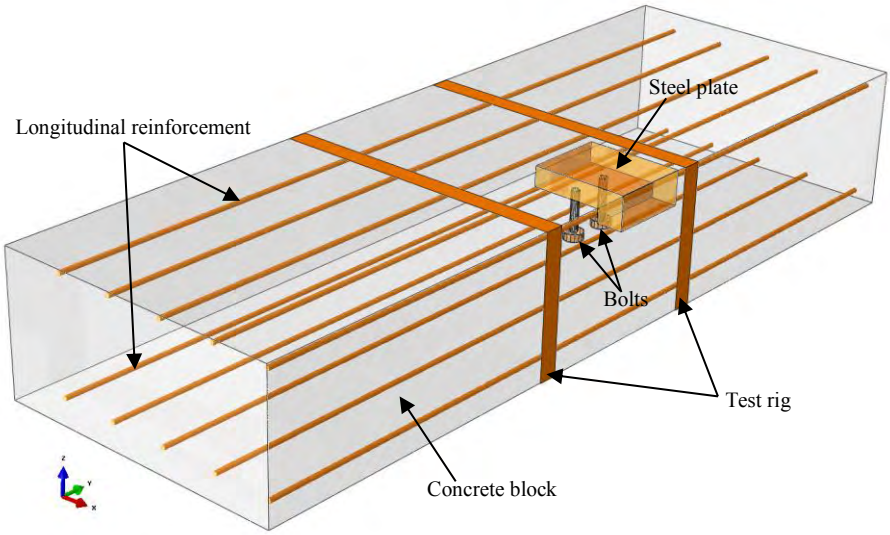

Figure 7-63: Transparent perspective view of the different parts constituting the longitudinally reinforced concrete model.

Results in terms of force-displacement relations for a non-reinforced concrete model and the FE-model including longitudinal reinforcement are shown in figure 7-64. The fracture surface is shown in figure 7-65. Additional result plots are presented in Appendix 2.9.

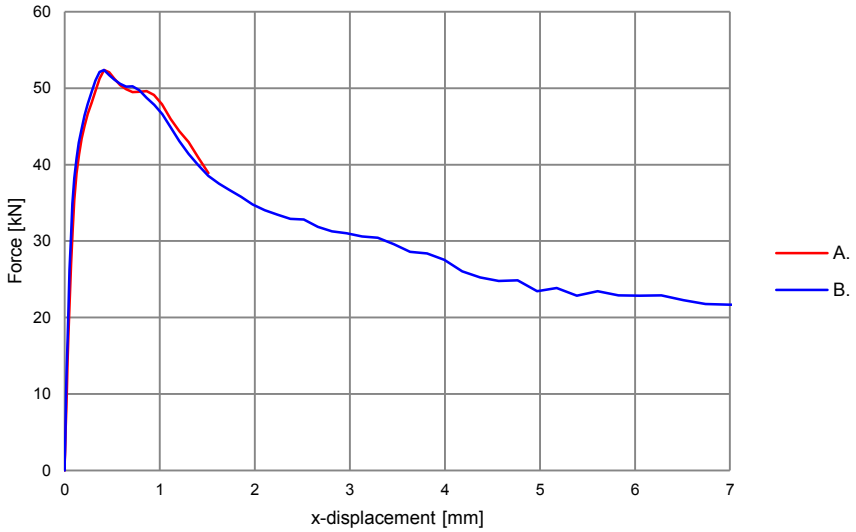

A. Non-reinforced concrete (main analysis as described in section 7.4.1)
B. Longitudinal reinforcement Φ12cc150

Figure 7-64: Relation between force and displacement for group of anchors in non-reinforced and longitudinally reinforced concrete.

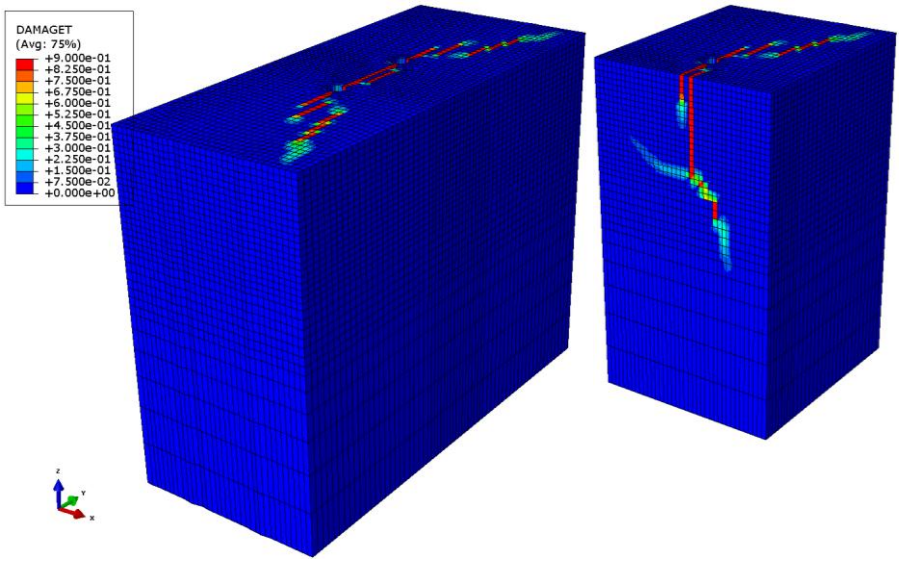

Figure 7-65: Damage tension parameter for longitudinally reinforced concrete at the time of peak load (52.4kN).

The maximum rebar normal force amount approximately 13.4kN (118 MPa) and occurs after the failure load has been reached, see figure 7-66. This means that when cracks have developed the reinforcement gets more utilized.

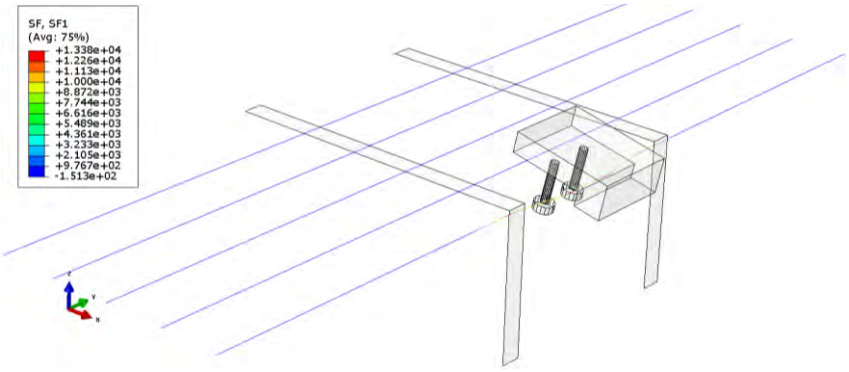

Figure 7-66: Maximum rebar normal force (13.4kN). Deformations are scaled 5 times.

Since there is only one rebar situated between the anchor bolts and the concrete edge this is the only one affecting the results for actuated shear loading scenario. As earlier stated the maximum rebar normal force is 13.4kN, resulting in a normal stress of 118 MPa. As stated in section 7.3.1 the steel is elastically modelled. By anyhow assuming a reasonable steel yield value of f_y = 450 MPa one can conclude that the rebar is not remarkably utilized. Since there is no reinforcement in the direction of the applied load the force will not be anchored more than for a non-reinforced concrete. This conclusion correlates with the results presented in figure 7-64.

Shear reinforced concrete

The diameter of the rebars is consistently 12 mm but different reinforcement setups, e.g. spacing has been studied in different cases. The concrete cover regarding the longitudinal reinforcement is 30 mm meaning there is an 18 mm concrete cover to the shear reinforcement.

Apart from the reinforcement the finite element model is the same as the model described in section 7.4.1. The different parts constituting the model are shown in figure 7-67.

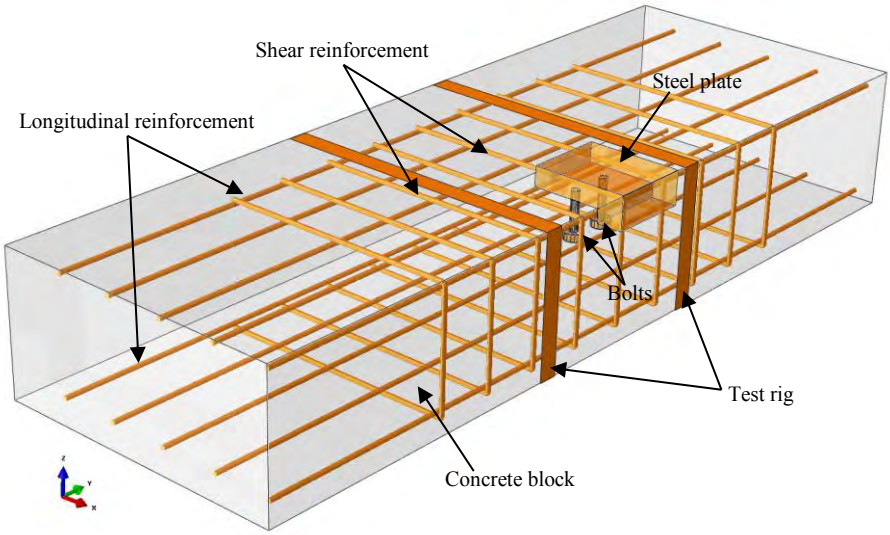

Figure 7-67: Transparent perspective view of the different parts constituting the shear reinforced concrete model.

Results in terms of force-displacement relations for non-reinforced concrete and different types of reinforcement setups are shown in figure 7-68. Figure 7-69 shows the reinforcement placing around the anchor bolt.

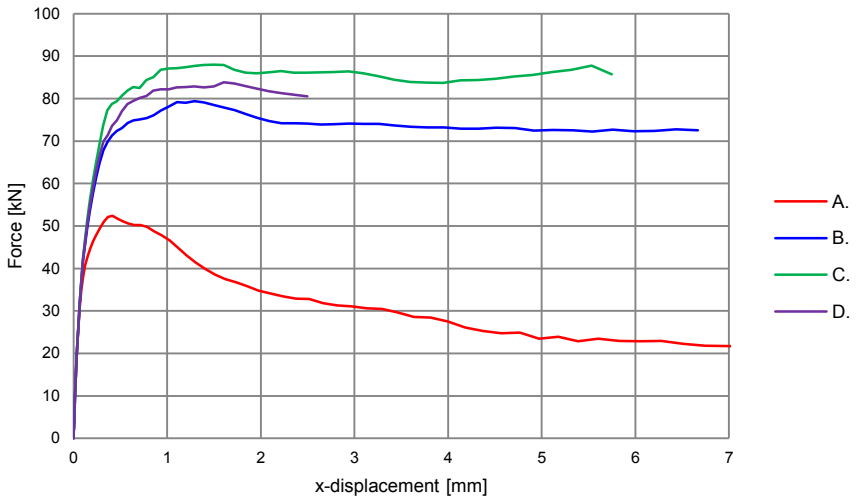

A. Longitudinal reinforcement Φ12cc150
B. Longitudinal reinforcement Φ12cc150 + shear reinforcement Φ12cc150 (see figure 7-69 for reinforcement setup)
C. Longitudinal reinforcement Φ12cc150 + shear reinforcement Φ12cc100
D. Longitudinal reinforcement Φ12cc150 + 25 mm ecc. shear reinforcement Φ12cc150 (see figure 7-69 for reinforcement setup)

Figure 7-68: Relation between force and displacement for a group of anchors in different reinforcement setups.

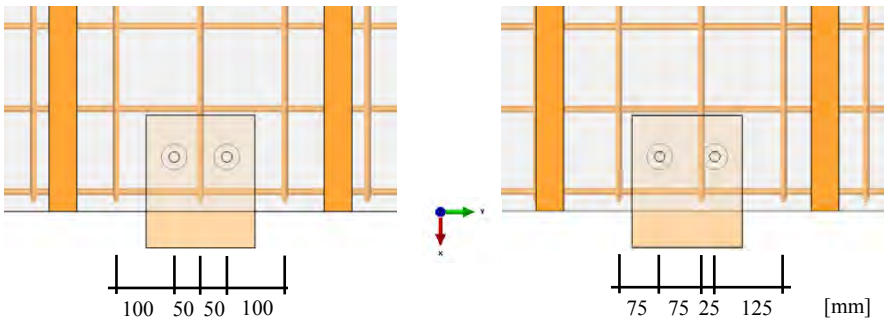

Figure 7-69: Top view showing reinforcement placings. To the left the shear reinforcement has no eccentricity and to the right a 25 mm eccentricity.

In table 7-12, the failure load for the different reinforcement setups is presented. The figures referred to show fracture surfaces where part of the concrete block in the vicinity of the anchor bolts is visualized. Additional result plots are presented in Appendix 2.9-2.12.

Table 7-12: Failure load magnitudes and fracture surfaces for the different reinforcement setups presented in figure 7-68.

Reinforcement setup (see figure 7-68)	Failure load [kN]	Fracture surface
A	52.4	See figure 7-65
B	79.4	See figure 7-70 to 7-74
C	87.9	See figure 7-75 to 7-79
D	83.8	See figure 7-80 to 7-84

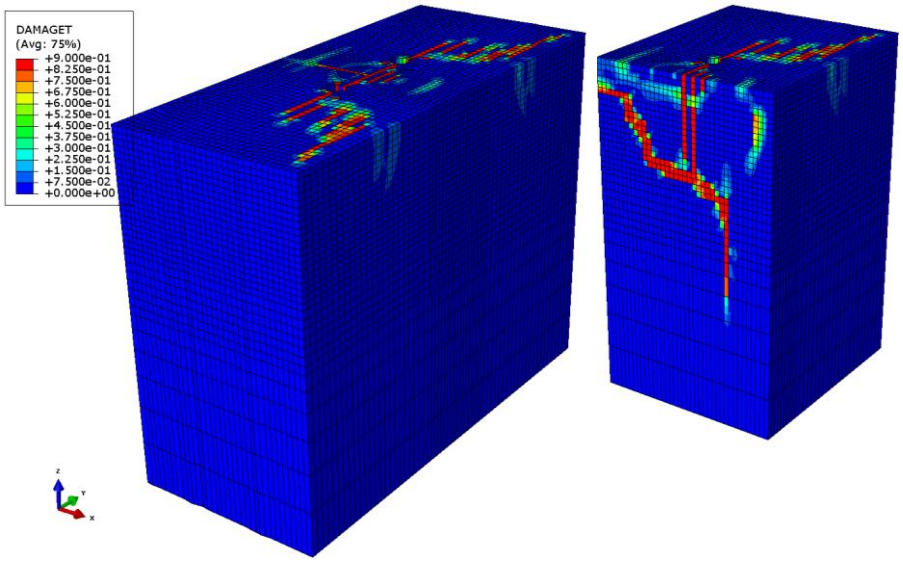

Figure 7-70: Reinforcement setup B. Damage tension parameter at the time of peak load (79.4kN).

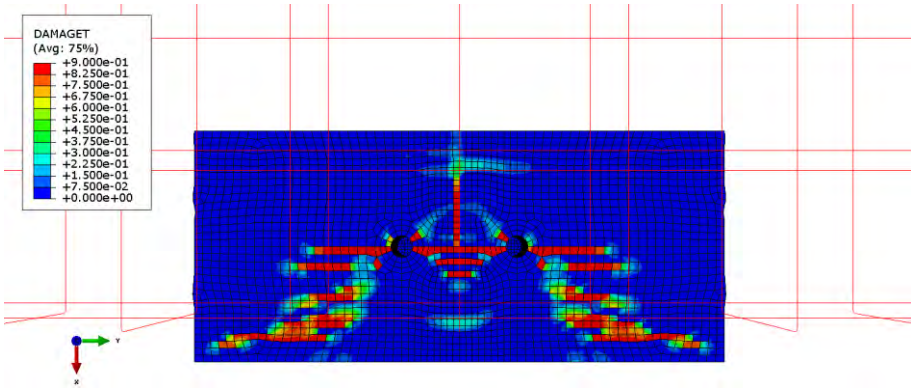

Figure 7-71: Reinforcement setup B. Top perspective view with highlighted reinforcement. Damage tension parameter at the time of peak load (79.4kN).

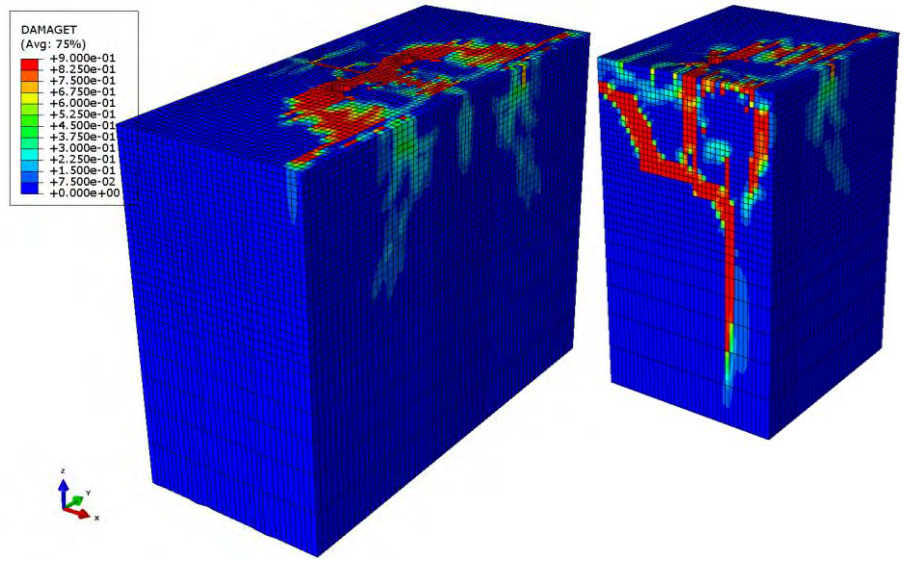

Figure 7-72: Reinforcement setup B. Damage tension parameter at the last increment.

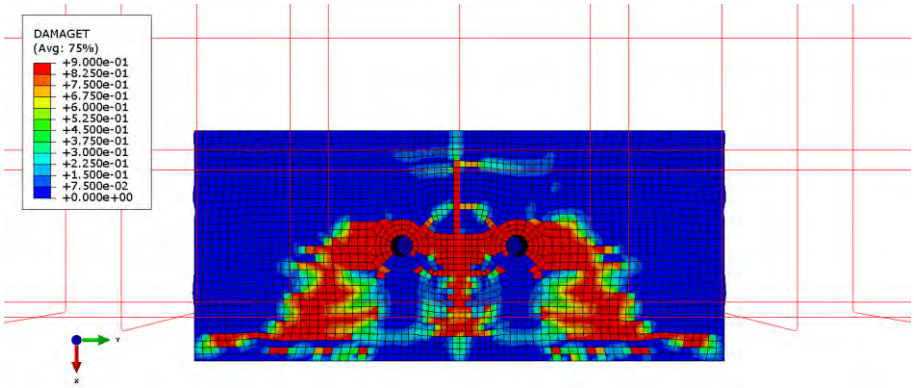

Figure 7-73: Reinforcement setup B. Top perspective view with highlighted reinforcement. Damage tension parameter at the last increment.

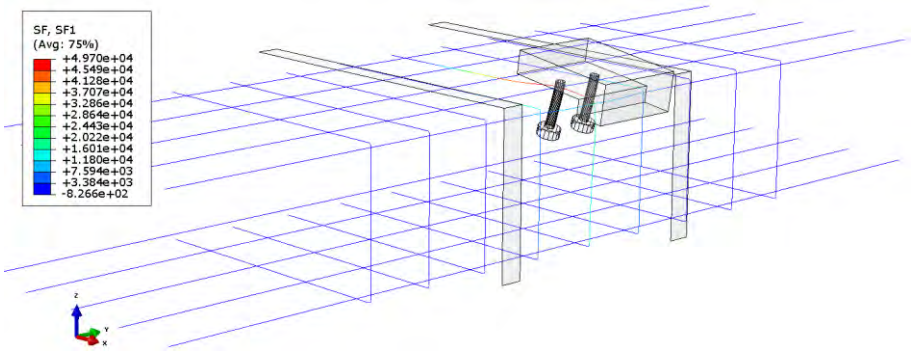

Figure 7-74: Reinforcement setup B. Maximum rebar normal force (49.7kN / 440MPa). Deformations are scaled 5 times.

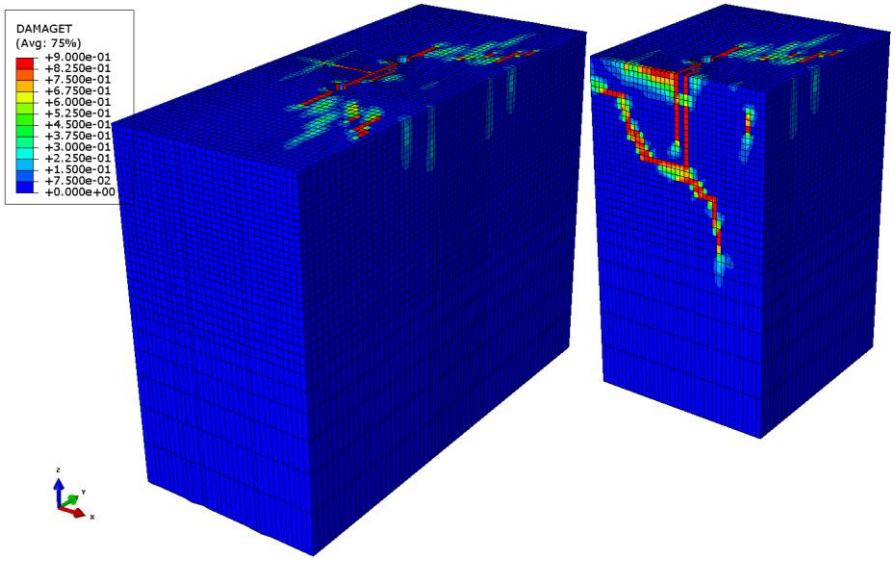

Figure 7-75: Reinforcement setup C. Damage tension parameter at the time of peak load (87.9kN).

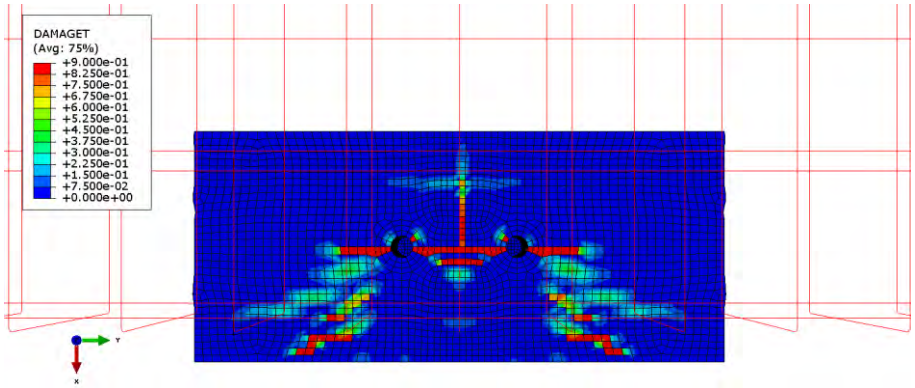

Figure 7-76: Reinforcement setup C. Top perspective view with highlighted reinforcement. Damage tension parameter at the time of peak load (87.9kN).

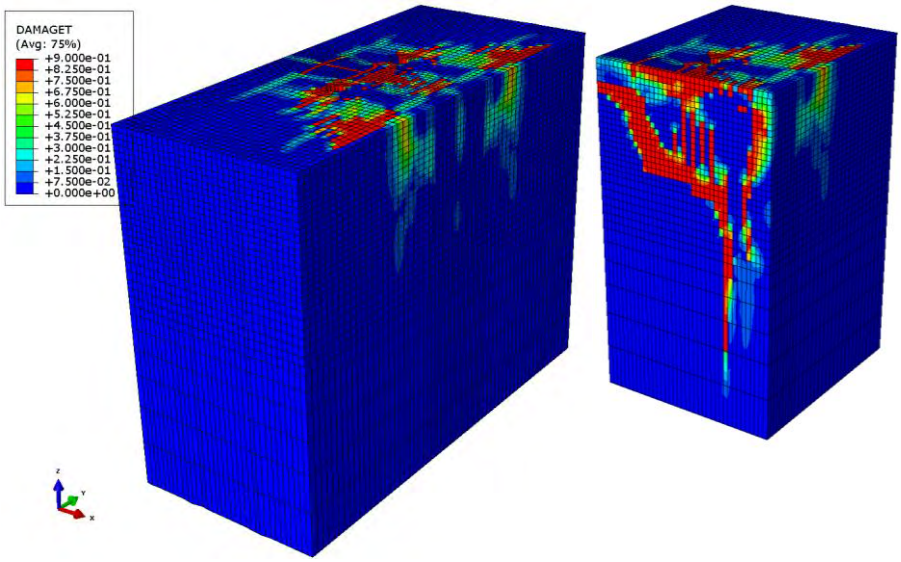

Figure 7-77: Reinforcement setup C. Damage tension parameter at the last increment.

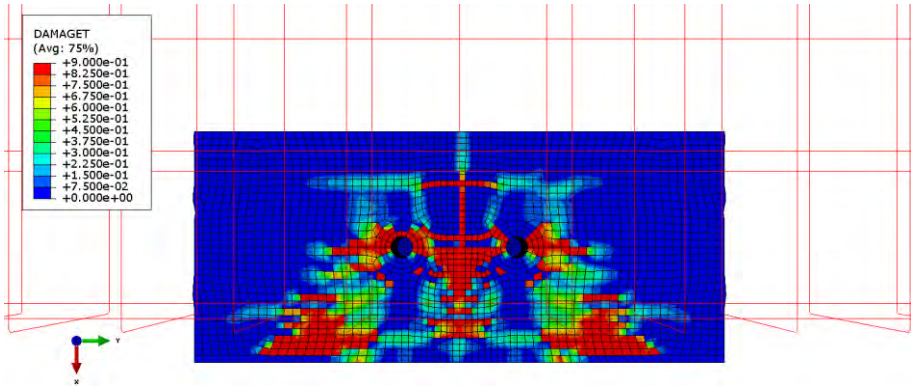

Figure 7-78: Reinforcement setup C. Top perspective view with highlighted reinforcement. Damage tension parameter at the last increment.

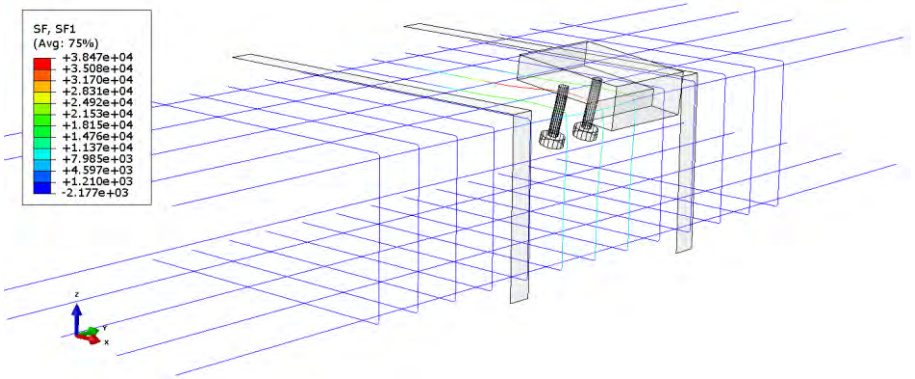

Figure 7-79: Reinforcement setup C. Maximum rebar normal force (38.5kN / 340 MPa). Deformations are scaled 5 times.

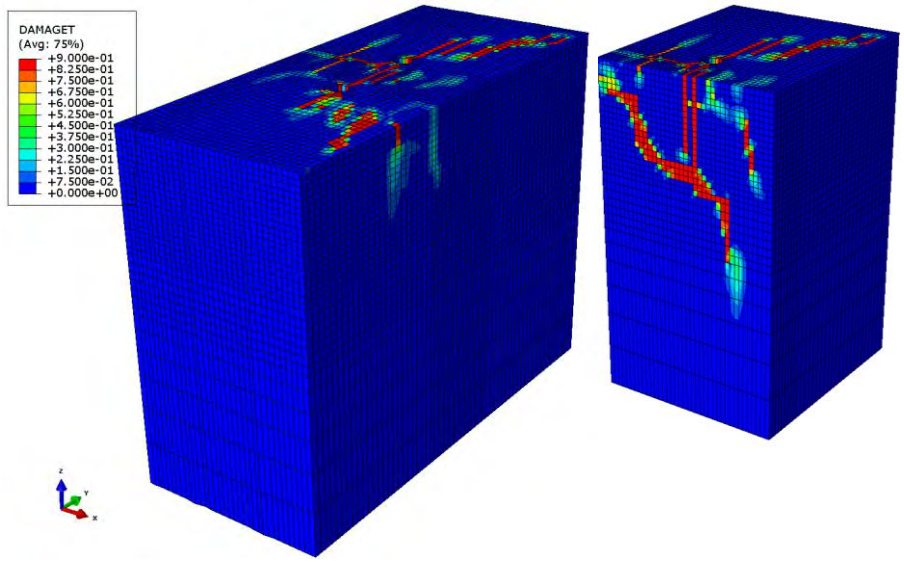

Figure 7-80: Reinforcement setup D. Damage tension parameter at the time of peak load (83.8kN).

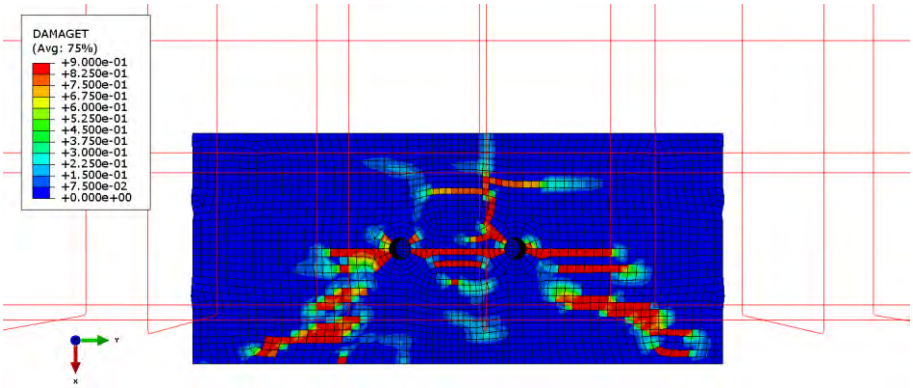

Figure 7-81: Reinforcement setup D. Top perspective view with highlighted reinforcement. Damage tension parameter at the time of peak load (83.8kN).

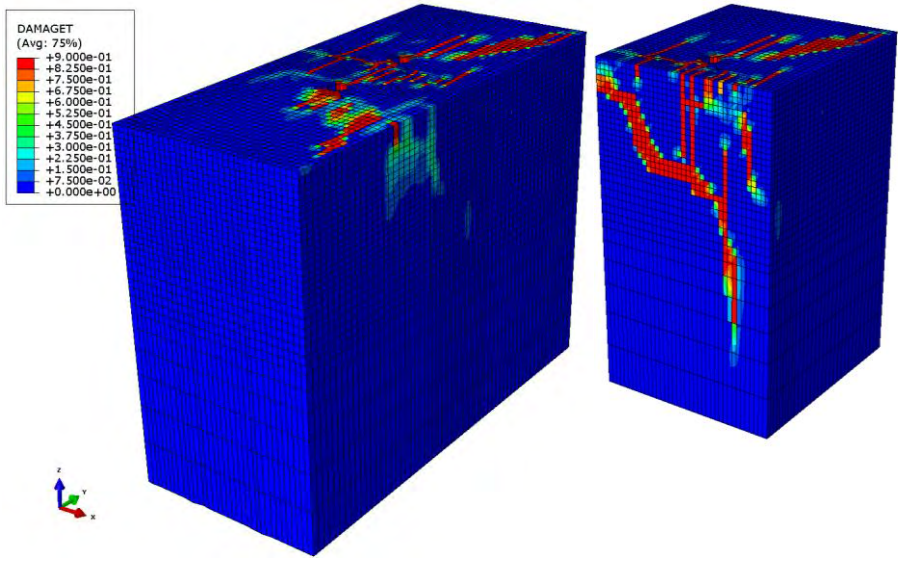

Figure 7-82: Reinforcement setup D. Damage tension parameter at the last increment.

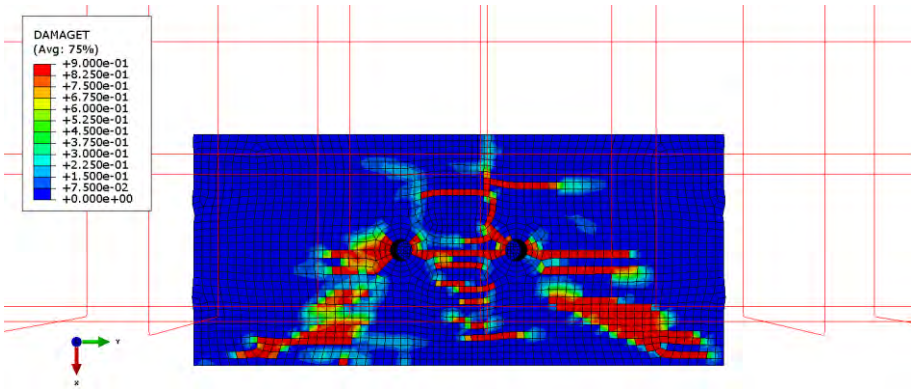

Figure 7-83: Reinforcement setup D. Top perspective view with highlighted reinforcement. Damage tension parameter at the last increment.

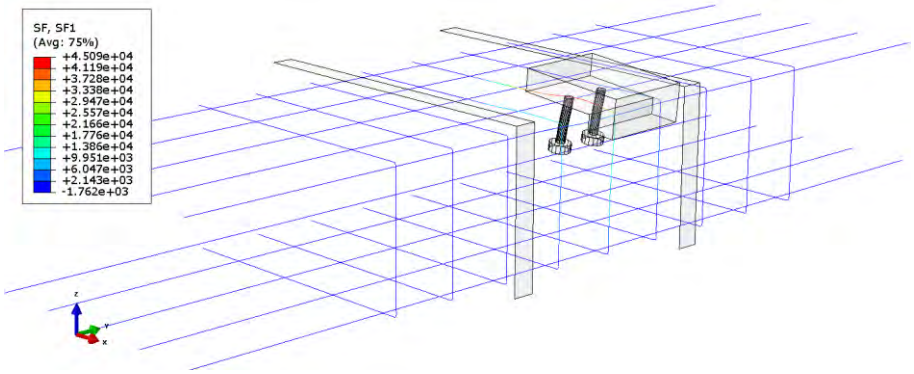

Figure 7-84: Reinforcement setup D. Maximum rebar normal force (45.1kN / 399MPa). Deformations are scaled 10 times.

The analyses are driven as long as possible but all of them were aborted due to excessive element distortion. This evidently means that the maximum reinforcement utilizations presented in contour plot figures within section 7.4.2 not necessarily are given in the same analysis time increment. Hence, the stresses are not directly comparable. Nevertheless, the stresses in all the rebars located within the failure breakout cone for each of the studied cases are presented in table 7-13 at the time of peak load. In addition, figure 7-85 presents the propagating rebar normal stresses in the most utilized elements for the different reinforcement setups.

Table 7-13: Stresses in shear reinforcement tying the failure prisms.

Reinforcement setup (see figure 7-85)	Failure load [kN]	Corresponding shear reinforcement stresses [MPa]
B	79.4	47.4; 307.9; 46.7
C	87.9	9.8; 112.0; 222.3; 112.7; 10.0
D	83.8	58.4; 303.4; 19.4

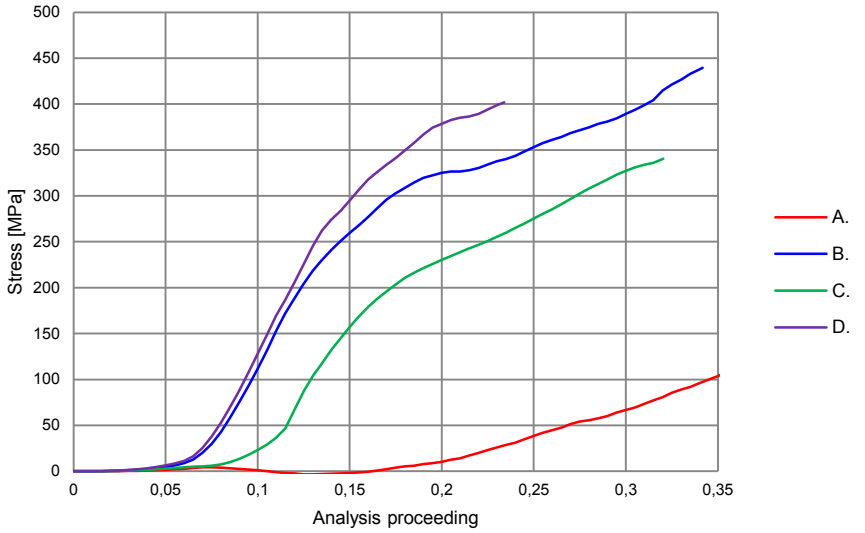

A. Longitudinal reinforcement Φ12cc150
B. Longitudinal reinforcement Φ12cc150 + shear reinforcement Φ12cc150 (see figure 7-69 for reinforcement setup)
C. Longitudinal reinforcement Φ12cc150 + shear reinforcement Φ12cc100
D. Longitudinal reinforcement Φ12cc150 + 25 mm ecc. shear reinforcement Φ12cc150 (see figure 7-69 for reinforcement setup)

Figure 7-85: Anchor group - Stress propagation in most utilized rebar for different reinforcement setups.

At a first glance the results presented in figure 7-85 may seem somewhat surprising since the maximum rebar normal stress is higher for reinforcement setup B than C. However, because of the wider shear reinforcement spacing in setup B the rebar situated between the two anchors will get far more utilized than the two immediate equally distanced rebars. For reinforcement setup C on the other hand the distance from each anchor bolt to the two surrounding shear rebars is 50 mm, hence the force is distributed on a greater total reinforcement area consequently lowering the maximum rebar normal stress.

As seen in figure 7-68 the concrete edge capacity seems to increase with approximately 60 % when there is shear reinforcement in the vicinity of the anchor bolts, i.e. rebars located inside the failure concrete cone. Regardless of the amount of reinforcement and distances to the anchor bolts for the different cases studied, the failure load magnitudes are in the same region. Even though the simulations presented are few, the trend is that if there is sufficient shear reinforcement (meaning denser reinforcement than the sufficient amount will not have a particularly uprate effect on the capacity) the concrete edge capacity may be enumerated by approximately 1.6. But then again, this has to be further investigated with a greater number of samples in order to make solid conclusions.

The CEN/TS 1992-4-2 concrete edge capacity expression for a group of anchor bolts includes an uprating capacity factor $\psi_{re,V}$ that depends on the position of the fastening. For fastenings in cracked concrete with edge reinforcement and closely spaced stirrups or wire mesh with a spacing $a \leq 100$ mm and $a \leq 2 \cdot c_1$, or for fastening in non-cracked concrete, the mentioned factor is $\psi_{re,V} = 1.4$ [CEN/TS 1992-4-2 2009].

8. Discussion

The response of mechanically loaded anchors in reinforced concrete structures can only be understood by a combination of testing and numerical simulations. As concrete is a complex material, interaction between anchors, reinforcement and concrete is consequently also complex. Reported work within this area in the open literature is limited why efforts are needed to fill this gap.

In this research project, the response of headed anchors in non-reinforced and reinforced concrete structures is investigated by means of finite element simulations. Single anchor and anchor groups loaded in tension or shear are studied. Focus is on anchors in reinforced concrete structures. However, as most of available testing is conducted on non-reinforced concrete and as codes for design of anchors also are based on non-reinforced concrete, simulations in this project cover both types of structures.

Simulations are conducted with the general purpose finite element program Abaqus [Dassault Systémes 2010]. Among three available constitutive models, the concrete damaged plasticity model is found to best fit the purpose. A number of parameters are investigated such as dilation angle, fracture energy of concrete, element size, width and thickness of concrete structure, number of anchors, eccentricity of anchor group, type and amount of reinforcement and boundary conditions.

Simulations show that reinforcement has a beneficial effect on anchor capacity both in tension and shear. Firstly, it increases the global stiffness of the concrete structure which means that the risk for splitting of the concrete at the location of the anchor is reduced. Secondly, it increases the confinement in the vicinity of the anchor which increases the capacity. Thirdly, in the case of supplementary reinforcement close to the anchors, such as shear reinforcement for an anchor in shear, the shear reinforcement can directly transfer the load from the anchor into the concrete structure and thereby increase the capacity substantially. Fourthly, in general reinforcement makes the failure of anchors loaded in tension or shear more ductile. The effect of all these phenomena is investigated in this work.

Numerical simulations show good agreement with available results from testing of anchor bolts in tension and shear. The level of failure loads is better simulated than the shape of force-displacement curves. In most cases, simulated displacement at failure load is smaller than that in corresponding testing. One explanation for this discrepancy might be the way the test setup, such as support and loading equipment, is modelled in the simulation. Initial gaps in the testing equipment are for example not considered in the numerical simulations.

Table 8-1 summarises failure loads from testing, simulations and predictions based on CEN/TS for single anchor and anchor groups subjected to tension in concrete slabs. Results from testing and simulation are taken from table 6-9 and 6-14. Failure load predictions with CEN/TS are done for anchors in non-reinforced concrete as described in chapter 6.

Table 8-1: Summary of failure loads from testing, simulations and predictions based on CEN/TS for single anchor and anchor groups subjected to tension in concrete slabs. CEN/TS predictions are done without considering the reinforcement.

	No	Slab dimension [m]	Top reinforcement	Pre-crack [mm]	$\bar{N}_{u,test}$ [kN]	$N_{u,simul.}$ [kN]	$N_{u,CEN/TS}$ [kN]	$\frac{\bar{N}_{u,test}}{N_{u,CEN/TS}}$ [-]	$\frac{N_{u,simul.}}{N_{u,CEN/TS}}$ [-]
Single	1	1.2x1.2x0.3	-	0	196	270	296	0.66	0.91
	2	1.2x1.2x0.3	Ø12cc300	0	280	284	296	0.95	0.96
	3	1.2x1.2x0.3	Ø16cc150	0	319	305	296	1.08	1.03
	4	1.2x1.2x0.3	Ø16cc100	0	317	346	296	1.07	1.17
	5	1.2x1.2x0.6	Ø12cc300	0	357	349	296	1.21	1.18
	6	2.2x2.2x0.3	Ø12cc400	0	241	267	296	0.81	0.90
	7	2.2x2.2x0.3	Ø12cc150	0	262	288	296	0.89	0.97
	8	2.2x2.2x0.6	Ø12cc150	0	327	354	296	1.10	1.20
Single	9	1.2x1.2x0.3	-	0.5	144	212	212	0.68	1.00
	10	1.2x1.2x0.3	Ø12cc300	0.5	292	245	212	1.38	1.16
	11	1.2x1.2x0.3	Ø16cc150	0.5	303	266	212	1.43	1.25
	12	1.2x1.2x0.3	Ø16cc100	0.5	256	325	212	1.21	1.53
	13	2.2x2.2x0.3	Ø12cc500	0.5	217	249	212	1.02	1.17
Anchor group	1	2.2x2.2x0.3	Ø12cc300	0	-	341	526	-	0.65
	2	2.2x2.2x0.3	Ø12cc150	0	-	464	526	-	0.88
	3	2.2x2.2x0.3	Ø12cc100	0	-	492	526	-	0.94
	4	2.2x2.2x0.3	Ø12cc150	0	-	461	526	-	0.88
	5	2.2x2.2x0.3	Ø12cc300	0	-	340	526	-	0.65
	6	2.2x2.2x0.3	Ø12cc150	0	-	443	526	-	0.84
	7	2.2x2.2x0.3	Ø12cc100	0	-	502	526	-	0.95
	8	2.2x2.2x0.6	Ø12cc150	0	-	612	526	-	1.16
	9	2.2x2.2x0.6	Ø12cc150	0	-	622	526	-	1.18
	10	3x3x0.6	Ø12cc300	0	-	600	526	-	1.14
	11	3x3x0.6	Ø12cc300	0	-	618	526	-	1.17

The purpose of comparing failure loads from testing and simulations with CEN/TS predictions is to get an indication of the effect of reinforcement for each concrete slab configuration. The ratio $N_{u,simul.}/N_{u,CEN/TS}$ is given as an indicator in this comparison where $N_{u,CEN/TS}$ is calculated for anchors without considering the reinforcement. As seen in table 8-1, this ratio can be both higher and lower than 1. For reinforced slabs with dimension 1.2x1.2x0.3 m, the ratio is higher than 1 for all slabs except one. For all non-cracked reinforced slabs with dimension 2.2x2.2x0.3 m, the ratio is lower than 1 where those with anchor groups show the lowest ratio. In general, the ratio increases with increasing slab thickness and with increasing amount of reinforcement.

Codes for analysis of anchors such as CEN/TS do not consider the global stiffness of the concrete structure. The capacity of an anchor group loaded in tension is calculated based on the capacity of corresponding single anchor assuming sufficient global stiffness. However, if the concrete structure is not sufficiently stiff, the anchor group capacity according to CEN/TS can be non-conservative. Higher loads on the anchor group compared to that on the single anchor might result in different conditions in the concrete in the vicinity of the anchors. Thus, with a more flexible concrete structure, the failure mechanism splitting instead of concrete cone breakout might limit the anchor group capacity. The results in table 8-1 indicate that this is the case for anchor groups in non-cracked reinforced slabs with dimension 2.2x2.2x0.3 m. As the thickness of these slabs is increased to 0.6 m, the global

stiffness increases and the ratio $N_{u,simul.}/N_{u,CEN/TS}$ increases to a value higher than 1.

For all anchor group simulations, non-cracked concrete is assumed. Hence, the failure load prediction based on CEN/TS is also done with this condition. However, for the more flexible slabs with a thickness of 0.3 m and a lower amount of reinforcement, it might be more correct to assume cracked concrete in doing the CEN/TS prediction. The reason for this is that pre-cracking caused by splitting precedes the concrete cone failure in slabs with insufficient global stiffness. In doing so, the ratio $N_{u,simul.}/N_{u,CEN/TS}$ increases by a factor of 1.4 and thus $N_{u,CEN/TS}$ better corresponds with simulated failure loads.

Highest ratio $N_{u,simul.}/N_{u,CEN/TS}$ is seen for single anchor in pre-cracked slabs. An explanation for this is that CEN/TS uses a reduction factor of 1.4 on the capacity if the concrete is cracked instead of non-cracked. Such a large reduction is not found from testing or simulations.

For non-reinforced slabs it would be expected that failure loads from testing, simulations and predictions based on CEN/TS were comparable. Instead, testing of anchors loaded in tension shows failure loads that are more than 30% lower than that of simulations and predicted with CEN/TS. The reason for this deviation is probably that splitting occurs in the tests. An increase of slab thickness would increase the global stiffness of the slab and thereby reduce the risk for splitting. Results in section 6.3.1 indicate this. It is furthermore obvious that simulations as well as predictions based on CEN/TS overestimate the failure load if the concrete structure is non-reinforced and not sufficiently stiff.

In summary, failure loads from simulations in table 8-1 agree fairly well with failure loads from testing, particularly for anchors in non-cracked concrete. CEN/TS predicted concrete cone failure loads agree somewhat better with simulated failure loads than those from testing.

As demonstrated in this project, global stiffness of the concrete structure is of importance for the capacity of anchors loaded in tension. For anchors loaded in shear, sufficient global stiffness is in general often fulfilled as the anchors are loaded within the plane of the concrete structure. This is confirmed by the simulation results in chapter 7.

9. Conclusions

This research project has resulted in the following conclusions:

1. Concrete cone failure and concrete edge failure of headed single anchors and anchor groups in non-reinforced as well as in reinforced concrete can be simulated with confidence using finite element analyses.

2. The simulations show good agreement with results from physical tests. The failure load is better predicted than force-displacement curves.

3. The concrete damaged plasticity constitutive model in Abaqus is found to work very well for the simulation of the failure modes studied in this report.

4. The use of mean concrete cylinder compressive strength together with corresponding tensile strength in the concrete damaged plasticity constitutive model seems to be most appropriate for simulation of the physical response of concrete structures.

5. In general, reinforcement makes the failure of anchors loaded in tension or shear more ductile.

6. Global stiffness of the concrete structure is not considered by design codes such as CEN/TS in the design of anchors. For anchor groups loaded in tension, this lack might result in reduced safety margin against concrete cone failure if the concrete structure is too flexible. This is particularly true when non-cracked concrete is assumed.

7. For studied cases of single anchor in tension, simulated concrete cone failure loads for anchors in non-cracked reinforced concrete show better agreement with physical tests than that of anchors in pre-cracked reinforced concrete.

8. The simulations show that reinforcement in the direction of the applied load leads to a distinct increase of the concrete edge failure capacity. However, the simulations show that the normal stress in the reinforcement bars close to the anchors is considerably higher than in the rest of the bars tying the breakout body to the concrete member.

10. Further work

Further work is suggested within the following areas:

1. Anchor plates installed in concrete with shear reinforcement and loaded in tension. Simulations of several configurations with different distances between anchors and reinforcement. Comparison with capacities according to CEN/TS and other design codes.

2. Anchor plates installed close to a free concrete edge and loaded in tension. Numerical simulation and comparison with capacities according to CEN/TS and other design codes.

3. Pry-out failure of headed single anchor and anchor group in non-reinforced and reinforced concrete. Numerical simulation and comparison with capacities according to CEN/TS and other design codes.

4. Anchor plates loaded by eccentric tension load (i.e. tension and bending moment). Numerical simulation of both non-reinforced and reinforced members and comparison with capacities according to CEN/TS and other design codes.

5. Anchor plates loaded in tension and shear simultaneously. Numerical simulation of both non-reinforced and reinforced members and comparison with capacities according to CEN/TS and other design codes.

6. Anchor plates loaded in shear with hairpin reinforcement. Numerical simulation of both non-reinforced and reinforced members and comparison with capacities according to CEN/TS and other design codes.

7. Anchor plates loaded with cyclic load. Simulations of both non-reinforced and reinforced concrete members.

8. Development of recommendations for design of anchor plates by use of numerical simulations compatible with CEN/TS.

Acknowledgement

The Swedish Radiation Safety Authority (SSM) has sponsored this research project. This support is acknowledged.

References

ACI 349-76, 1978. Code requirements for nuclear safety related concrete structures. ACI Journal Vol. 75, pp. 329-347.

ACI 349-06, 2006. Code Requirements for Nuclear Safety-Related Concrete Structures (ACI 349-06) and Commentary. American Concrete Institute.

Bazant Z P, 1984. Size effect in blunt fracture: Concrete, rock, metal. J. Eng. Mechanics (ASCE), Vol 110(4), pp. 518-535.

Betonghandbok - Material, 2008. Betonghandbok - Material, utgåva 2. Svensk Byggtjänst.

Boverket, 2004. Boverkets handbok om betongkonstruktioner, BBK04. Karlskrona, 2004.

CEN/TS 1992-4-2, 2009. European committee for standardization. Design of fastenings for use in concrete – Part 4-2: Headed fasteners. Brussels, May 2009.

Comité Euro-International du Beton, 1991. CEB-FIP Model Code 1990. London, June 1991. Thomas Telford House, pp 36-37.

Cornelissen H, Hordijk D, Reinhardt H, 1986. Experimental determination of crack softening characteristics of normalweight and lightweight concrete. Delft University of Technolog, pp. 50-51, 1986.

Dassault Systémes, 2010. Abaqus *Analysis User's Manual Volume I-V*, *Version 6.10*, Abaqus INC.

EC2, 2005, European committee for standardization. Dimensionering av betongkonstruktioner. SS-EN 1992-1-1:2005.

Eligehausen R, Bouska P, Cervenka V, Pukl R, 1992. Size effect of the concrete cone failure load of anchor bolts. In: Bazant, Z.P. (Editor), Fracture Mechanics of Concrete Structures, pp. 517-525, Elsevier Applied Science, London, New York.

Gordon N, McMahon T, Finlayson B, Gippel C, Nathan R, 2004. Stream Hydrology: An Introduction for Ecologists, second edition. 2004, Chichester.

Hallowell Gross J, Klingner R, Graves H, 2001. ACI Structural Journal: Dynamic Behavior of Single and Double Near-Edge Anchors Loaded in Shear. October 2001.

Hillerborg A, Modeer M, Petersson P, 1976. Analysis of Crack Formation and Crack Growth in Concrete by Means of Fracture Mechanics and Finite Elements, Cement and Concrete Research, vol. 6, pp. 773-782, 1976.

Lee J, Fenves G, 1998. Plastic-Damage Model for Cyclic Loading of Concrete Structures, Journal of Engineering Mechanics, vol. 124, no. 8, pp. 892-900, 1998.

Lubliner J, Oliver J, Oller S, Oñate E, 1989. A Plastic-Damage Model for Concrete, International Journal of Solids and Structures, vol. 25, pp. 299-329, 1989.

Nilsson M, Elfgren L, 2009. Fastenings (Anchor Bolts) in Concrete Structures – Effect of Surface Reinforcement on. Nordic Symposium on Nuclear Technology, 25-26 November 2009, Stockholm.

Weibull W, 1939. A statistical theory of the strength of materials. Royal Swedish Academy Eng. Sci. Proc., 151, pp. 1-45.

APPENDIX 1

Extended result figures regarding numerical simulation of anchors loaded in tension

In this Appendix, figures with the damage tension parameter (DAMAGET) are shown at failure load and at end of simulation for a number of single anchors and anchor groups loaded in tension. Single anchor configurations and anchor group configurations are summarised in table A1-1 and table A1-2, respectively. Table A1-1 is identical to table 6-9 and table A1-2 is identical to table 6-14.

Table A1-1: Summary of results from physical tests [Nilsson and Elfgren 2009] and corresponding simulation results.

No.	*L*	*H*	Top reinforce-ment	Pre-crack	$\bar{N}_{u,test}$	$N_{u,simulation}$	$\frac{N_{u,simulation}}{\bar{N}_{u,test}}$
	[m]	[m]		[mm]	[kN]	[kN]	[-]
1	1.2	0.3	-	0	196	270	1.38
2	1.2	0.3	ø12cc300	0	280	284	1.01
3	1.2	0.3	ø16cc150	0	319	305	0.96
4	1.2	0.3	ø16cc100	0	317	346	1.09
5	1.2	0.6	ø12cc300	0	357	349	0.98
6	2.2	0.3	ø12cc400	0	241	267	1.11
7	2.2	0.3	ø12cc150	0	262	288	1.10
8	2.2	0.6	ø12cc150	0	327	354	1.08
9	1.2	0.3	-	0.5	144	212	1.47
10	1.2	0.3	ø12cc300	0.5	292	245	0.84
11	1.2	0.3	ø16cc150	0.5	303	266	0.88
12	1.2	0.3	ø16cc100	0.5	256	325	1.27
13	2.2	0.3	ø12cc500	0.5	217	249	1.15

Table A1-2: Investigated configurations of anchor groups in reinforced concrete slabs. $N_{u,group}$ is the failure load of the group.

Slab	Slab dimension [m]	Top rein-forcement	Support	Anchor group	Cross-section of profile [mm]	$N_{u,group}$ [kN]
1	2.2x2.2x0.3	ø12cc300	Ring	2x2	120x120	341
2	2.2x2.2x0.3	ø12cc150	Ring	2x2	120x120	464
3	2.2x2.2x0.3	ø12cc100	Ring	2x2	120x120	492
4	2.2x2.2x0.3	ø12cc150	Ring	2x2	220x220	461
5	2.2x2.2x0.3	ø12cc300	Ring	2x3	120x120	340
6	2.2x2.2x0.3	ø12cc150	Ring	2x3	120x120	443
7	2.2x2.2x0.3	ø12cc100	Ring	2x3	120x120	502
8	2.2x2.2x0.6	ø12cc150	Ring	2x2	120x120	612
9	2.2x2.2x0.6	ø12cc150	Ring	2x2	220x220	622
10	3x3x0.6	ø12cc300	Simply supported	2x2	220x220	600
11	3x3x0.6	ø12cc300	Clamped	2x2	220x220	618

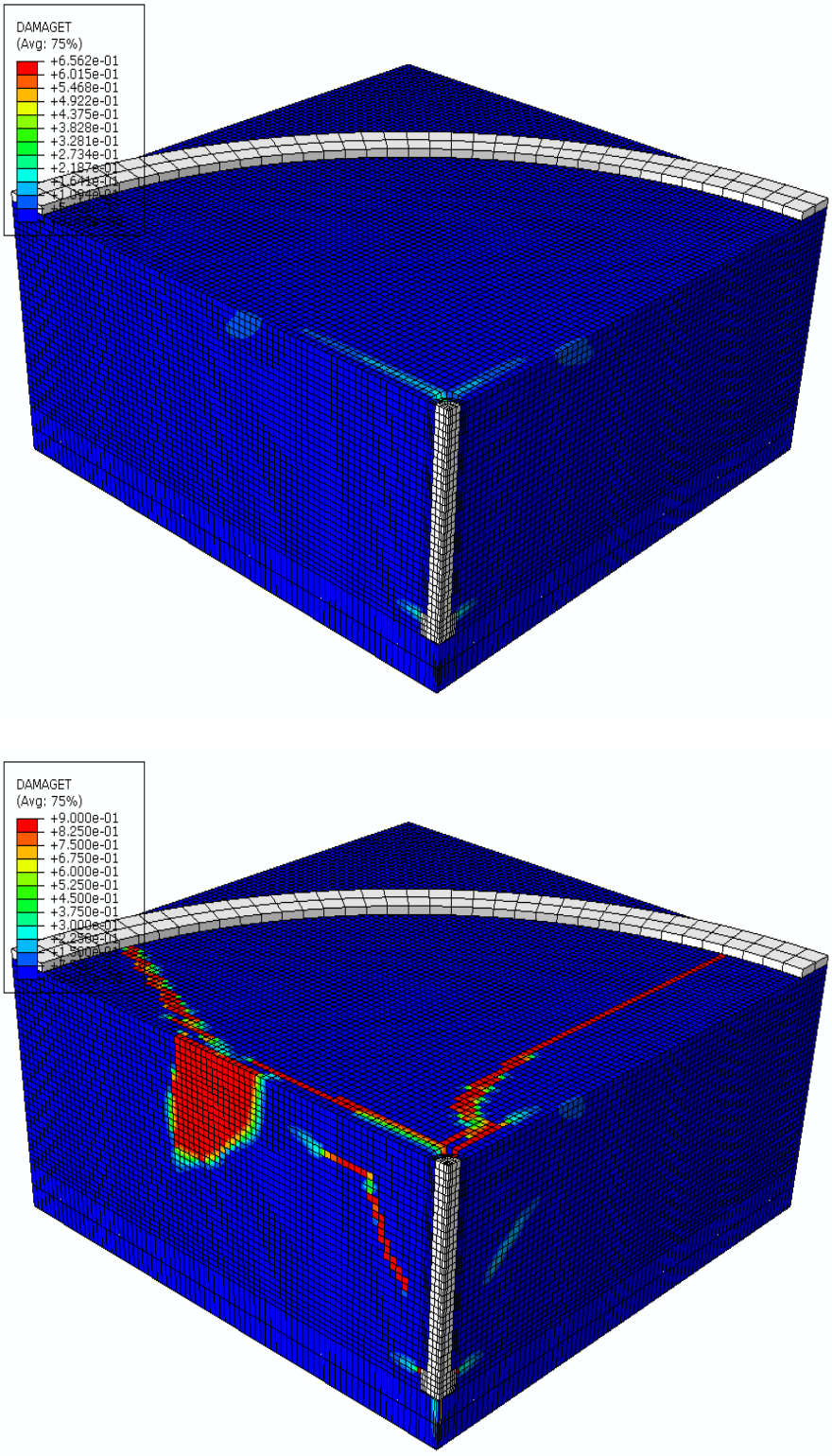

Figure A1-1: Damage tension parameter (DAMAGET) at failure load and at end of simulation for configuration 1 in table A1-1.

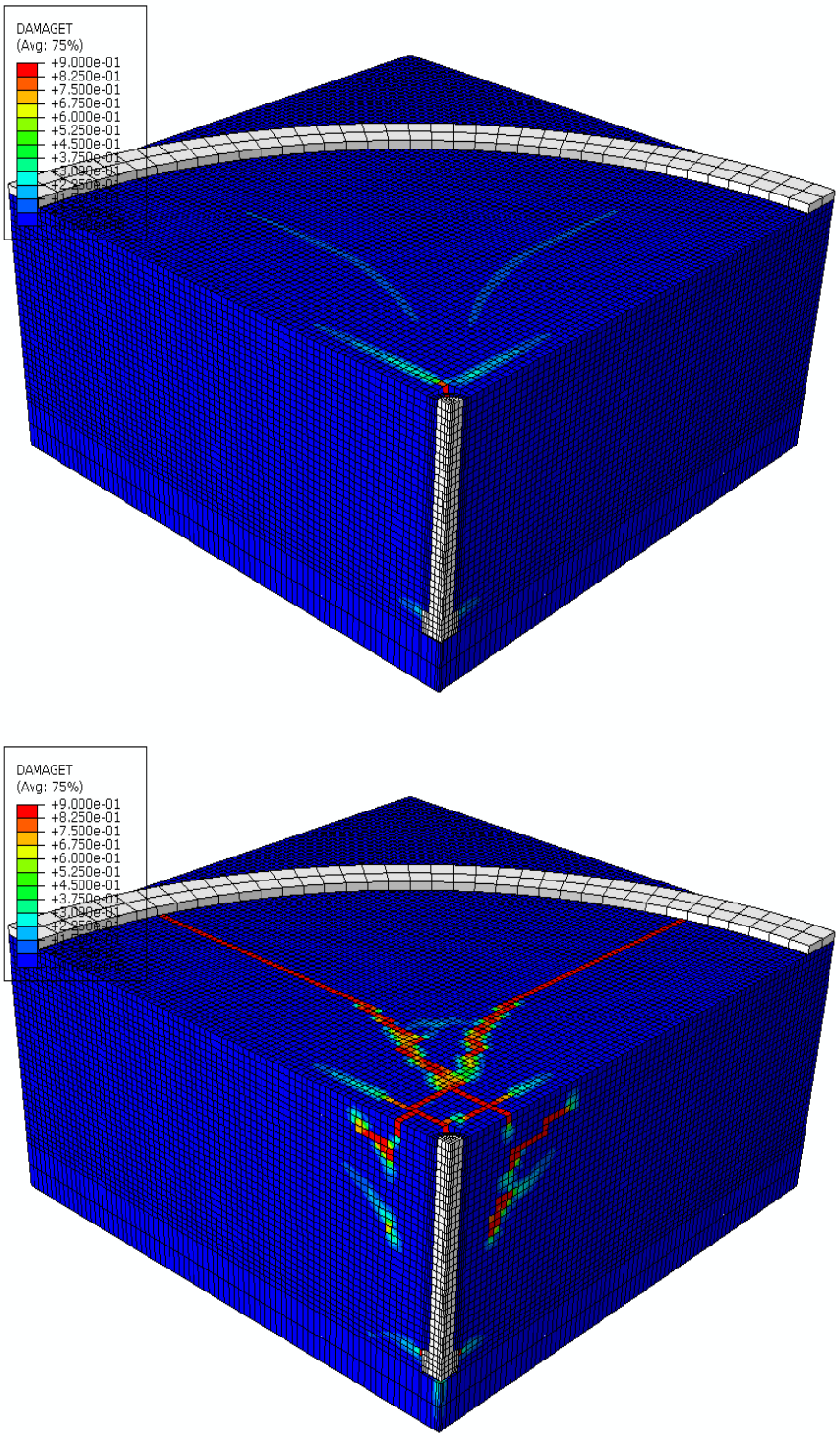

Figure A1-2: Damage tension parameter (DAMAGET) at failure load and at end of simulation for configuration 2 in table A1-1.

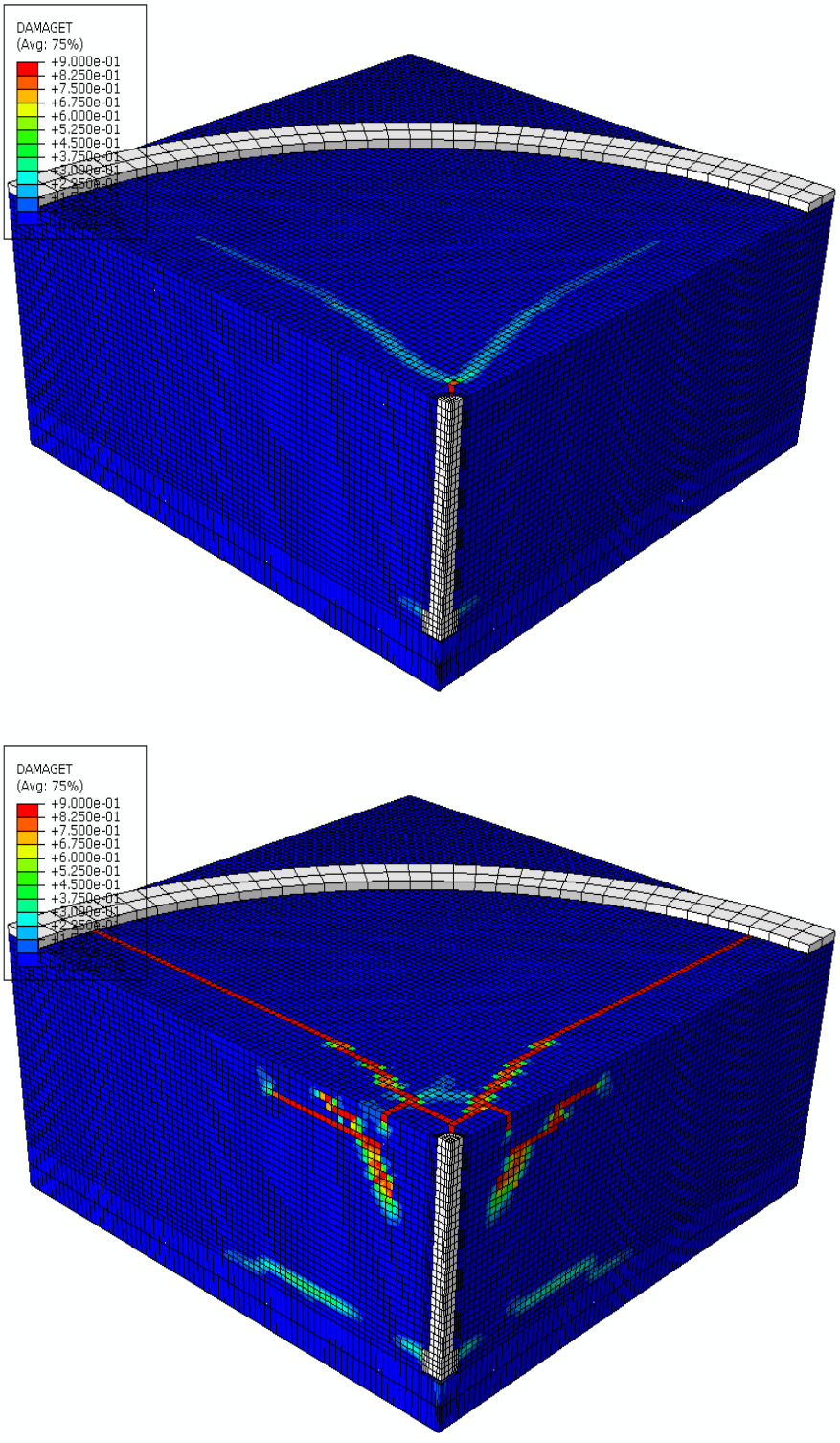

Figure A1-3: Damage tension parameter (DAMAGET) at failure load and at end of simulation for configuration 3 in table A1-1.

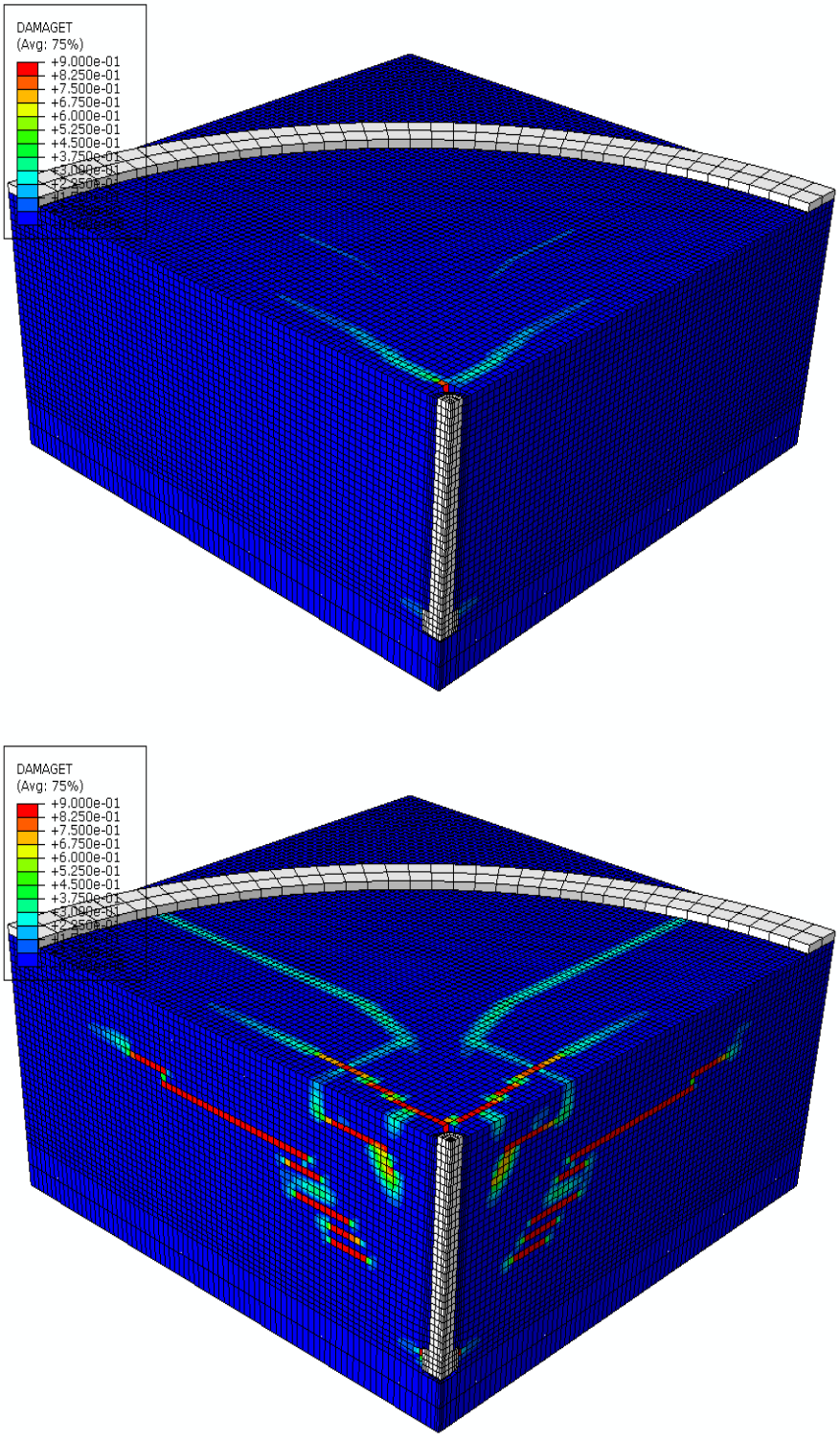

Figure A1-4: Damage tension parameter (DAMAGET) at failure load and at end of simulation for configuration 4 in table A1-1.

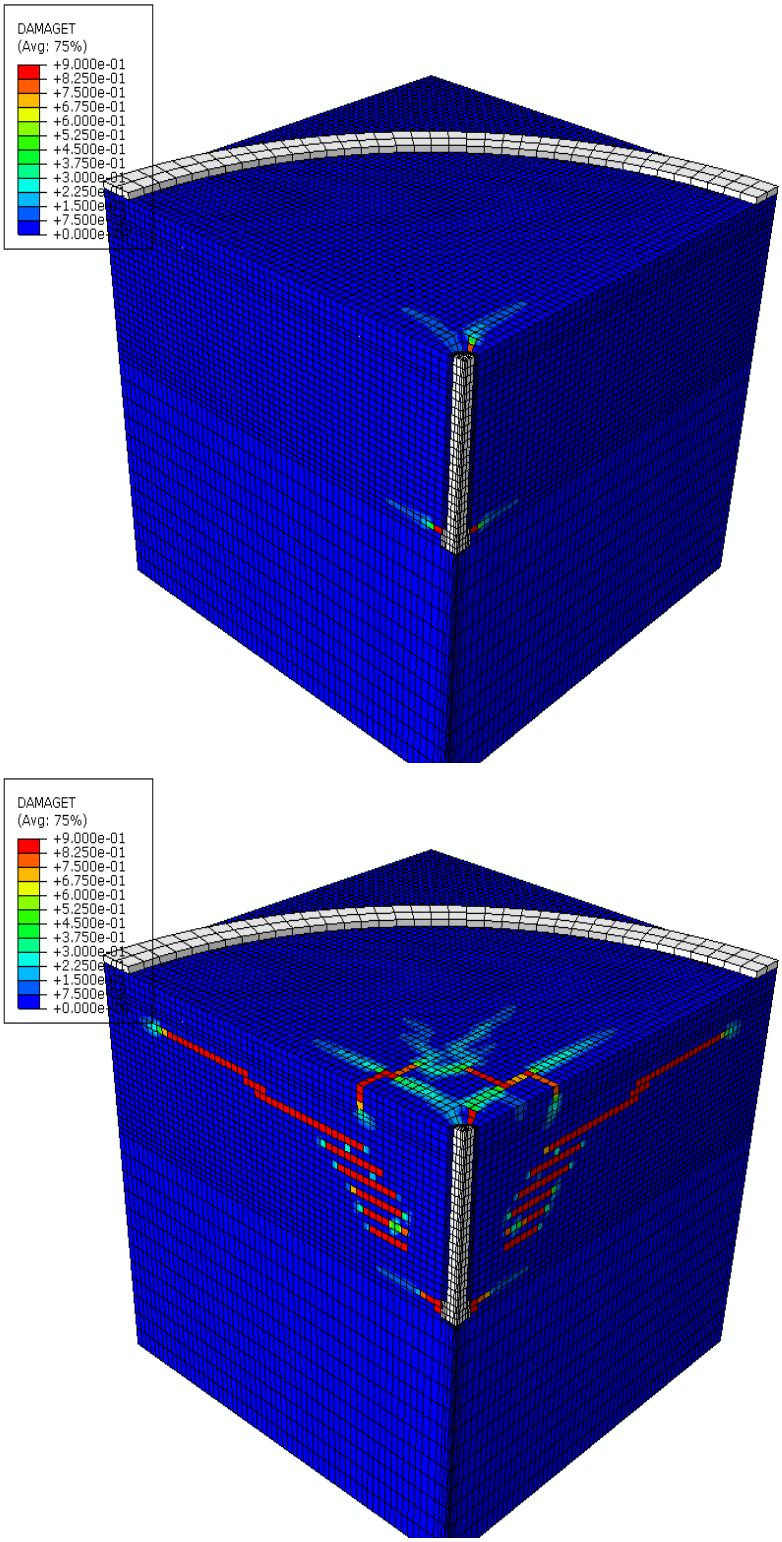

Figure A1-5: Damage tension parameter (DAMAGET) at failure load and at end of simulation for configuration 5 in table A1-1.

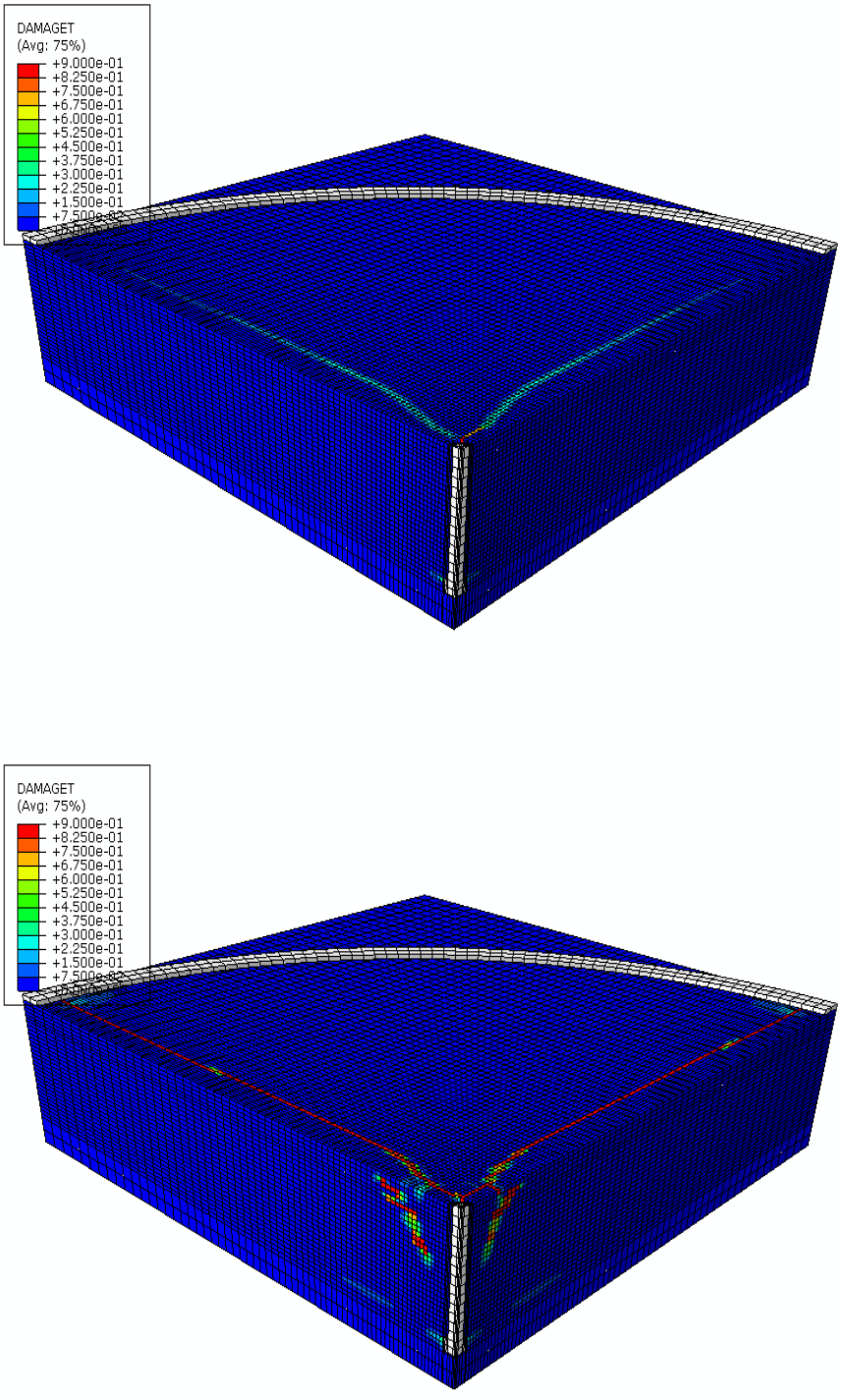

Figure A1-6: Damage tension parameter (DAMAGET) at failure load and at end of simulation for configuration 7 in table A1-1.

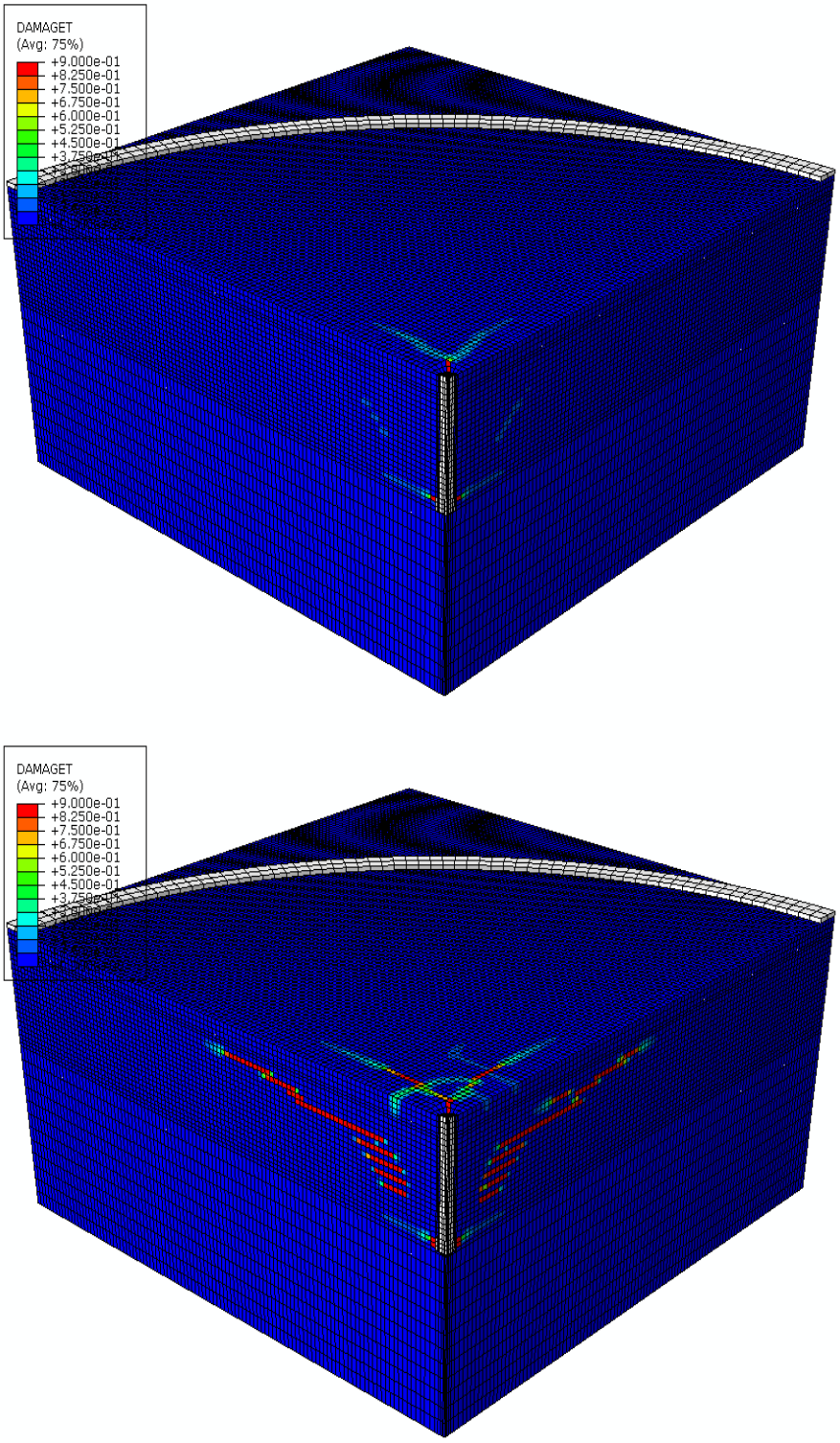

Figure A1-7: Damage tension parameter (DAMAGET) at failure load and at end of simulation for configuration 8 in table A1-1.

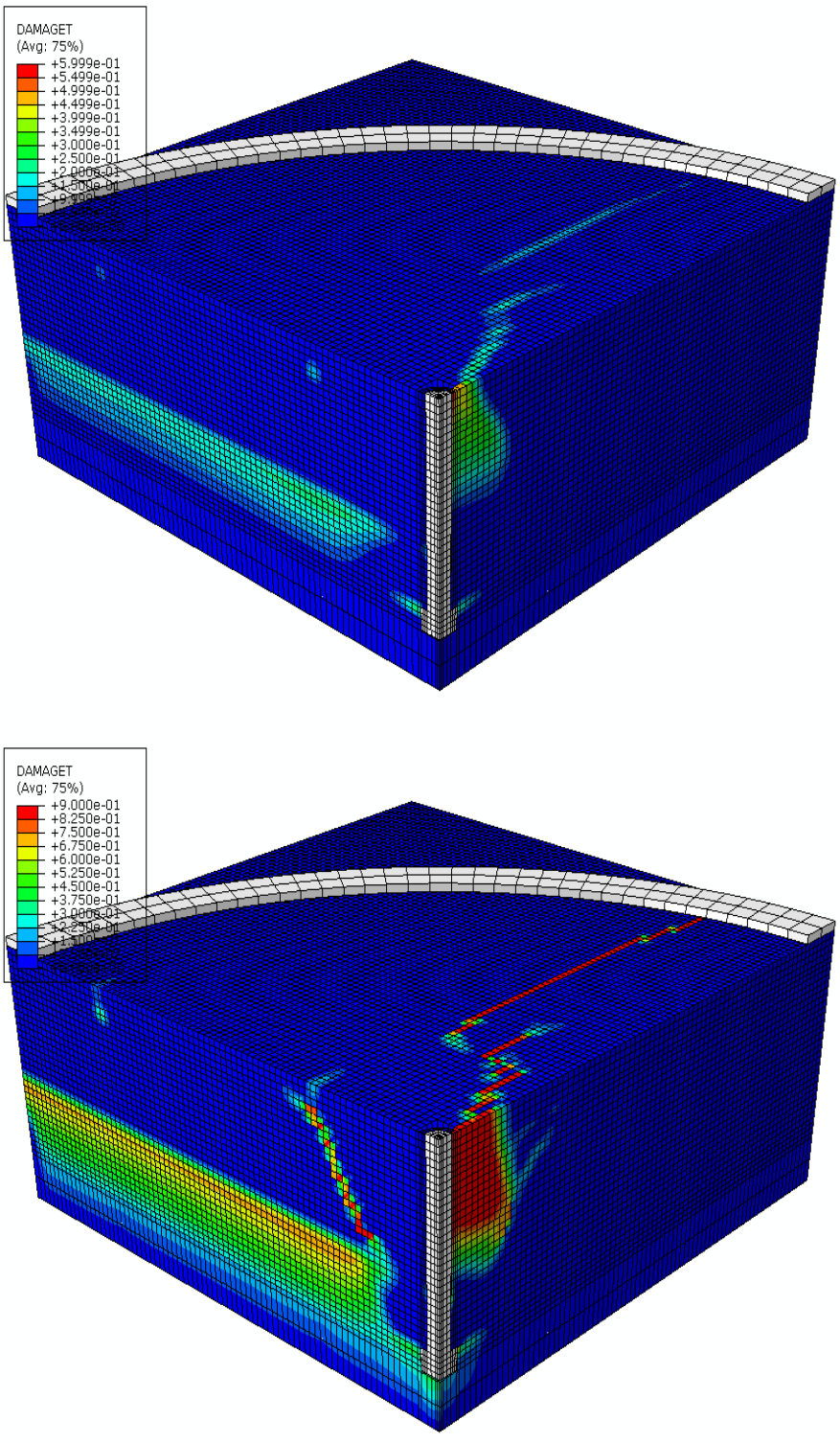

Figure A1-8: Damage tension parameter (DAMAGET) at failure load and at end of simulation for configuration 10 in table A1-1.

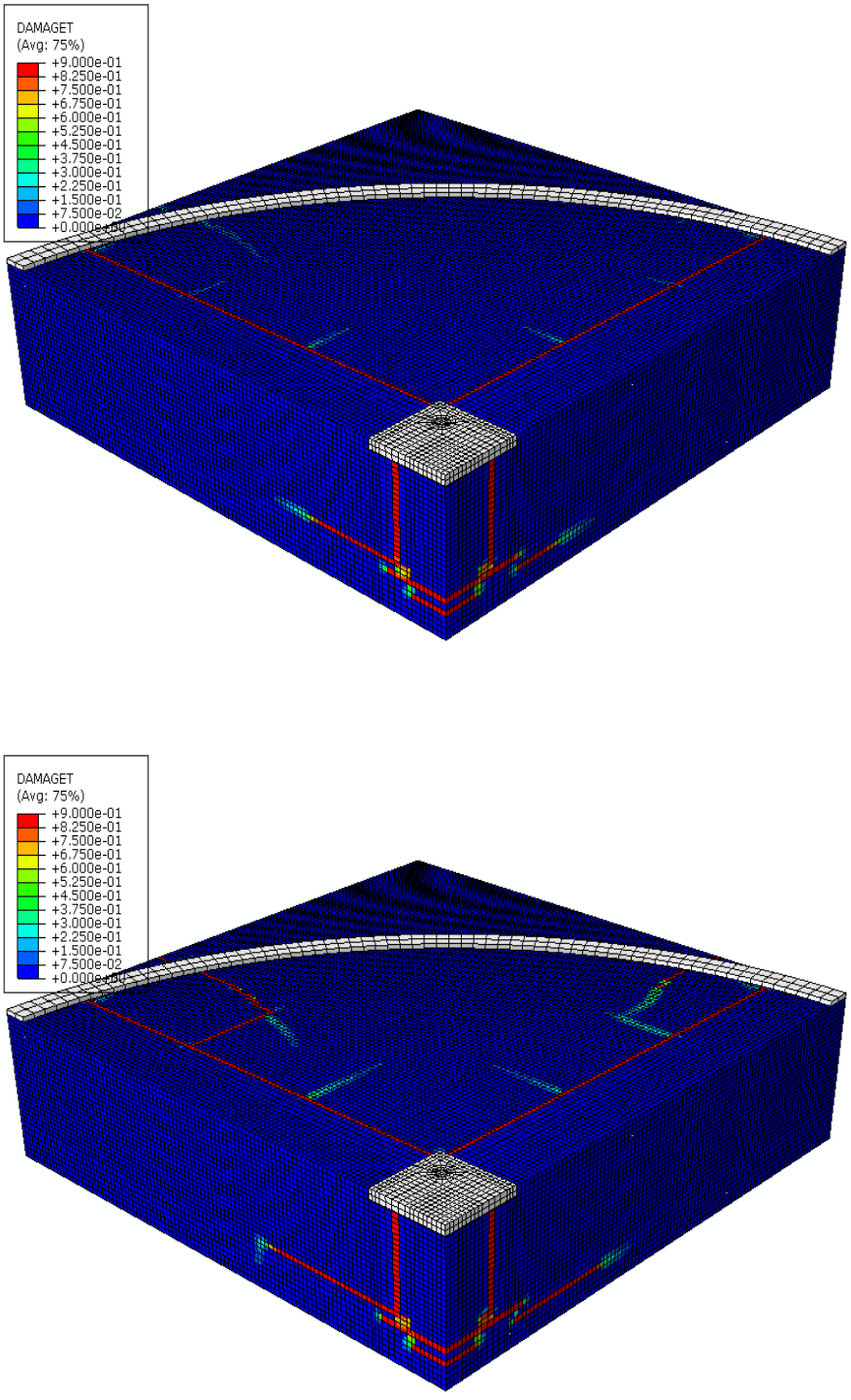

Figure A1-9: Damage tension parameter (DAMAGET) at failure load and at end of simulation for configuration 1 in table A1-2.

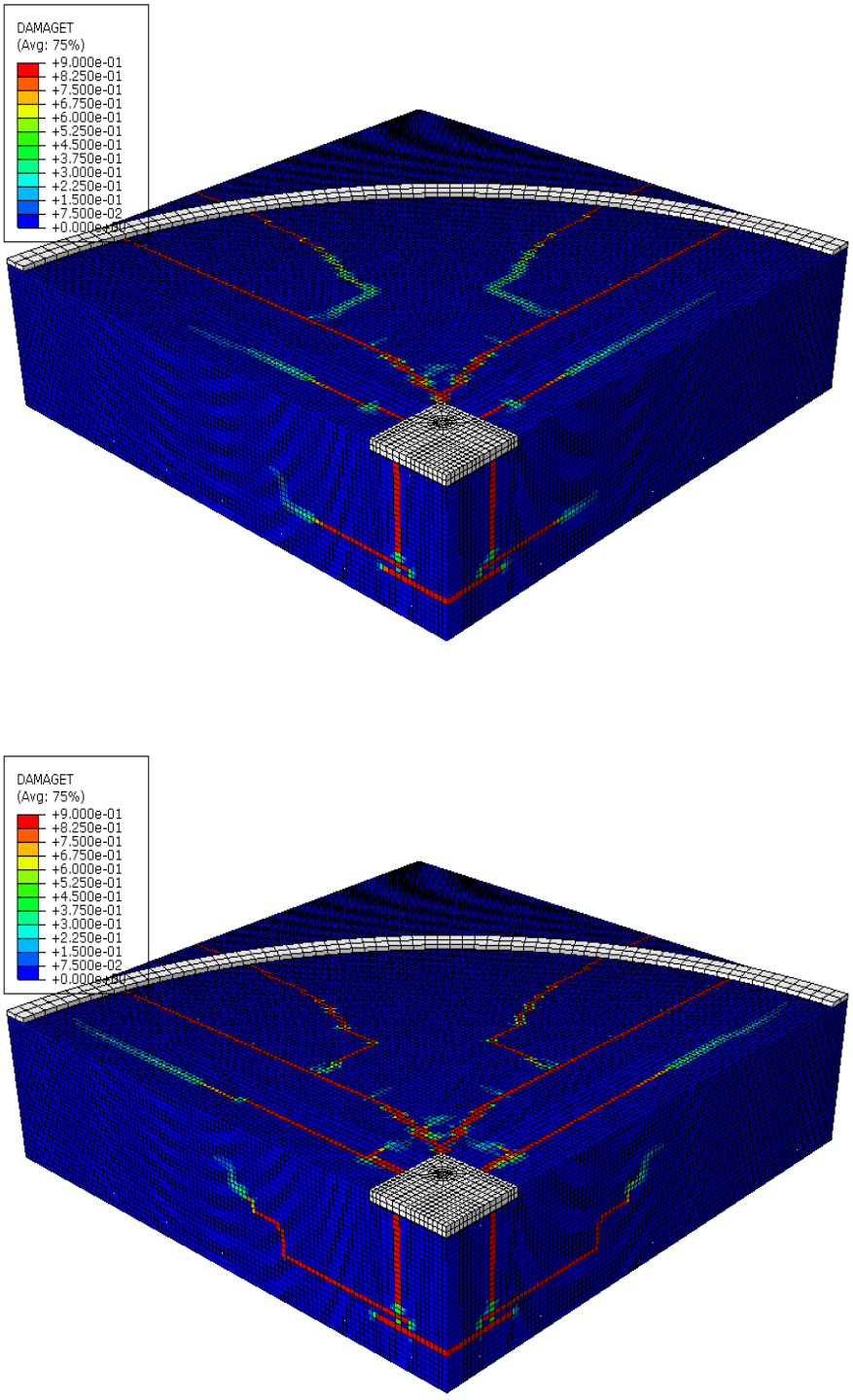

Figure A1-10: Damage tension parameter (DAMAGET) at failure load and at end of simulation for configuration 2 in table A1-2.

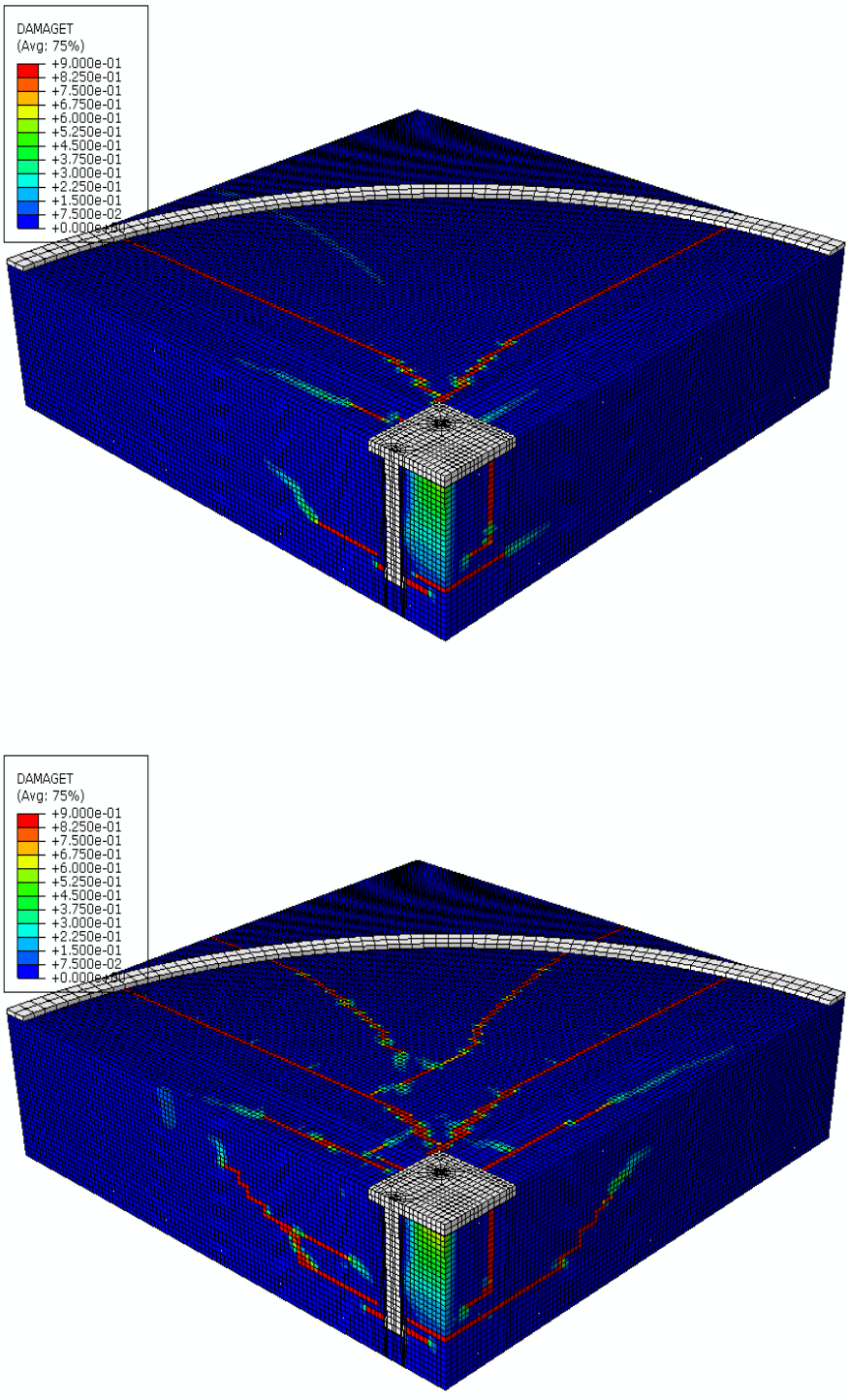

Figure A1-11: Damage tension parameter (DAMAGET) at failure load and at end of simulation for configuration 6 in table A1-2.

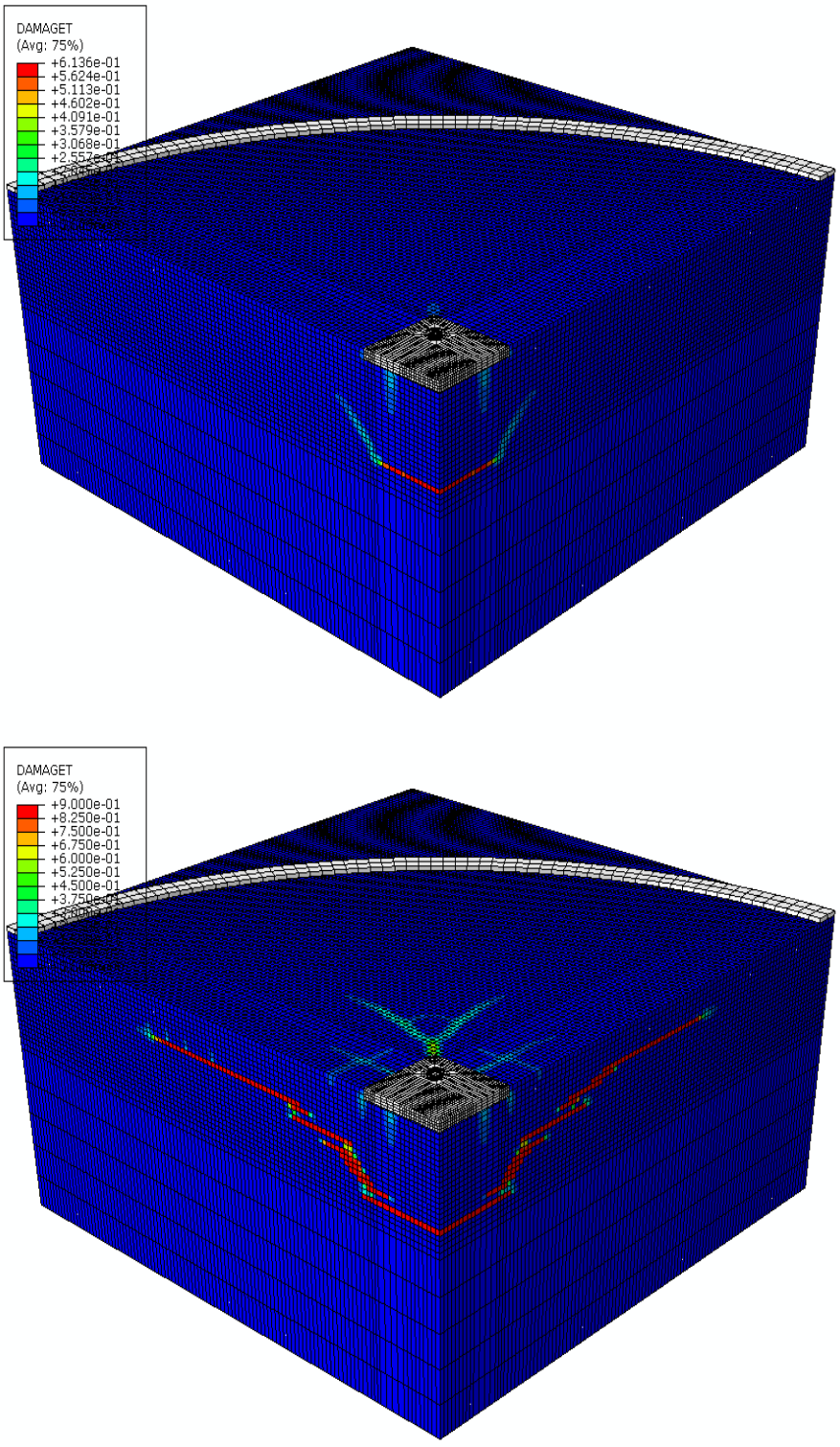

Figure A1-12: Damage tension parameter (DAMAGET) at failure load and at end of simulation for configuration 8 in table A1-2.

APPENDIX 2

Anchors loaded in shear: Additional result plots

CONTENT

A2.1 FINITE ELEMENT MODEL STIFFNESS - HOURGLASSING

Results in terms of force-displacement relations for the different hourglass control methods presented in table 7-2 are shown in figure A2.1-1. The concrete cylinder compressive strength in the study has been 25 MPa (differ from the main analysis described in section 7.3.1), hence the results are not comparable to physical test results. Anyhow the intermutual relation between the results is of interest.

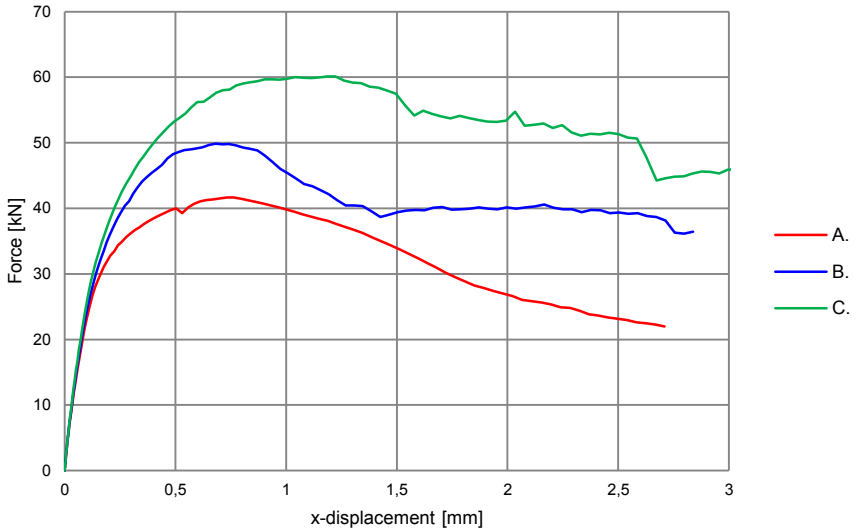

A. Relax stiffness
B. Stiffness
C. Enhanced

Figure A2.1-1: Relation between force and displacement for different Abaqus hourglass control methods.

Due to excessive hourglassing when using the viscous hourglass control method the results are discarded. In table A2.1-1 the failure loads for the other investigated hourglass control methods are presented. The figures referred to show fracture surfaces where part of the concrete block in the vicinity of the anchor bolt is visualized.

Table A2.1-1 Abaqus hourglass control methods with corresponding failure load and fracture surface.

Hourglass control method	Failure load [kN]	Fracture surface
Relax stiffness	41.7	See figure A2.1-2 to A2.1-3
Stiffness	49.9	See figure A2.1-4 to A2.1-5
Enhanced	60.1	See figure A2.1-6 to A2.1-7
Viscous	N/A	N/A

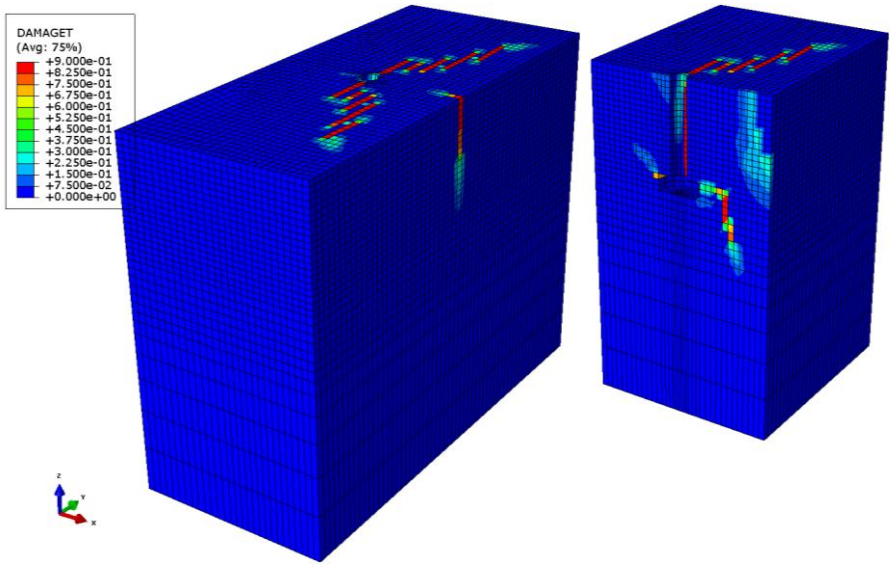

Figure A2.1-2: Hourglass control method – Relax stiffness. Damage tension parameter at the time of peak load (41.7kN).

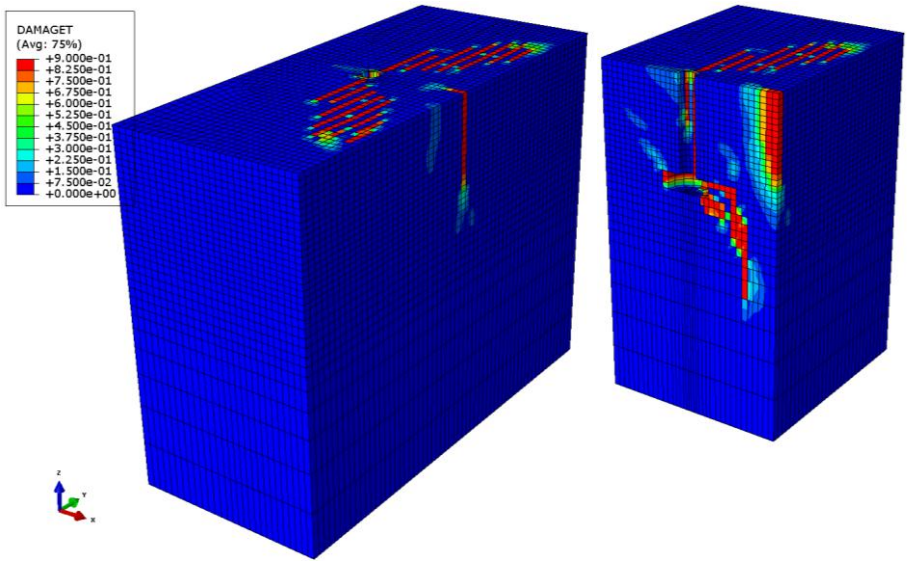

Figure A2.1-3: Hourglass control method – Relax stiffness. Damage tension parameter at the last increment.

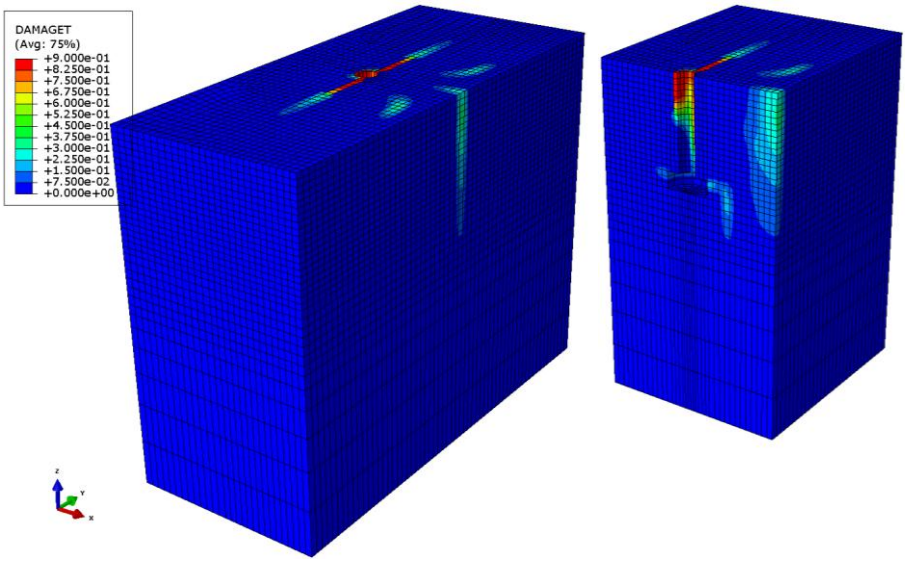

Figure A2.1-4: Hourglass control method – Stiffness. Damage tension parameter at the time of peak load (49.9kN).

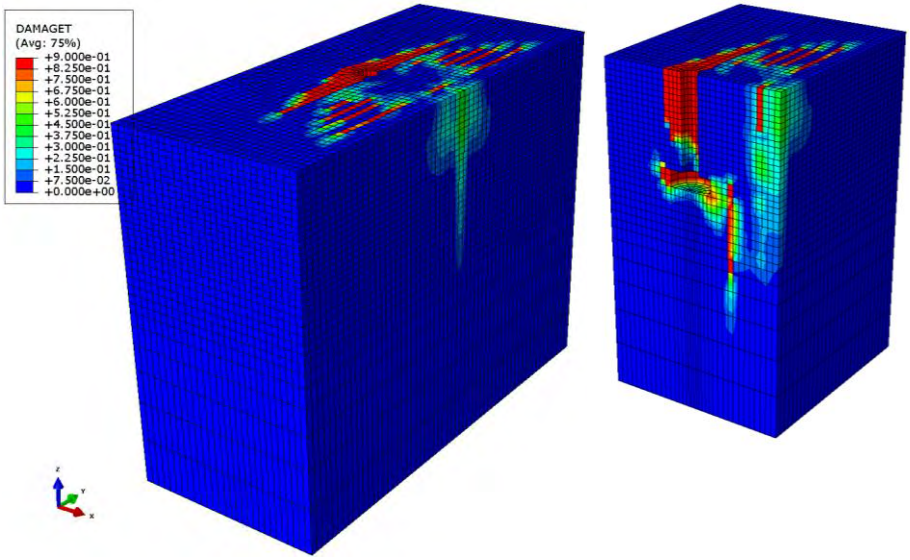

Figure A2.1-5: Hourglass control method – Stiffness. Damage tension parameter at the last increment.

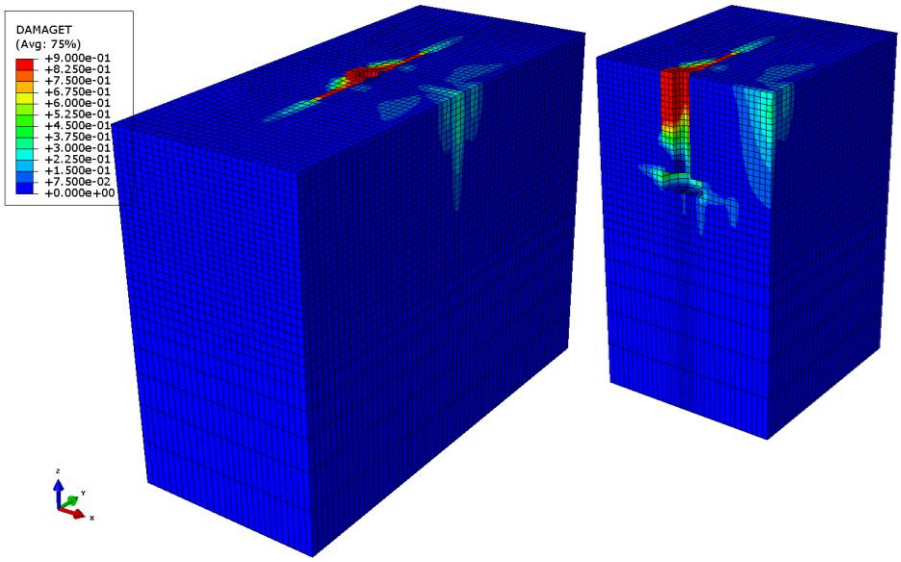

Figure A2.1-6: Hourglass control method – Enhanced. Damage tension parameter at the time of peak load (60.1kN).

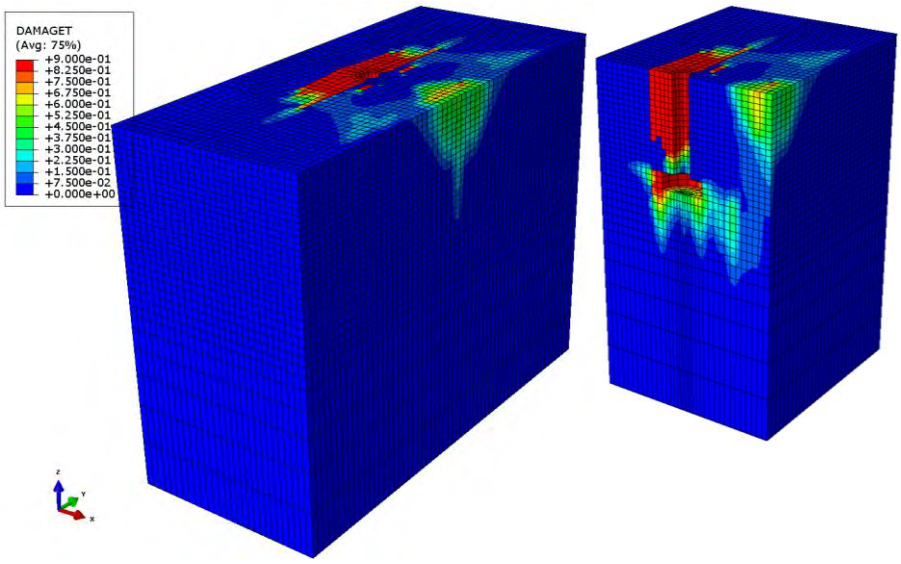

Figure A2.1-7: Hourglass control method – Enhanced. Damage tension parameter at the last increment.

A2.2 PARAMETRIC STUDY – DILATION ANGLE

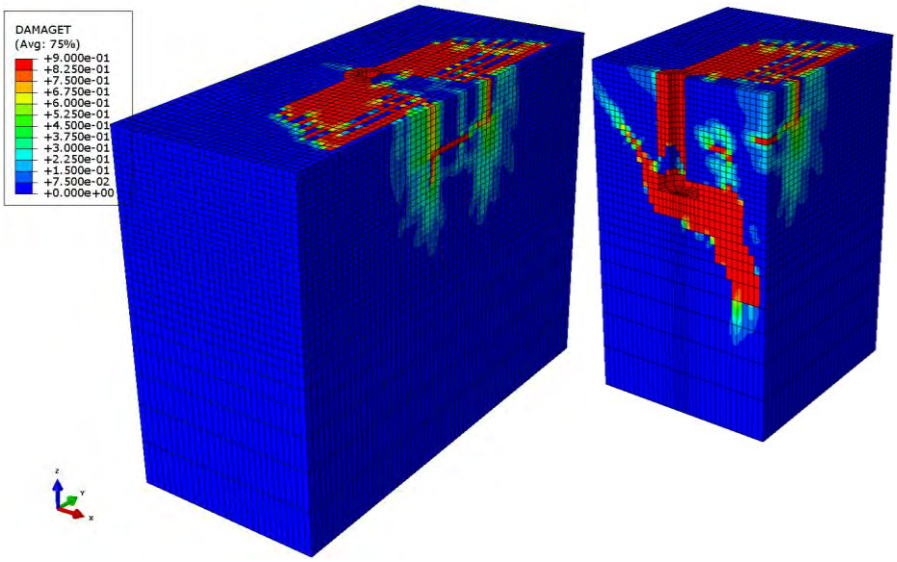

Figure A2.2-1: Dilation angle 28°. Damage tension parameter at the last increment.

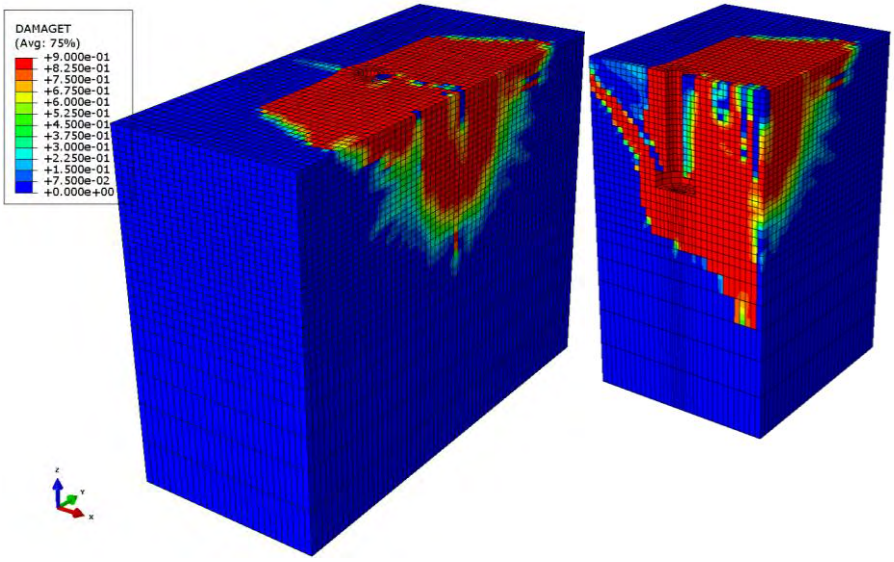

Figure A2.2-2: Dilation angle 35°. Damage tension parameter at the last increment.

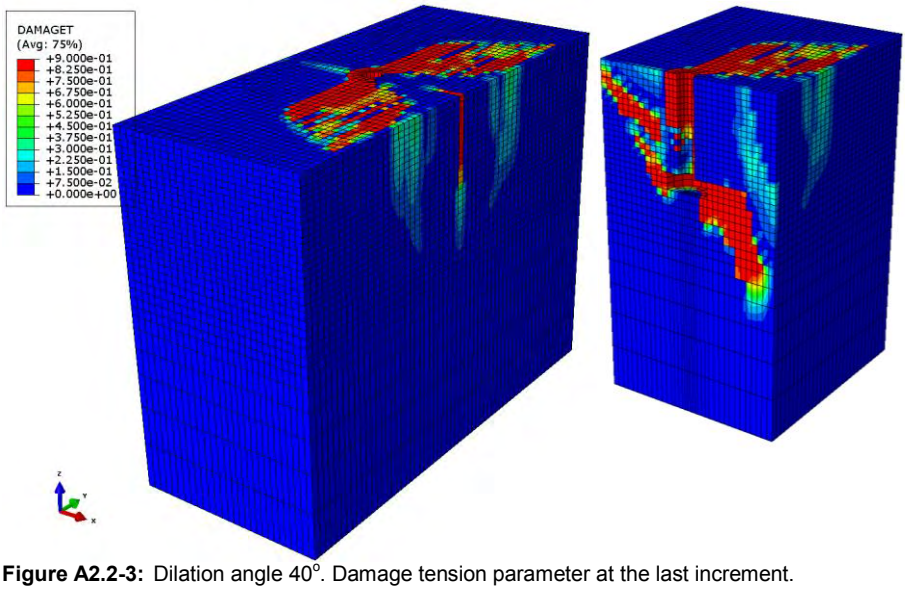

Figure A2.2-3: Dilation angle 40°. Damage tension parameter at the last increment.

A2.3 PARAMETRIC STUDY – FRACTURE ENERGY

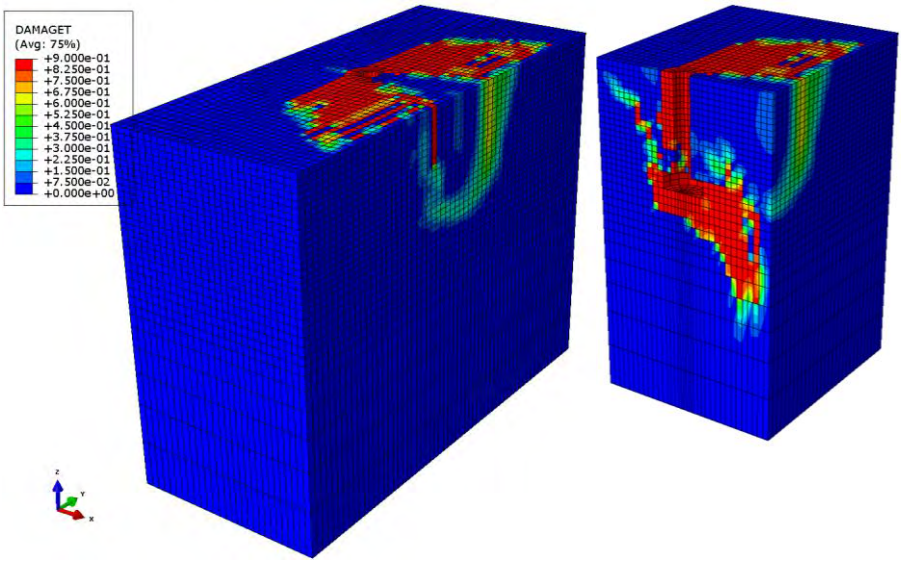

Figure A2.3-1: Damage tension parameter at the last increment for concrete with fracture energy 85 Nm/m^2 (dilation angle 35^o).

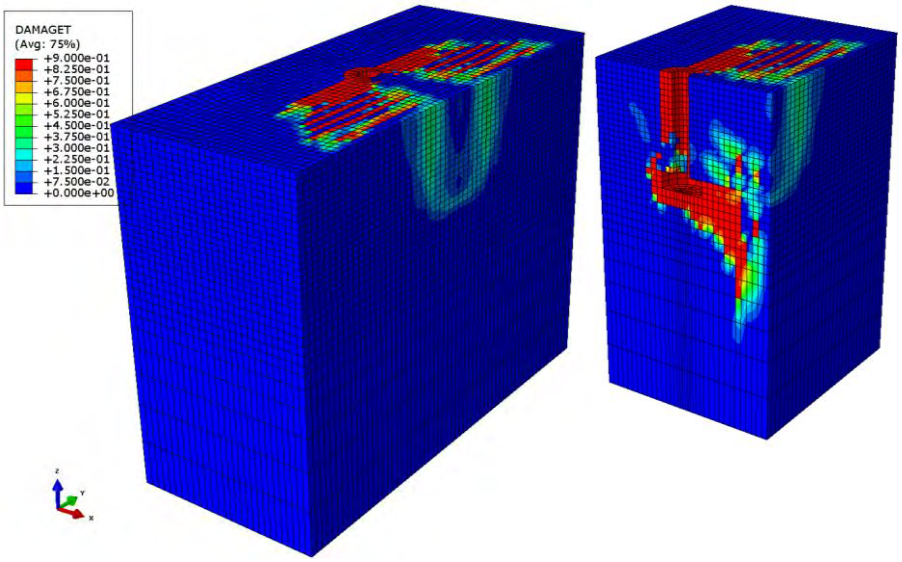

Figure A2.3-2: Damage tension parameter at the last increment for concrete with fracture energy 134 Nm/m^2 (dilation angle 35^o).

A2.4 SINGLE ANCHOR – REINFORCEMENT IN LONGITUDINAL DIRECTION

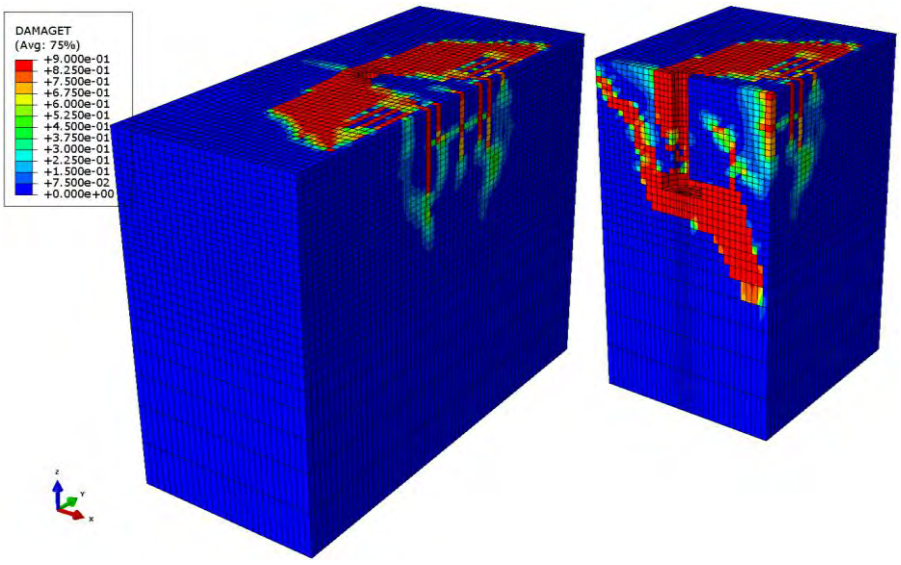

Figure A2.4-1: Damage tension parameter at last increment.

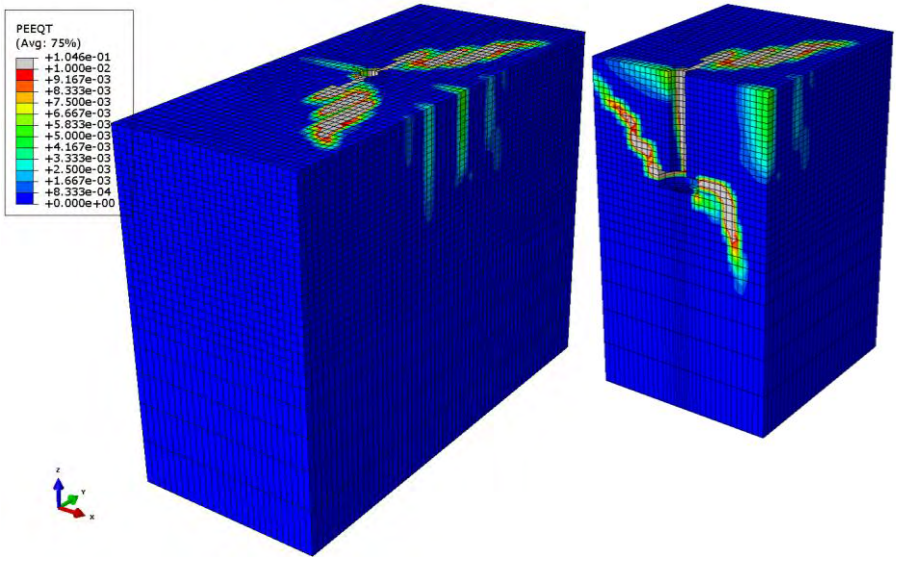

Figure A2.4-2: Plastic strains (PEEQT) at the time of peak load (42.6kN). Grey areas indicate strains greater than 10‰.

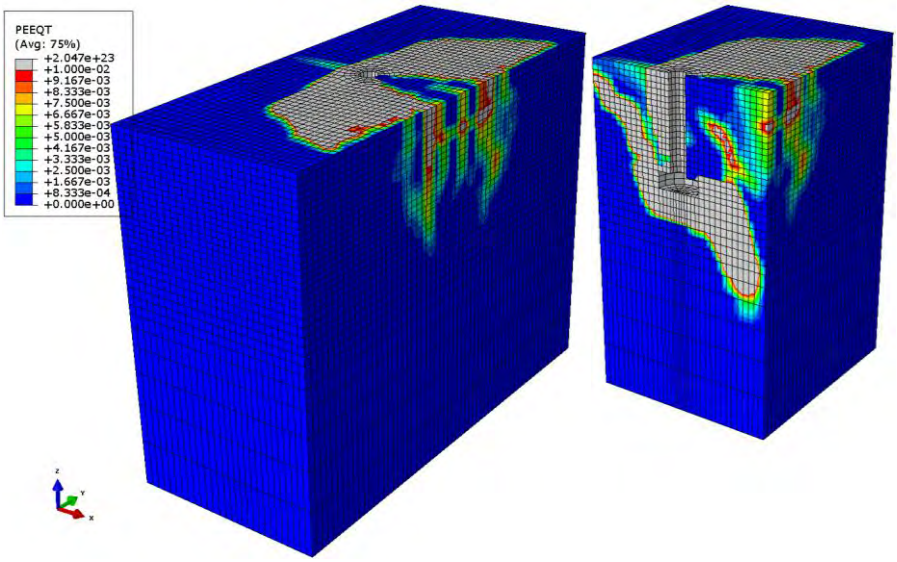

Figure A2.4-3: Plastic strains (PEEQT) at last increment. Grey areas indicate strains greater than 10‰.

A2.5 SINGLE ANCHOR – SHEAR REINFORCEMENT SETUP B

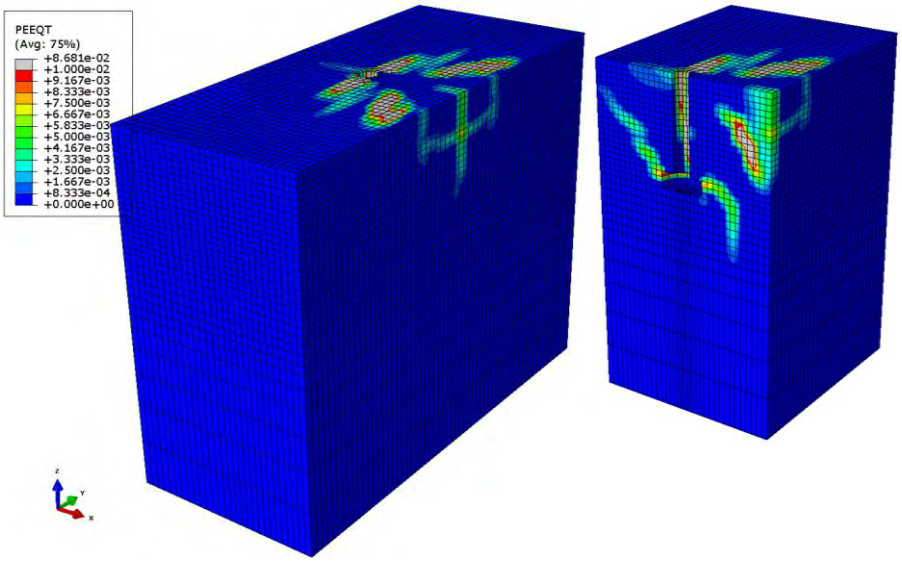

Figure A2.5-1: Reinforcement setup B. Plastic strains (PEEQT) at the time of peak load (52.6kN). Grey areas indicate strains greater than 10‰.

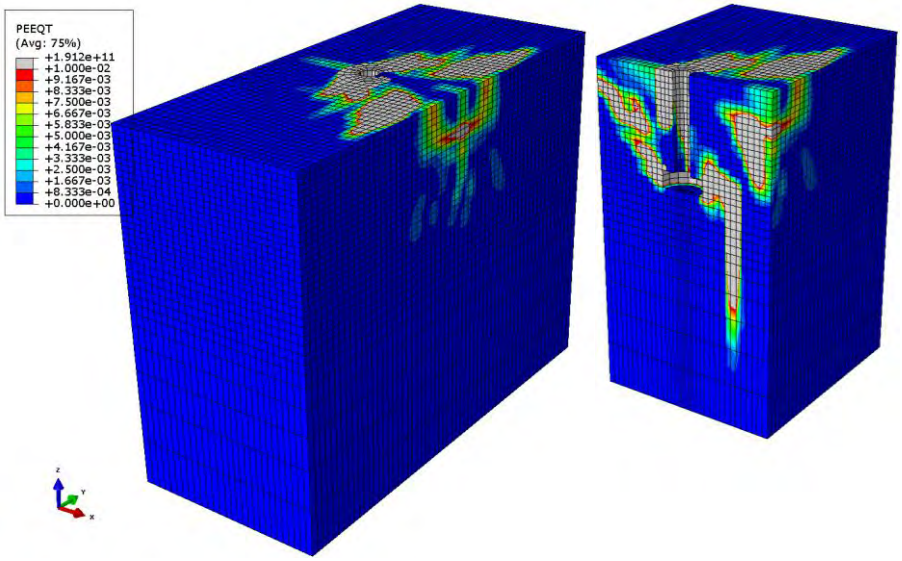

Figure A2.5-2: Reinforcement setup B. Plastic strains (PEEQT) at the last increment. Grey areas indicate strains greater than 10‰.

Following sequence of figures show the propagation of the concrete failure for reinforcement setup B. The fifth sequence figure is at the time of the peak load (52.6kN).

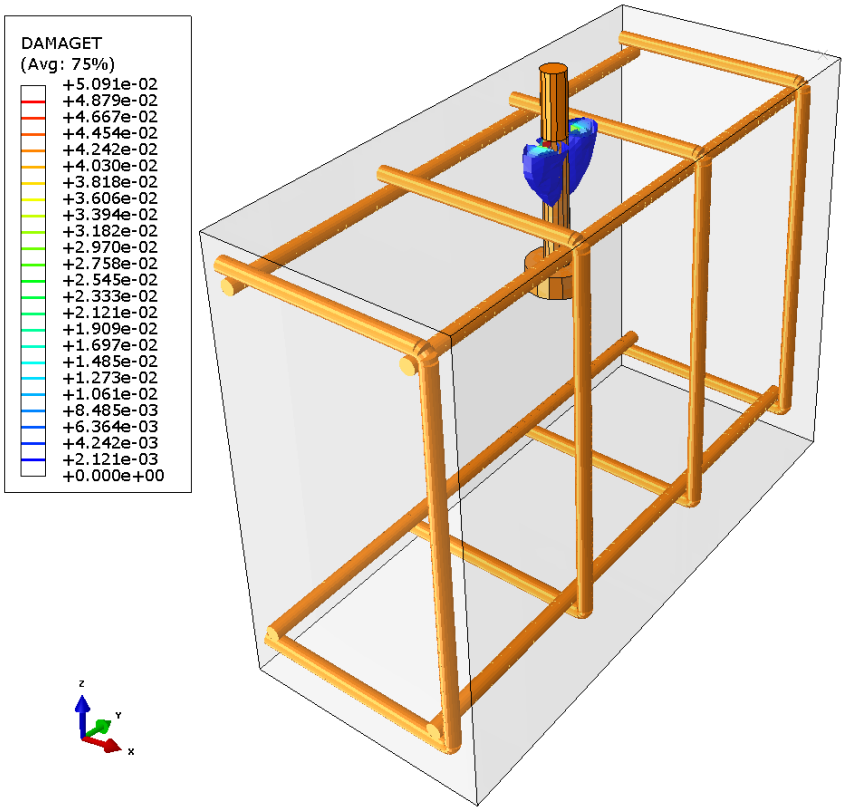

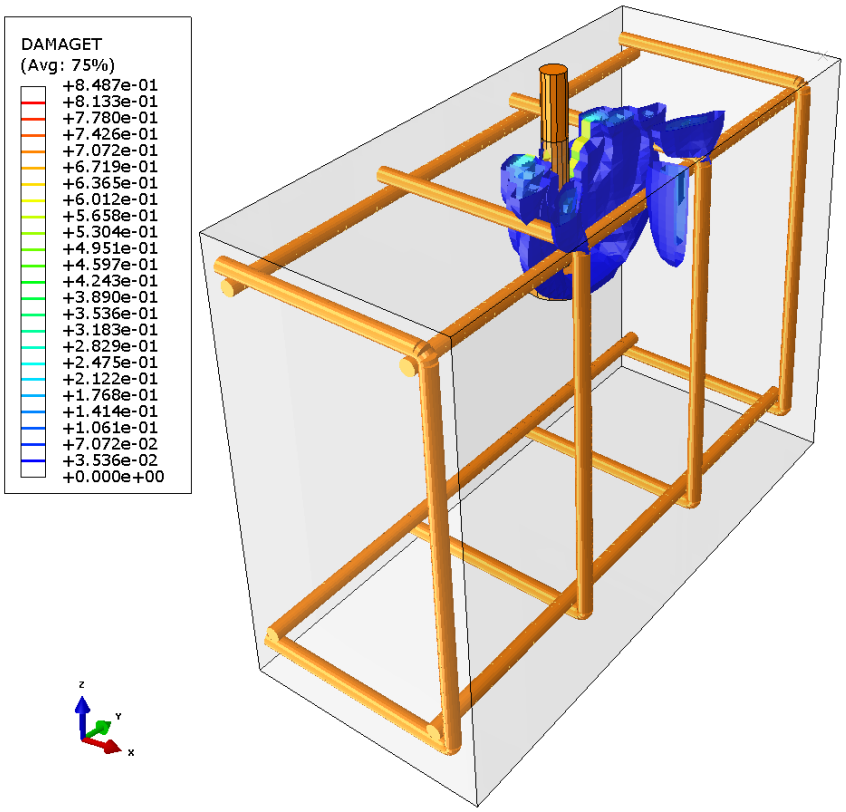

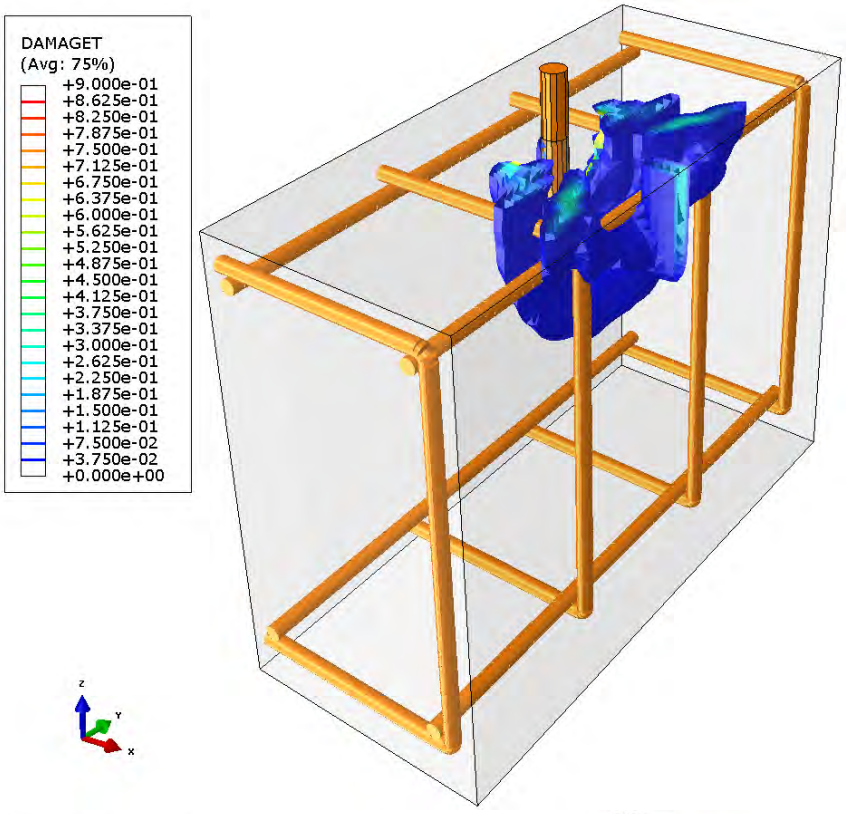
DAMAGET
(Avg: 75%)
+9.000e-01
+8.625e-01
+8.250e-01
+7.875e-01
+7.500e-01
+7.125e-01
+6.750e-01
+6.375e-01
+6.000e-01
+5.625e-01
+5.250e-01
+4.875e-01
+4.500e-01
+4.125e-01
+3.750e-01
+3.375e-01
+3.000e-01
+2.625e-01
+2.250e-01
+1.875e-01
+1.500e-01
+1.125e-01
+7.500e-02
+3.750e-02
+0.000e+00
Z
Y
X

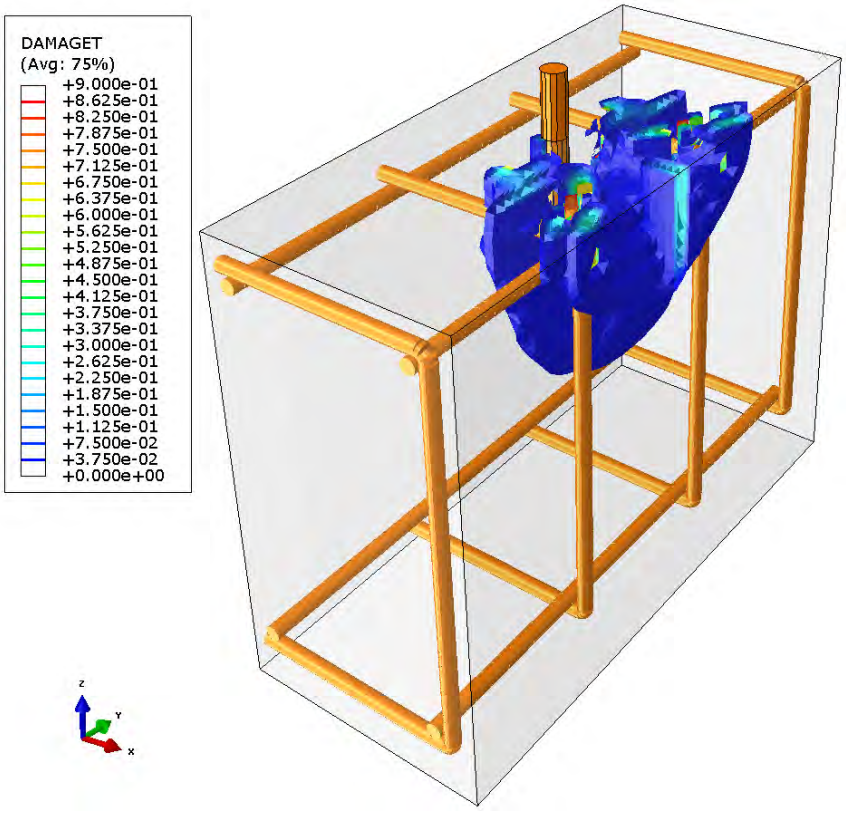
DAMAGET
(Avg: 75%)
+9.000e-01
+8.625e-01
+8.250e-01
+7.875e-01
+7.500e-01
+7.125e-01
+6.750e-01
+6.375e-01
+6.000e-01
+5.625e-01
+5.250e-01
+4.875e-01
+4.500e-01
+4.125e-01
+3.750e-01
+3.375e-01
+3.000e-01
+2.625e-01
+2.250e-01
+1.875e-01
+1.500e-01
+1.125e-01
+7.500e-02
+3.750e-02
+0.000e+00
Z
Y
X

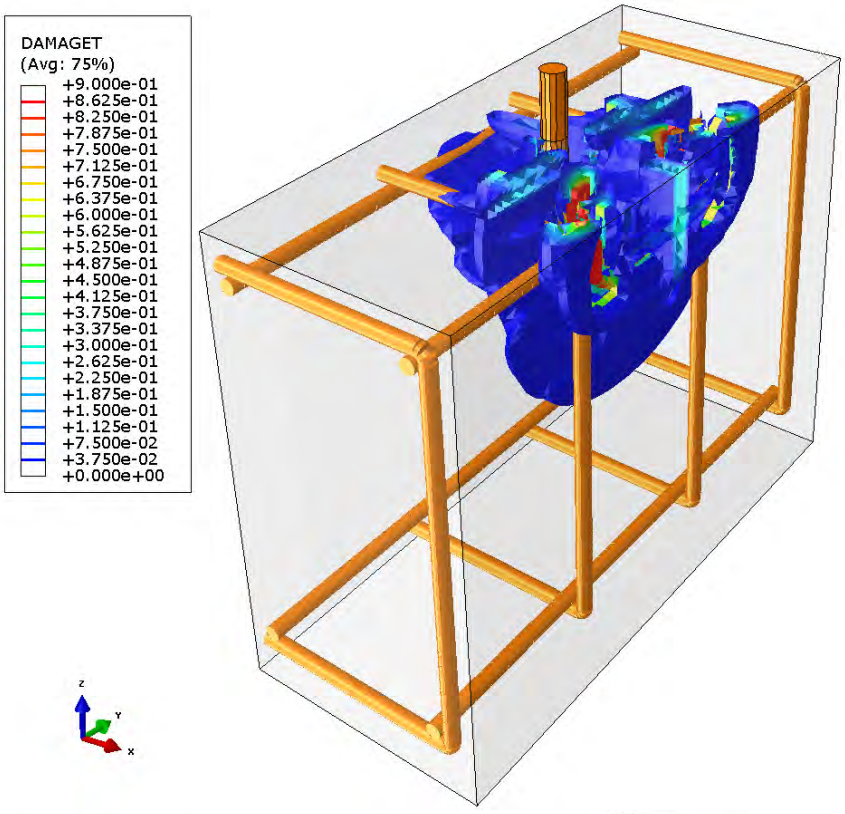
DAMAGET
(Avg: 75%)
+9.000e-01
+8.625e-01
+8.250e-01
+7.875e-01
+7.500e-01
+7.125e-01
+6.750e-01
+6.375e-01
+6.000e-01
+5.625e-01
+5.250e-01
+4.875e-01
+4.500e-01
+4.125e-01
+3.750e-01
+3.375e-01
+3.000e-01
+2.625e-01
+2.250e-01
+1.875e-01
+1.500e-01
+1.125e-01
+7.500e-02
+3.750e-02
+0.000e+00
Z
Y
X

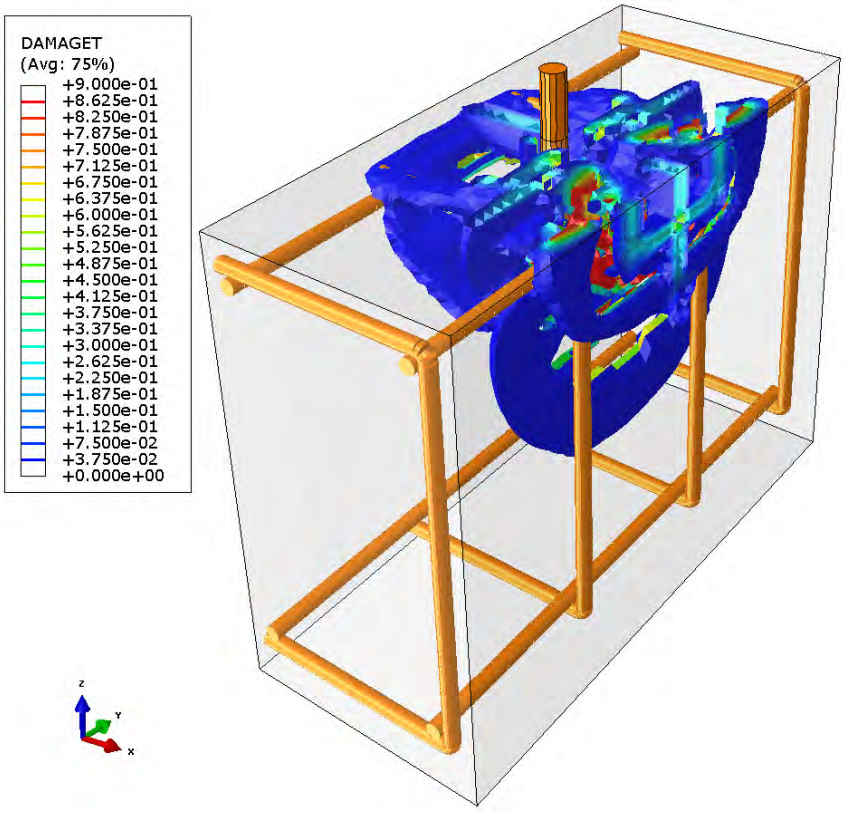
DAMAGET
(Avg: 75%)
+9.000e-01
+8.625e-01
+8.250e-01
+7.875e-01
+7.500e-01
+7.125e-01
+6.750e-01
+6.375e-01
+6.000e-01
+5.625e-01
+5.250e-01
+4.875e-01
+4.500e-01
+4.125e-01
+3.750e-01
+3.375e-01
+3.000e-01
+2.625e-01
+2.250e-01
+1.875e-01
+1.500e-01
+1.125e-01
+7.500e-02
+3.750e-02
+0.000e+00
Z
Y
X

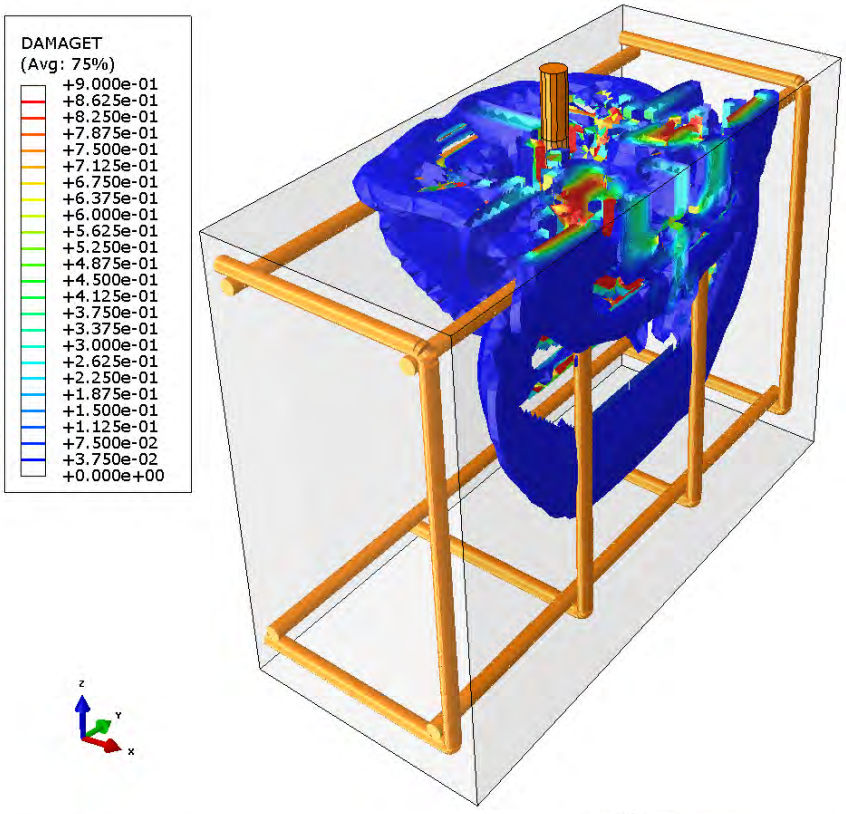
DAMAGET
(Avg: 75%)
+9.000e-01
+8.625e-01
+8.250e-01
+7.875e-01
+7.500e-01
+7.125e-01
+6.750e-01
+6.375e-01
+6.000e-01
+5.625e-01
+5.250e-01
+4.875e-01
+4.500e-01
+4.125e-01
+3.750e-01
+3.375e-01
+3.000e-01
+2.625e-01
+2.250e-01
+1.875e-01
+1.500e-01
+1.125e-01
+7.500e-02
+3.750e-02
+0.000e+00
Z
Y
X

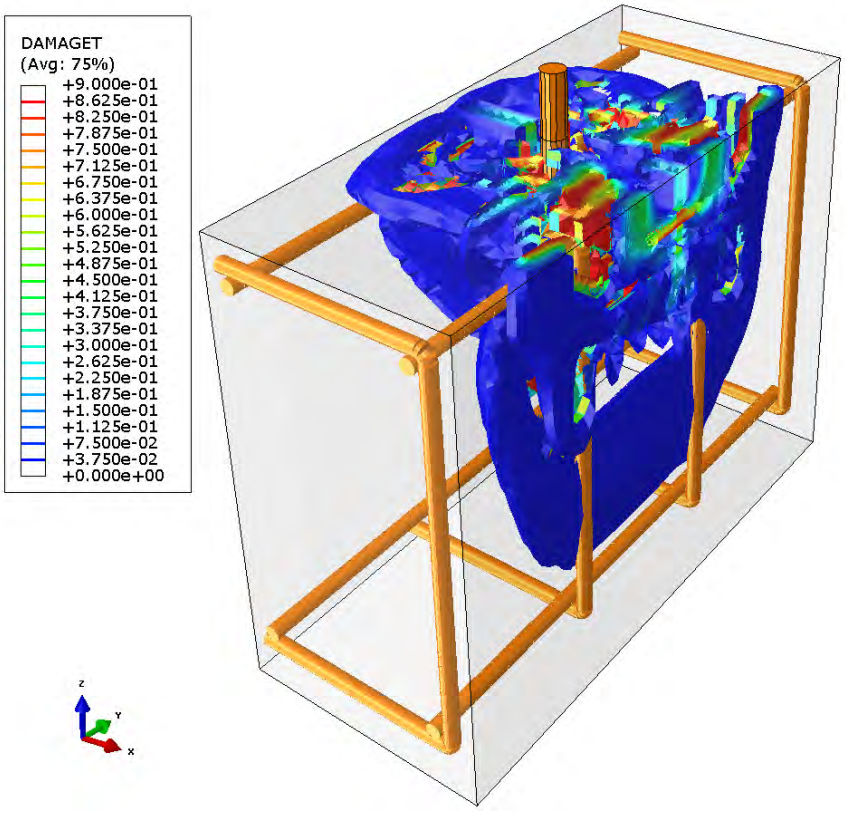
DAMAGET
(Avg: 75%)
+9.000e-01
+8.625e-01
+8.250e-01
+7.875e-01
+7.500e-01
+7.125e-01
+6.750e-01
+6.375e-01
+6.000e-01
+5.625e-01
+5.250e-01
+4.875e-01
+4.500e-01
+4.125e-01
+3.750e-01
+3.375e-01
+3.000e-01
+2.625e-01
+2.250e-01
+1.875e-01
+1.500e-01
+1.125e-01
+7.500e-02
+3.750e-02
+0.000e+00
Z
Y
X

A2.6 SINGLE ANCHOR – SHEAR REINFORCEMENT SETUP C

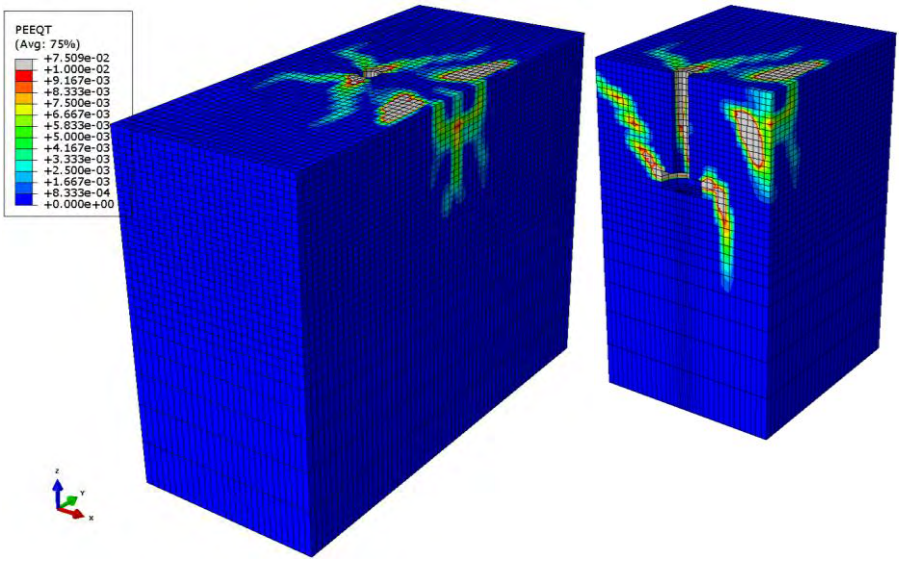

Figure A2.6-1: Reinforcement setup C. Plastic strains (PEEQT) at the time of peak load (66.3kN). Grey areas indicate strains greater than 10‰.

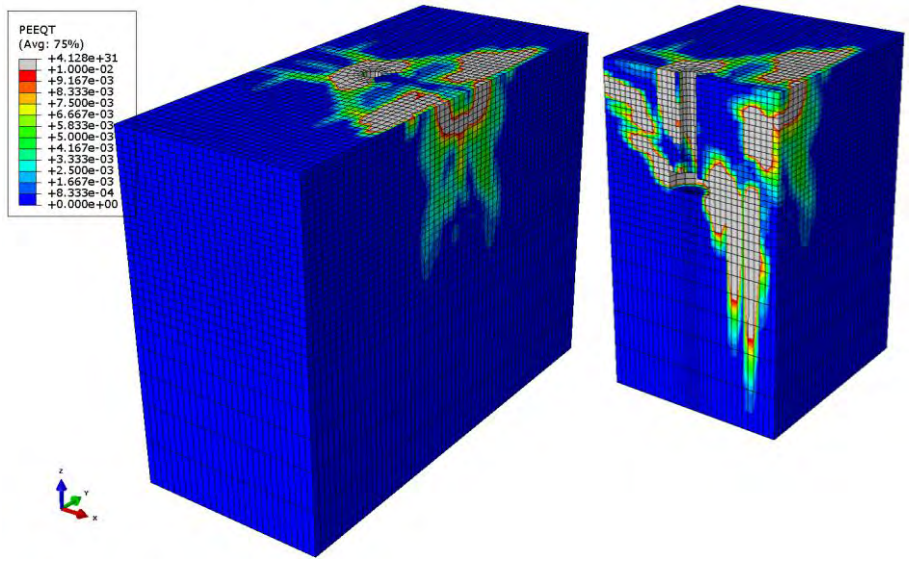

Figure A2.6-2: Reinforcement setup C. Plastic strains (PEEQT) at the last increment. Grey areas indicate strains greater than 10‰.

A2.7 SINGLE ANCHOR – SHEAR REINFORCEMENT SETUP D

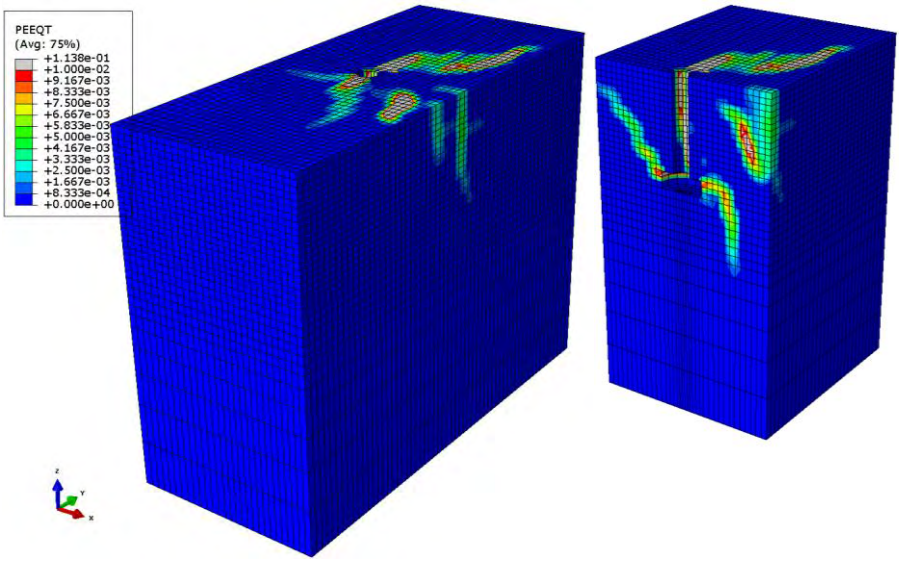

Figure A2.7-1: Reinforcement setup D. Plastic strains (PEEQT) at the time of peak load (54.8kN). Grey areas indicate strains greater than 10‰.

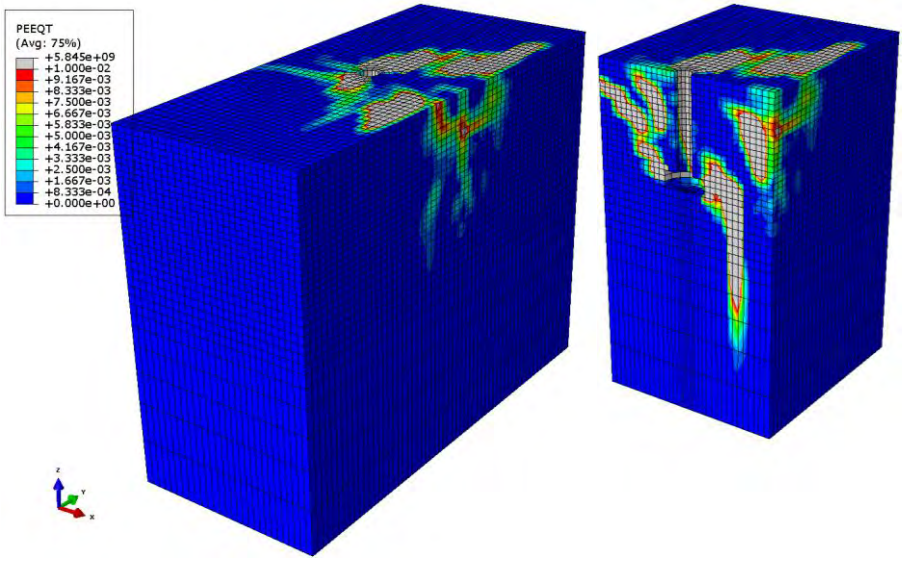

Figure A2.7-2: Reinforcement setup D. Plastic strains (PEEQT) at the last increment. Grey areas indicate strains greater than 10‰.

A2.8 SINGLE ANCHOR – SHEAR REINFORCEMENT SETUP E

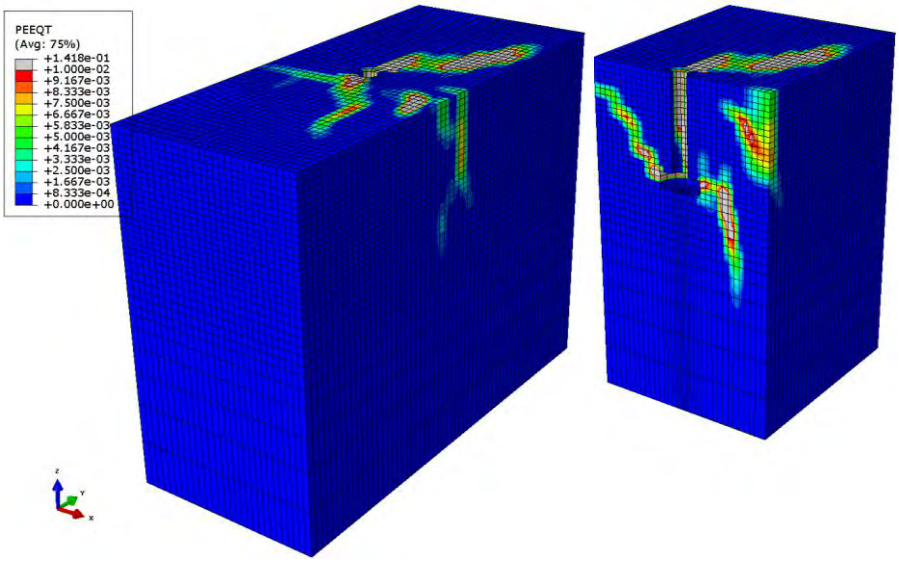

Figure A2.8-1: Reinforcement setup E. Plastic strains (PEEQT) at the time of peak load (57.2kN). Grey areas indicate strains greater than 10‰.

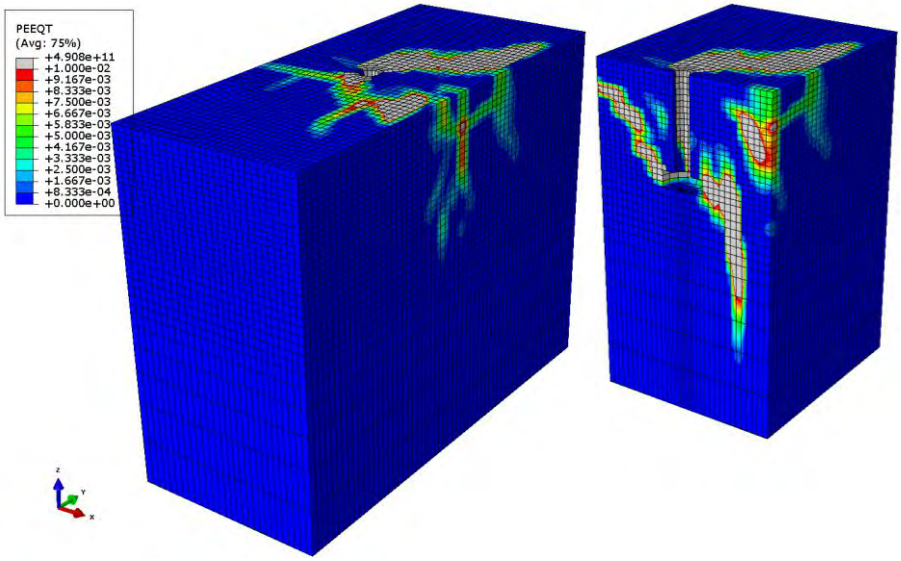

Figure A2.8-2: Reinforcement setup E. Plastic strains (PEEQT) at the last increment. Grey areas indicate strains greater than 10‰.

A2.9 ANCHOR GROUP – REINFORCEMENT IN LONGITUDINAL DIRECTION

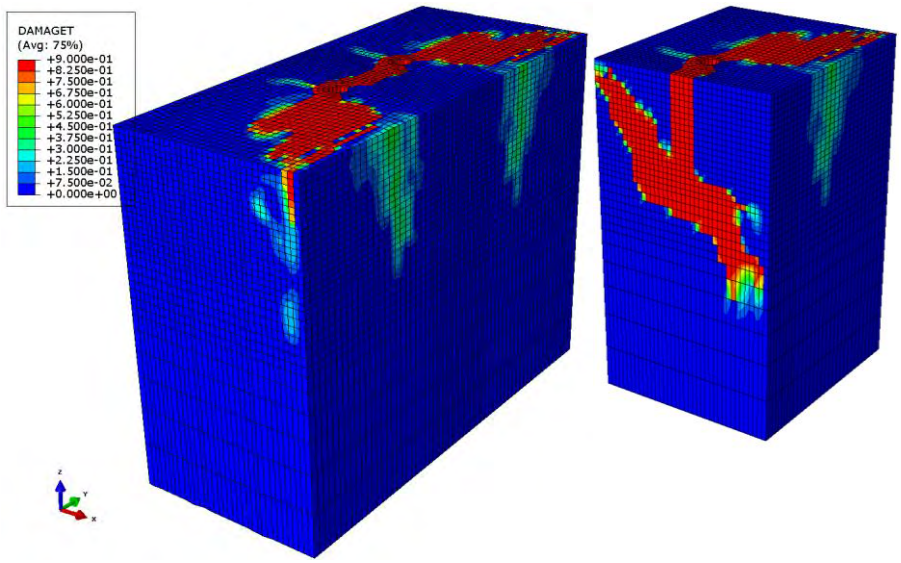

Figure A2.9-1: Damage tension parameter at the last increment.

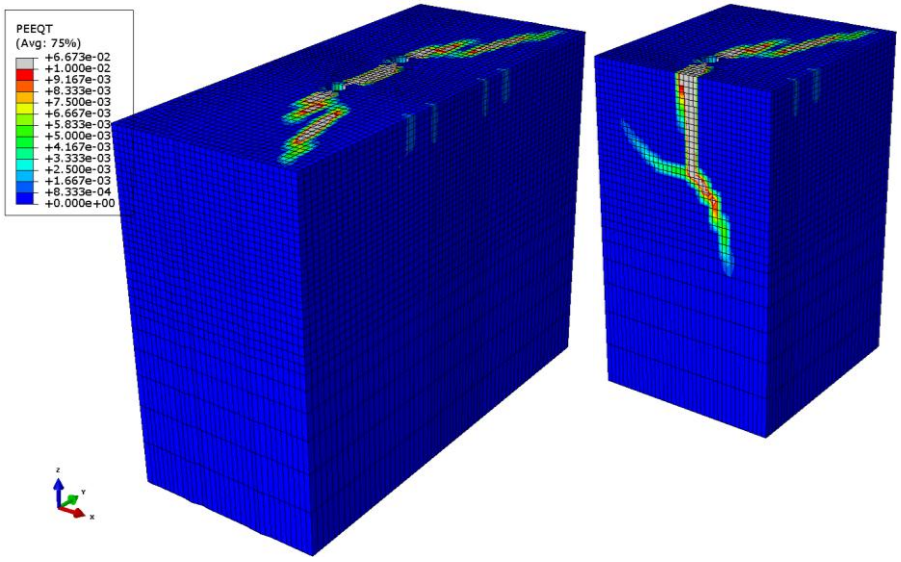

Figure A2.9-2: Plastic strains (PEEQT) at the time of peak load (52.4kN). Grey areas indicate strains greater than 10‰.

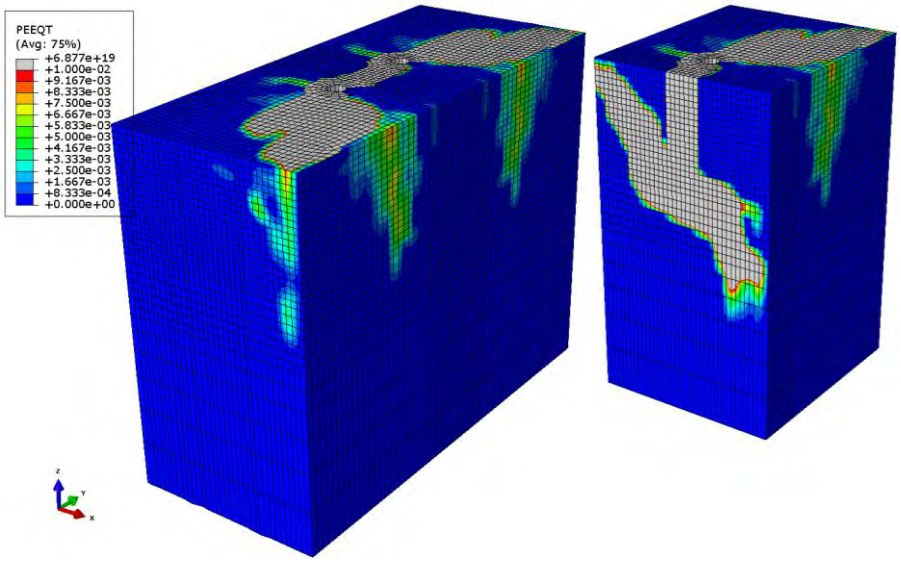

Figure A2.9-3: Plastic strains (PEEQT) at the last increment. Grey areas indicate strains greater than 10‰.

A2.10 ANCHOR GROUP – SHEAR REINFORCEMENT SETUP B

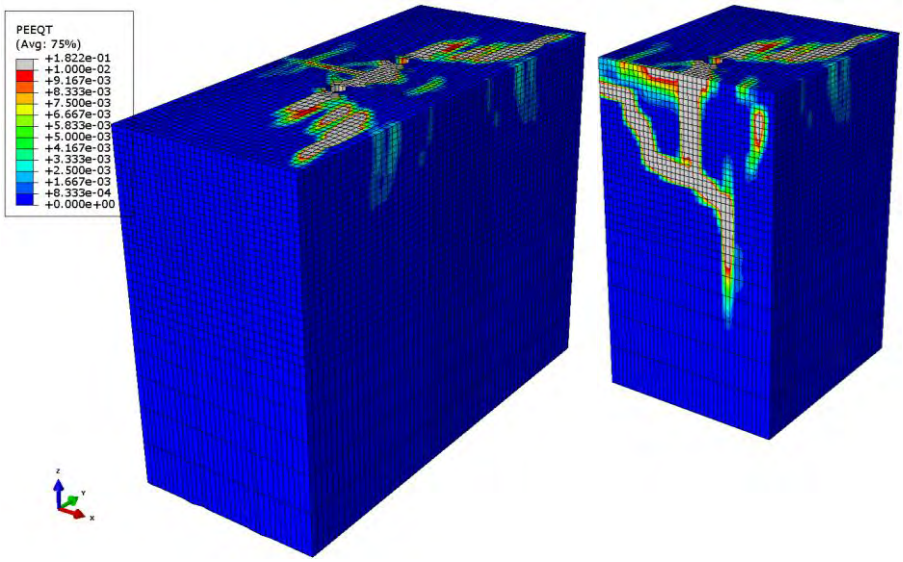

Figure A2.10-1: Reinforcement setup B. Plastic strains (PEEQT) at the time of peak load (79.4kN). Grey areas indicate strains greater than 10‰.

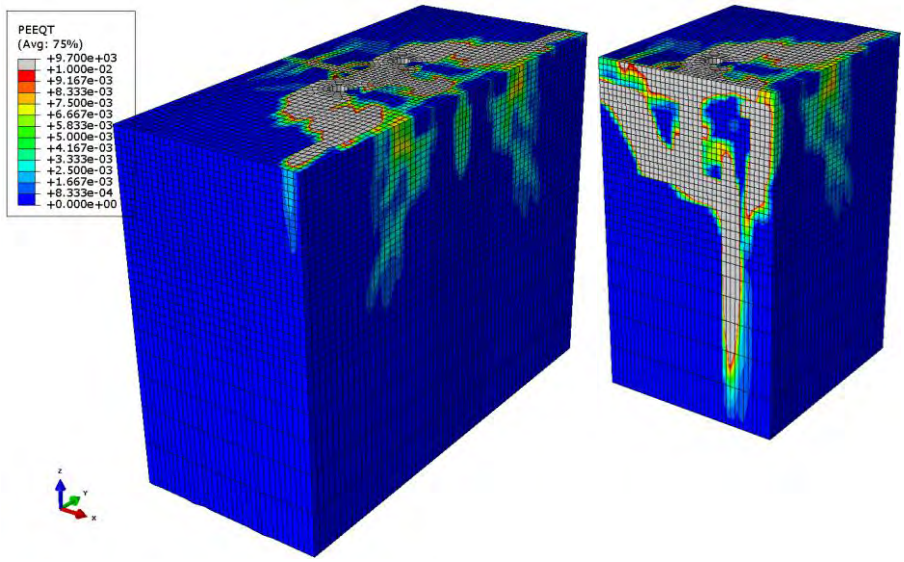

Figure A2.10-2: Reinforcement setup B. Plastic strains (PEEQT) at the last increment. Grey areas indicate strains greater than 10‰.

A2.11 ANCHOR GROUP – SHEAR REINFORCEMENT SETUP C

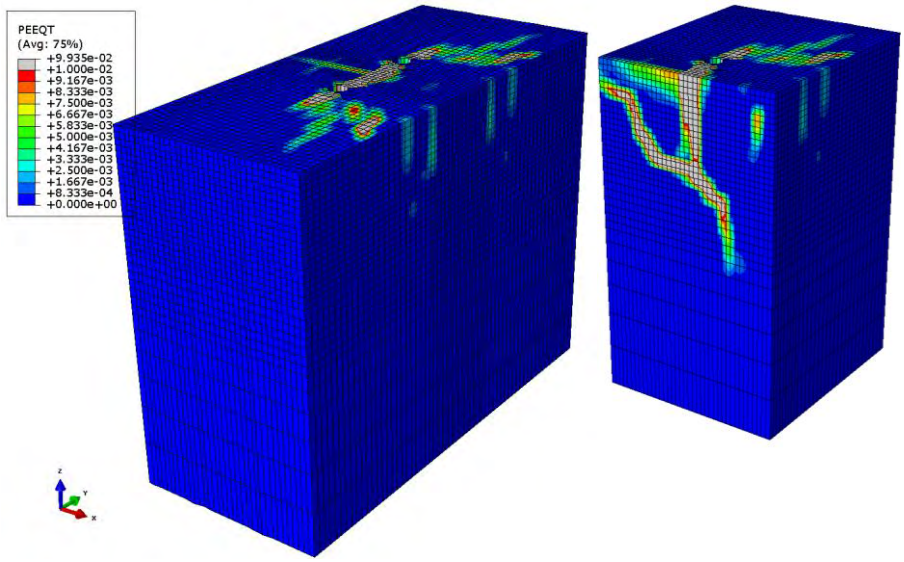

Figure A2.11-1: Reinforcement setup C. Plastic strains (PEEQT) at the time of peak load (87.9kN). Grey areas indicate strains greater than 10‰.

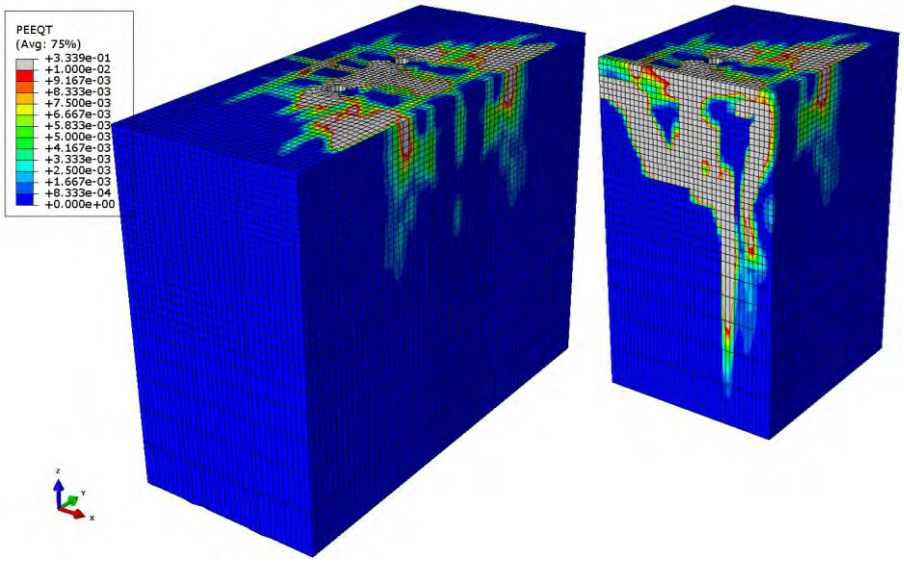

Figure A2.11-2: Reinforcement setup C. Plastic strains (PEEQT) at the last increment. Grey areas indicate strains greater than 10‰.

A2.12 ANCHOR GROUP – SHEAR REINFORCEMENT SETUP D

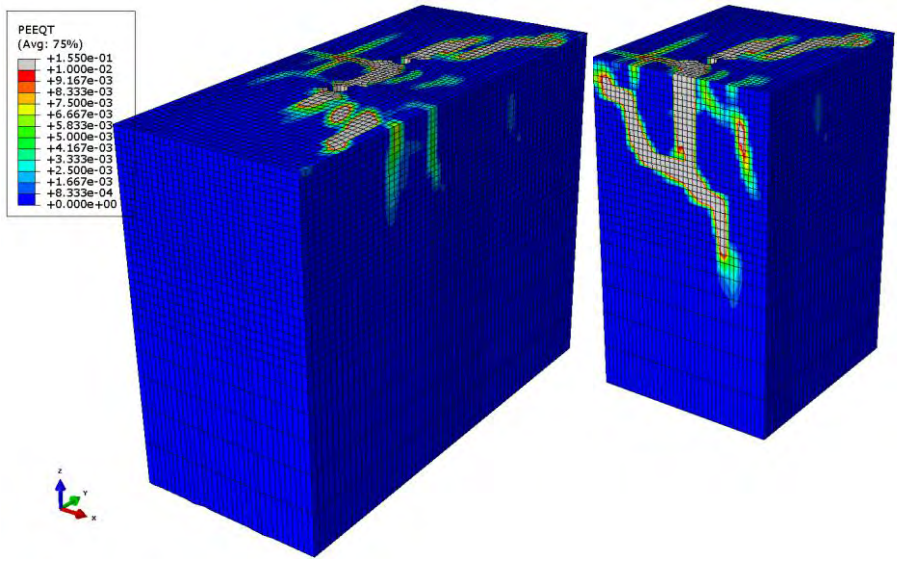

Figure A2.12-1: Reinforcement setup D. Plastic strains (PEEQT) at the time of peak load (83.8kN). Grey areas indicate strains greater than 10‰.

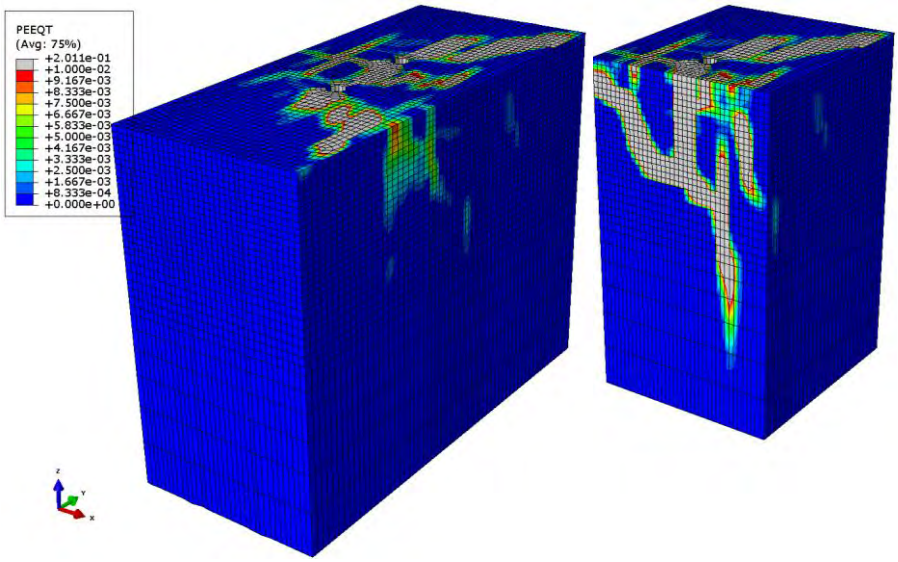

Figure A2.12-2: Reinforcement setup D. Plastic strains (PEEQT) at the last increment. Grey areas indicate strains greater than 10‰.

2013:27

The Swedish Radiation Safety Authority has a comprehensive responsibility to ensure that society is safe from the effects of radiation. The Authority works to achieve radiation safety in a number of areas: nuclear power, medical care as well as commercial products and services. The Authority also works to achieve protection from natural radiation and to increase the level of radiation safety internationally.

The Swedish Radiation Safety Authority works proactively and preventively to protect people and the environment from the harmful effects of radiation, now and in the future. The Authority issues regulations and supervises compliance, while also supporting research, providing training and information, and issuing advice. Often, activities involving radiation require licences issued by the Authority. The Swedish Radiation Safety Authority maintains emergency preparedness around the clock with the aim of limiting the aftermath of radiation accidents and the unintentional spreading of radioactive substances. The Authority participates in international co-operation in order to promote radiation safety and finances projects aiming to raise the level of radiation safety in certain Eastern European countries.

The Authority reports to the Ministry of the Environment and has around 270 employees with competencies in the fields of engineering, natural and behavioural sciences, law, economics and communications. We have received quality, environmental and working environment certification.

Strålsäkerhetsmyndigheten
Swedish Radiation Safety Authority

SE-171 16 Stockholm
Solna strandväg 96

Tel: +46 8 799 40 00
Fax: +46 8 799 40 10

E-mail: registrator@ssm.se
Web: stralsakerhetsmyndigheten.se